Citrate carrier links chromatin, metabolism and stemness upon ageing and exposure to high oxygen

Inaugural-Dissertation

zur

Erlangung des Doktorgrades

der Mathematisch-Naturwissenschaftlichen Fakultät

der Universität zu Köln

vorgelegt von

Andromachi Pouikli

aus Thessaloniki

Köln, January 2022

Berichterstatter/in:	*Dr. Peter Tessarz*
	Prof. Dr. Elena Rugarli
Prüfungsvorsitzender:	*Prof. Dr. Jan Riemer*
Tag der Disputation:	*24.01.2022*

The aim of science is not to open the door to infinite wisdom,

but to set a limit to infinite error.

– Bertolt Brecht, The life of Galileo

Kurzzusammenfassung

Die Alterung geht mit einer allgemeinen Abnahme der Funktion vieler zellulärer Signalwege einher. Obwohl der Beitrag der einzelnen Signalwege zur Alterung in den letzten Jahren eingehend untersucht wurde, ist nicht klar, wie diese Signalwege zusammenwirken, um die Entwicklung und das Fortschreiten der Alterung zu regulieren. Das Ziel dieser Arbeit war zu untersuchen, ob altersbedingte Veränderungen der mitochondrialen Funktion, der epigenetischen Modifikationen und der Stammzellaktivität miteinander kausal und funktionell verbunden sind. Daher untersuchte ich die Auswirkungen der mitochondrial-nukleären Kommunikation auf die Stammzellfunktion während des Alterns. Ich fand heraus, dass gealterte mesenchymale Stammzellen, die aus dem Knochenmark isoliert wurden (BM-MSCs), eine verringerte Chromatin-Zugänglichkeit und eine geringere Histon-Azetylierung aufweisen, insbesondere an Promotoren und Enhancern von Genen, die für die Osteogenes wichtig sind. Die verringerte Histon-Azetylierung ist auf einen gestörten Export von mitochondrialem Azetyl-CoA zurückzuführen, der durch die geringeren Mengen an Citrat-Carrier (CiC) bedingt ist. Ich konnte nachweisen, dass gealterte Zellen einen verstärkten lysosomalen Abbau von CiC aufweisen, der über aus den Mitochondrien stammende Vesikel (MDV – *mitochondrial derived vesicles*) vermittelt wird. Hervorzuheben ist, dass die Wiederherstellung des zytosolischen Azetyl-CoA-Spiegels entweder durch exogene CiC-Expression oder durch Azetat-Supplementierung das Chromatin verjüngern kann und Defekt der Osteogenese in gealterten BM-MSCs behebt. Insgesamt belegen meine Ergebnisse eine enge, altersabhängige Verbindung zwischen mitochondrialer Qualitätskontrolle, Chromatin und dem Schicksal der Stammzellen, die alle durch CiC miteinander verbunden sind.

Das Knochenmarkstroma ist durch eine niedrige Sauerstoffkonzentration (Hypoxie) gekennzeichnet, die für die Aufrechterhaltung der BM-MSC-Stammzellen unerlässlich ist. Die In-vitro-Kultur von BM-MSC im Rahmen von Stammzelltherapien erfolgt jedoch unter hohen Sauerstoffkonzentrationen (Normoxie), was die Aktivität der BM-MSC erheblich beeinträchtigen könnte. Hier habe ich untersucht, wie die Achse Stoffwechsel-Chromatin-Stammzellen durch die Sauerstoffspannung

beeinflusst wird. Ich fand heraus, dass ein hoher Sauerstoffgehalt die Osteogenese irreversibel beeinträchtigt, was auf eine höhere Chromatinverdichtung und eine geringere Histonacetylierung an Promotoren und Enhancern osteogener Gene zurückzuführen ist. Obwohl Normoxie eine Stoffwechselumstellung induziert, die zu einer höheren Azetyl-CoA-Produktion führt, konnte ich zeigen, dass Azetyl-CoA in den Mitochondrien gefangen bleibt. Dies ist möglicherweise auf eine geringere CiC-Aktivität zurückzuführen. Ähnlich zu den Vorgängen im Alter kann die Modulation der CiC-Aktivität sowohl das metabolische als auch das epigenetische Profil von BM-MSCs beeinflussen und eine exogene Supplementierung mit Azetat die osteogene Differenzierungsfähigkeit der in Normoxie kultivierten Zellen wiederherstellen.

Abstract

Ageing is accompanied by a general decline in the function of many cellular pathways. Although the contribution of each individual pathway in ageing has been extensively studied over the last years, how these pathways crosstalk to regulate the development and progression of ageing remained elusive. Here, I sought to determine whether age-associated changes in mitochondrial function, epigenetic modifications and stem cell activity are causally or functionally interconnected. Therefore, I studied the effects of mitochondrial–nuclear communication on stem cell function upon ageing. I found that aged mesenchymal stem cells isolated from the bone marrow (BM-MSCs) exhibit reduced chromatin accessibility and lower histone acetylation, particularly on promoters and enhancers of osteogenic genes. The reduced histone acetylation is due to impaired export of mitochondrial acetyl-CoA, owing to the lower levels of citrate carrier (CiC). I demonstrated that aged cells show enhanced lysosomal degradation of CiC, which is mediated via mitochondrial-derived vesicles. Strikingly, restoring cytosolic acetyl-CoA levels either by exogenous CiC expression or via acetate supplementation, remodels the chromatin landscape and rescues the osteogenesis defects of aged BM-MSCs. Collectively, my results establish a tight, age-dependent connection between mitochondrial quality control, chromatin and stem cell fate, which are altogether linked by CiC.

The bone marrow stroma is characterized by low oxygen concentration (hypoxia), which is essential for the maintenance of BM-MSC stemness. However, *in vitro* BM-MSC culture during stem cell therapies is performed under high oxygen conditions (normoxia), which could dramatically impact BM-MSC activity. Here, I explored how the metabolism-chromatin-stemness axis is affected by oxygen tension. I found that high oxygen impairs osteogenesis irreversibly, due to higher chromatin compaction and lower histone acetylation on promoters and enhancers of osteogenic genes. Although normoxia induces a metabolic switch which results in production of higher acetyl-CoA levels, I showed that this remains trapped inside the mitochondria, potentially due to lower CiC activity. Impressively, modulating CiC function impacts both the metabolic and the epigenetic profile of BM-MSCs, whereas exogenous

supplementation with acetate restores the osteogenic differentiation capacity of normoxia-cultured cells.

Acknowledgements

This PhD thesis would have not been completed successfully without the constant help, being scientific or personal, of the people around me, to whom I would like to express my immense gratitude.

First and foremost, I am grateful to my supervisor Dr. Peter Tessarz, who allowed me to conduct my doctoral thesis in his lab and offered me this great project to work on. His scientific guidance and constant support at every single step of my PhD research have helped me to become a better scientist. I thank him heartily for being a mentor who believed in me from the very start, listening to my concerns and giving me invaluable advice.

Furthermore, I would like to thank the members of my PhD Thesis advisory board, Prof. Aleksandra Trifunovic and Prof. Thorsten Hoppe for their constructive feedback and insightful discussions during our meetings.

Special thanks to Prof. Elena Rugarli for kindly agreeing to be a tutor on my PhD Thesis advisory committee and taking over the task as second reviewer of this Thesis. Accordingly, I am grateful to Prof. Jan Riemer for kindly agreeing to be a tutor on my PhD Thesis advisory committee and taking over the chairmanship of my disputation and to Prof. Hartmut Geiger who agreed to review my PhD Thesis.

I would also like to thank Andrea Mesaros (MPI-AGE Phenotyping Core) for carrying out the bone quality-related measurements and Patrick Giavalisco (MPI-AGE Metabolomic Core) for running the metabolomic analyses and for proof-reading one of my publications.

Thank you, Kat Folz-Donahue and Lena Schumacher (MPI-AGE FACS & Imaging Core) for your assistance and patience during my time-consuming cell sorting experiments.

The Alexander S. Onassis Public Benefit Foundation in Greece funded the last year of my PhD research. I appreciate the trust the Foundation has placed in me and I would like to thank especially Mrs. Katerina Magkel for always being so kind, helpful and responsive.

I thank all current and former members of the Tessarz group and particularly Tonanzi, Niklas K., Mihaela, Niklas G., and Julia for their scientific feedback, for creating a pleasant working environment and for our relaxing moments during our lunch breaks and beer-hours. HUGE thanks to my colleagues and close friends Chrysa and Constantine; you both have helped me by all means during all these years. I am immensely grateful for your scientific and psychological support and I am very happy that I have met you.

I am very thankful to my good friends Lisonia, Chrysanthi, Danae and Chris and my friends in Greece who were always next to me celebrating my bright moments and supporting me in dire times.

I reserve my deepest thanks for my beloved family. Mam, Dad, Kleoniki and Antonis thank you for always being there for me, listening to my worries, and sharing your views. I would have never accomplished any of my goals, if you had given up on me.

Table of contents

1. Introduction ***1***

1.1 Introduction to bone marrow mesenchymal stem cells (BM-MSCs) *2*

1.2 Metabolic and epigenetic regulation of BM-MSC fate decisions *6*

1.3 Mitochondrial-derived vesicles (MDVs) contribute to mitochondrial proteostasis *18*

1.4 The BM-MSC differentiation balance in ageing and age-associated bone diseases *25*

1.5 The mitochondrial citrate carrier in physiology and disease *29*

1.6 Research aims of the thesis *36*

2.* Materials and Methods** ***38

2.1 Materials *39*

2.2 Methods *44*

3. Results ***62***

Part I: Chromatin remodeling due to degradation of Citrate Carrier impairs osteogenesis of aged stem cells *63*

3.1 Chromatin compaction and histone hypo-acetylation during BM-MSC ageing *63*

3.2 Age-induced changes in the abundance of histone marks on lineage-defining genes *73*

3.3 Lower CiC levels lead to acetyl-CoA trapping inside mitochondria of aged cells *77*

3.4 Functional role of CiC in the regulation of osteogenesis *82*

3.5 MDV-lysosomal degradation of CiC in aged BM-MSCs *89*

3.6 The CiC–histone acetylation axis is conserved in human BM-MSCs *95*

Part II: Citrate Carrier impacts the mito-nuclear communication and impairs osteogenesis in response to oxygen stress *96*

3.7 Normoxia impairs osteogenesis via changes on the epigenome *96*

3.8 High oxygen alters the cellular energetic profile *102*

3.9 High oxygen impairs export of mitochondrial acetyl-CoA to the cytosol *107*

4. Discussion ***111***

4.1 Ageing perturbs the mito-nuclear communication via degradation of CiC *112*

4.2 High oxygen impairs osteogenesis in a CiC-dependent manner *116*

5. **Conclusions and perspectives** ***119***

References ***123***

Appendix A Measurement of bone quality parameters ***139***

Appendix B Electron microscopy ***140***

Appendix C Targeted liquid chromatography mass spectrometry (LC-MS) analysis ***141***

Appendix D Analysis of sequencing data ***142***

List of Tables

Table 1. Cell culture reagents, growth media, antibiotics and drugs *39*

Table 2. Antibodies used for FACS analysis *40*

Table 3. Antibodies used for Western Blot *40*

Table 4. Antibodies used for Immunofluorescence and CUT&RUN-seq *41*

Table 5. Sequences of primers used for qRT-PCR analysis *46*

Table 6. Sequences of primers used for qRT-PCR analysis of mtDNA-encoded genes *47*

List of Figures

Figure 1.1. Isolation of BM-MSCs *3*

Figure 1.2. Enhanced BM-MSC activity in the PaS population *5*

Figure 1.3. Metabolic characteristics of uncommitted and differentiated BM-MSCs and major transcription factors driving lineage determination *8*

Figure 1.4. Metabolism-chromatin interplay *15*

Figure 1.5. Mitochondrial quality control mechanisms *19*

Figure 1.6. Current model for MDV formation *24*

Figure 1.7. Changes in the adipogenesis-osteogenesis differentiation balance upon ageing and osteoporosis *26*

Figure 1.8. Summary of the CiC activities *30*

Figure 3.1. Isolation and characterization of BM-MSCs derived from the bone endosteum *63*

Figure 3.2. Maintenance of BM-MSC properties during *in vitro* culture *65*

Figure 3.3. BM-MSCs lose their osteogenic capacity upon ageing *66*

Figure 3.4. Loss of trabecular bone volume and density in aged mice *67*

Figure 3.5. Quality control of ATAC-seq *68*

Figure 3.6. Chromatin compaction in aged BM-MSCs *69*

Figure 3.7. Reduced transcription rate in aged BM-MSCs *70*

Figure 3.8. Lower histone acetylation in aged BM-MSCs *71*

Figure 3.9. Altered abundance of H3K27ac on lineage-determining genes *73*

Figure 3.10. Age-associated changes in glucose metabolism *74*

Figure 3.11. Age-associated changes in H3K27me3 abundance *76*

Figure 3.12. Discrepancy between the levels of acetyl-CoA and histone acetylation *77*

Figure 3.13. Lower lipid content in aged cells is due to impaired lipogenesis 78

Figure 3.14. acetyl-CoA is trapped inside the mitochondria of aged cells *81*

Figure 3.15. CiC inhibition impairs mitochondrial acetyl-CoA export and osteogenesis in young BM-MSCs 82
Figure 3.16. CiC OE restores nuclear acetyl-CoA localization and osteogenesis *84*
Figure 3.17. Acetate restores nuclear acetyl-CoA localization and improves osteogenesis of aged BM-MSCs *85*
Figure 3.18. Acetate restores H3ac abundance on promoters of osteogenic genes *87*
Figure 3.19. Slc25a1 transcription remains stable upon ageing *89*
Figure 3.20. Lysosomal degradation of CiC in aged BM-MSCs *91*
Figure 3.21. MDVs transfer CiC to lysosomes for degradation *93*
Figure 3.22. The CiC–histone acetylation-cell fate axis is conserved in human BM-MSCs *95*
Figure 3.23. Isolation and culture scheme of BM-MSCs derived from the bone endosteum *96*
Figure 3.24. BM-MSCs lose their osteogenic capacity upon exposure to 21% O_2. *98*
Figure 3.25. Normoxia results in lower chromatin accessibility *99*
Figure 3.26. Loss of histone acetylation under high oxygen conditions *100*
Figure 3.27. Changes in the levels of epigenetic-related metabolites *102*
Figure 3.28. Normoxia suppresses glycolysis of BM-MSCs *104*
Figure 3.29. Induction of mitochondrial respiration under normoxia *105*
Figure 3.30. Normoxia impairs lipid biosynthesis *106*
Figure 3.31. Trapping of acetyl-CoA inside mitochondria in normoxia-cultured BM-MSCs *107*
Figure 3.32. Figure 3.34. Modulating CiC activity affects lipogenesis, acetylation and osteogenesis *109*
Figure 4.1. Model for CiC-mediated connection among mitochondrial quality control, chromatin and stemness in aged BM-MSCs *113*

List of Abbreviations

General

°C	degrees Celsius
v:v	volume:volume
acetyl-CoA	acetyl-coenzyme A
α-KG	alpha-ketoglutarate
ATP	adenosine triphosphate
BM-MSCs	bone marrow mesenchymal stem cells
bp	base pair(s)
cDNA	complementary DNA
D.melanogaster	*Drosophila melanogaster*
DANN	deoxyribonucleic acid
ECM	extracellular matrix
EDTA	ethylenediaminetetraacetic acid
ESCs	embryonic stem cells
et al.	et alia (and others)
etc.	et cetera (the rest)
ETC	electron transport complex
FAO	fatty acid oxidation
g	relative centrifugal force
GlcNAc	N-acetylglucosamine
GO	gene ontology
HG	hydroxyglutarate
HSCs	hematopoietic stem cells
i.e.,	id est (that is)
IMM	inner mitochondrial membrane
IMS	inter membrane space
ISCT	international society of cellular therapy
LDs	lipid droplets
LPS	lipopolysaccharides
MDVs	mitochondrial-derived vesicles
MET cycle	methionine cycle
MFI	mean fluorescence intensity
mPTP	mitochondrial permeability transition pore
mtDNA	mitochondrial DNA

NSCs	neural stem cells
OMM	outer mitochondrial membrane
OXPHOS	oxidative phosphorylation
RNA	ribonucleic acid
ROS	reactive oxygen species
rpm	rounds per minute
RT	room temperature
SAH	S-adenosyl-homocysteine
SAM	S-adenosyl-methionine
S.E.M.	standard error of mean
TCA cycle	tricarboxylic acid cycle
TSS	transcription Start Site
UDP-GlcNAc	uridine diphosphate N-acetylglucosamine
UPR^{mt}	mitochondrial unfolded protein response
UPS	ubiquitin-proteasome system
2-DG	2-deoxy-glucose

Reagents and methods

5-AzaC	5-azacytidine
5-EU	5-ethynyl uridine
APC	allophycocyanin
BafA1	bafilomycin A1
BTA	1,2,3-benzene-tricarboxylic acid
ChIP-seq	chromatin immunoprecipitation-sequencing
ECAR	extracellular acidification rate
EM	electron microscopy
FACS	fluorescence-activated cell sorting
FBS	fetal bovine serum
FCCP	carbonyl cyanide-p-trifuoromethoxyphenyl-hydrazone
FITC	fluorescein-5-isothiocyanate
HBSS	hanks balanced salt solution
HEPES	4-(2-hydroxyethyl)-1-piperazineethane-sulphonic acid
IBMX	3-Isobutyl-1-methylxanthine
ITS	insulin-transferrin-selenium
OCR	oxygen consumption rate

PBS	phosphate-buffered saline
PCR	polymerase chain reaction
PE	phycoerythrin
qRT-PCR	real-time quantitative reverse transcription-PCR

Gene and protein names

7AAD	7-aminoactinomysin D
Acan	*Aggrecan*
ACC1	acetyl-CoA carboxylase 1
ACLY	ATP citrate lyase
ACS	acetyl-CoA synthase
Alp	*Alkaline phosphatase*
AMPK	AMP-activated protein kinase
ATF5	activating transcription factor 5
Atp6	*ATP synthase membrane subunit 6*
BMP	bone morphogenetic protein
CAT	catalase
CBP	creb binding protein
CD proteins	cluster of differentiation
CiC	citrate carrier
Col2α1	*collagen-type 2 alpha 1*
Cox-1	*cytochrome c oxidase I*
CPT-1	carnitine palmitoyltransferase 1
CTCF	CCCTC-binding Factor
DLX5	distal-less homeobox 5
DNMTs	DNA methyltransferases
DRP1	dynamin-related protein 1
E2F5	E2F transcription factor 5
EZH2	enhancer of zeste homologue 2
FAS	fatty acid synthase
Foxo1	*forkhead-box O1*
GCN5	general control nonderepressible 5-related
GPx	glutathione peroxidase
HAT	histone acetyltransferase
HDACs	histone deacetylases

HIFs	hypoxia inducible factors
HMTs	histone methyltransferases
HOXA	homeobox A
IGF-1	insulin-like growth factor-1
IFN-γ	interferon-gamma
iNOS	inducible nitric oxide synthase
JmjC	jumonji C
LAMP2	lysosome-associated membrane protein 2
LdhA	*lactate dehydrogenase A*
MAPL	mitochondrial-anchored protein ligase
MLLs	mixed lineage leukemias
mTORC1	mammalian target of rapamycin complex1
NAD	nicotinamide adenine dinucleotide
NF-kB	nuclear factor 'kappa-light-chain-enhancer' of activated B cells
Nrf2	*nuclear factor erythroid 2-related factor 2*
Oc	*osteocalcin*
OCT-4	octamer-binding transcription factor 4
OPA1	optic atrophy type 1
Osx	*osterix*
PARL	presenilin associated rhomboid like
Pax6	*paired box 6*
PDH	pyruvate dehydrogenase
Pdk1	*pyruvate dehydrogenase kinase 1*
Pfk1	*phosphofructokinase 1*
PGC-1α	proliferator-activated receptor g co-activator 1 alpha
PGE2	prostaglandin E2
Pgk1	*phosphoglycerate kinase 1*
PPARγ	*proliferator-activated receptor gamma*
RUNX2	runt-related transcription factor 2
Sca-1	stem cell antigen-1
SIRT	sirtuin
SOD	sodium dismutase
Sox2	*SRY-box transcription factor 2*
SREBP1	sterol regulatory element-binding protein 1
Ssea-4	*stage-specific embryonic antigen 4*
STARD7	StAR related lipid transfer domain-containing 7

STX17	syntaxin 17
TFG-β	transforming growth factor-beta
TNF-α	tumor necrosis factor-aplha
TOMM20	translocase of outer mitochondrial membrane 20
T3	triiodothyronine
VAMP7	vesicle-associated membrane protein 7
VDAC	voltage-dependent anion channel
YME1L	YME1 like 1 ATPase

Chapter 1

Introduction

1.1 Introduction to bone marrow mesenchymal stem cells (BM-MSCs)

In multicellular organisms, stem cells are undifferentiated – or partly differentiated – cells with the dual capacity to undergo proliferation and differentiation into specific lineages in response to various internal and external stimuli (Seita and Weissman, 2010; Weissman et al., 2001). Therefore, stem cells play a vital role in the maintenance of tissue homeostasis throughout the lifetime of an organism. Stem cells are present in the embryonic, fetal and adult stages of life, displaying unique properties and defined characteristics at each developmental stage. Mesenchymal stem cells (MSCs) reside in various tissues within the adult organisms, with the bone marrow stroma (Haynesworth et al., 1992; Pittenger et al., 1999) and the vascular fraction of the adipose tissue (Baer and Geiger, 2012; Halvorsen et al., 2000; Zuk et al., 2001) being the most commonly used sources of adult MSCs.

Bone marrow mesenchymal stem cells (BM-MSCs) constitute a self-renewing cell population with the ability to give rise to osteoblasts, chondrocytes and adipocytes (Piersma et al., 1985; Pittenger et al., 1999). Due to their multi-lineage differentiation potential, BM-MSCs represent an ideal model to study how cell intrinsic networks co-operate with signals from the niche to regulate cell fate decisions. In this regard, a wide range of intra- and extra- cellular stimuli that regulate cellular metabolism have been demonstrated to influence stem cell fate, by promoting either stemness or lineage commitment (Rehman, 2010). In addition to energy metabolism, the chromatin landscape and the genome organization determine cell identity via regulation of gene expression. Integration of these signals and coordinated regulation of the downstream cellular processes is heavily perturbed upon ageing, leading to loss of stem cell function and tissue integrity.

Isolation and characterization of murine and human BM-MSCs

Although the currently used term “mesenchymal stem cell” was introduced in 1991 by Caplan (Caplan, 1991), it was Friedenstein and coworkers who first isolated and characterized BM-MSCs, in the 1960s and 1970s. With three landmark studies

Friedenstein: (i) found that transplantation of bone marrow into the kidney capsule results in ectopic bone formation, indicating that the bone marrow is a “reservoir” of a stem cell population that is able to give rise to bone precursors, (ii) isolated from the bone marrow, adherent, fibroblast-like cells that could rapidly form colonies and could differentiate *in vitro* to osteocytes, adipocytes and chondrocytes, and (iii) reported that these cells were capable of re-generating the bone marrow microenvironment after transplantation into recipient animals (Friedenstein et al., 1968, 1970, 1974) (**Figure 1.1**). Few years later, Owen expanded Friedenstein’s observations to rats and in 1992 Arnold Caplan isolated human BM-MSCs and demonstrated that they could give rise to various tissues, including bone, cartilage, tendon, ligament, marrow stroma, adipocytes, dermis and connective tissue (Caplan, 1991).

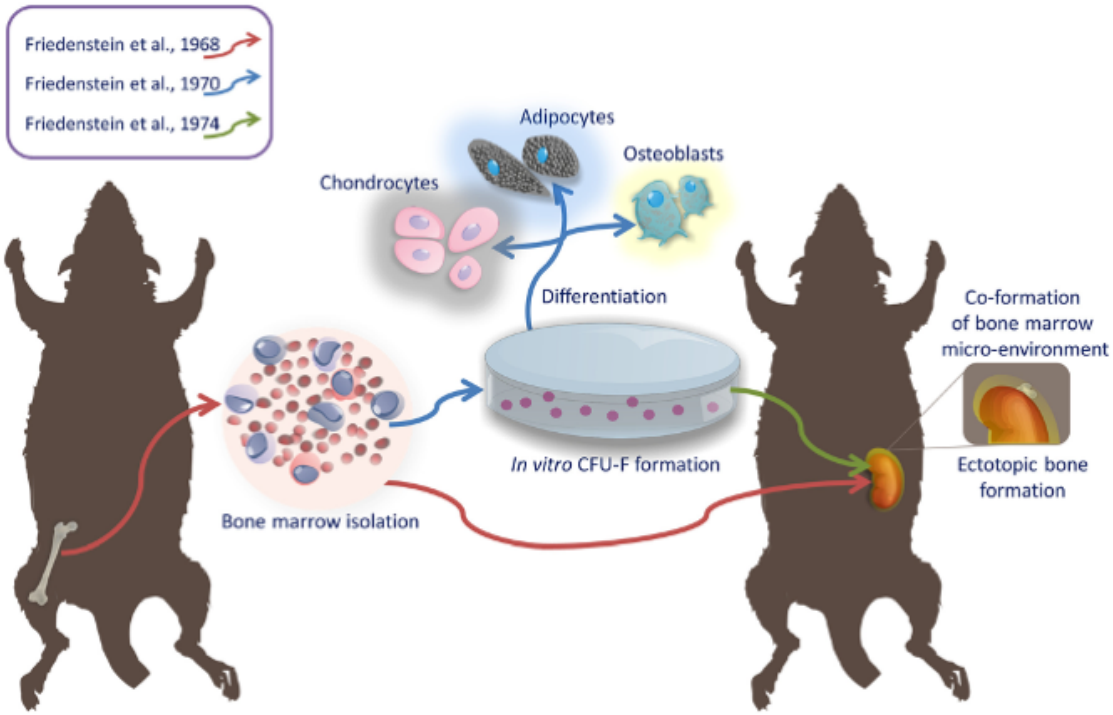

Figure 1.1. Isolation of BM-MSCs. The figure illustrates the three experimental approaches that Friedenstein followed to isolate and characterize BM-MSCs. In his first study published in 1968 (red arrows), Friedenstein observed ectopic bone formation after bone marrow transplantation into the kidney capsule. In a follow-up study published in 1970 (blue arrows) he isolated from the bone marrow a subset of cells that exhibited high proliferative potential and enhanced capacity to differentiate into adipocytes, osteoblasts and chondrocytes. His work published in 1974 (green arrows) demonstrated that these cells were able to re-shape the marrow microenvironment after transplantation. Figure obtained from Andrzejewska et al. (Andrzejewska et al., 2019).

Since their discovery, BM-MSCs have become widely used both in research studies and in clinical trials. However, the results of these studies have been considerably variable, mostly due to the lack of universal criteria and specific markers to define BM-MSCs. In fact, researchers used to enrich BM-MSCs from bone marrow aspirates by culturing the isolated cells over many passages. Cell passaging would dilute and eventually remove contaminating hematopoietic and endothelial cells, whereas the plastic-adherent BM-MSC population would be enriched. However, this approach results in a heterogeneous cell population, whereas long-term culture yields rapidly dividing stem cells that exhibit properties of immortalized cells. This is even more likely in BM-MSCs isolated from rodents, which exhibit higher immortalization rate compared to humans, due to differences in central cell-cycle checkpoint mechanisms (Josse et al., 2010; Prowse and Greider, 1995). To overcome these limitations, the International Society of Cellular Therapy (ISCT) proposed in 2006 the following criteria to define human BM-MSCs (Dominici et al., 2006):

- plastic-adherence under standard culture conditions,
- increased self-renewal capacity and differentiation potential towards adipocytes, osteoblasts and chondrocytes,
- expression of the mesenchymal stem cell surface markers: CD105, CD73, and CD90 and,
- absence of the hematopoietic and endothelial cell surface markers: CD45, CD34, CD14 or CD11b, CD79a or CD19 and HLA-DR

Regarding BM-MSC isolation from mice, it was shown that animals deficient for the Sca-1 protein display an osteopenic phenotype that could be explained by the loss of the BM-MSC population. Thus, Sca-1 could be used as a marker for mouse BM-MSCs (Bonyadi et al., 2003). However, Sca-1 is expressed in various cells, including endothelial cells. Therefore, in most recent studies, a combination of the Sca-1 marker with the PDGFRα mesenchymal marker is used to efficiently isolate BM-MSCs. Indeed, the PDGFRα-Sca-1 double positive population (PαS) displayed many of the standard properties associated with BM-MSCs, such as3 high colony-forming activity, increased proliferation and enhanced differentiation potential (Morikawa et al., 2009) (**Figure 1.2**).

The successful isolation and characterization of BM-MSCs from the bone marrow was a milestone towards their broader use in the fields of tissue engineering and regenerative medicine, mostly because of their increased differentiation capacity. Yet, we still have an incomplete understanding of the underlying molecular mechanisms contributing to BM-MSC unique functional properties and regulating BM-MSC fate decisions, which highlights the necessity of further preclinical studies.

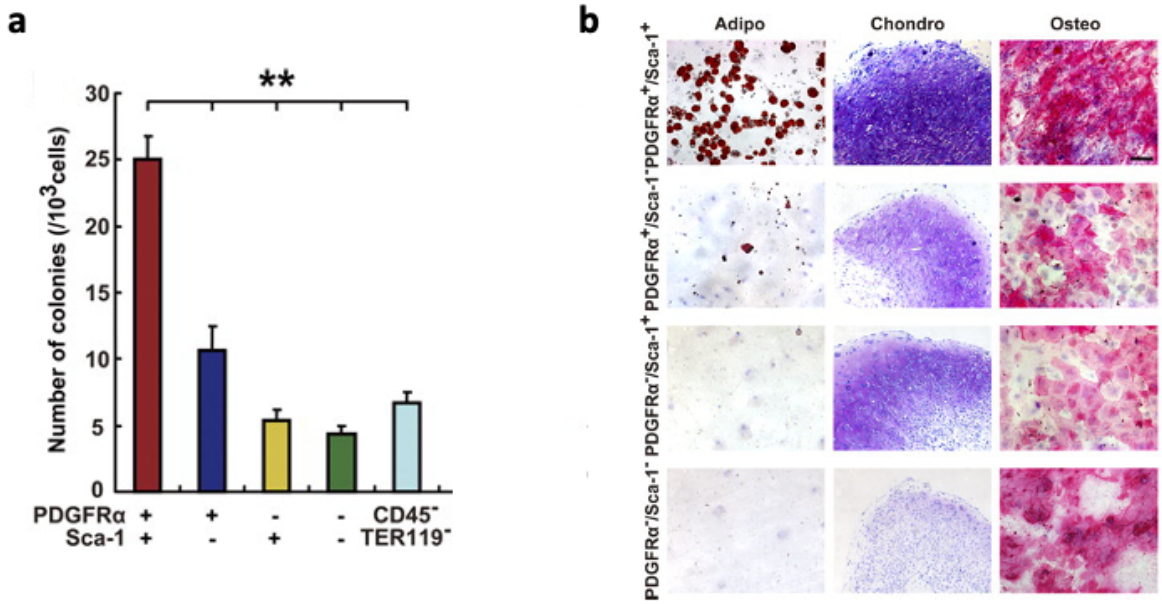

Figure 1.2. Enhanced BM-MSC activity in the PaS population. (**a**) Increased number of colonies of the PaS BM-MSC population. (**b**) Enhanced adipogenic, osteogenic and chondrogenic differentiation capacity of the PaS BM-MSC population. Adipo: adipocytes; Chondro: chondrocytes; Osteo: osteocytes. Figure adapted from Morikawa et al. (Morikawa et al., 2009).

1.2 Metabolic and epigenetic regulation of BM-MSC fate decisions

BM-MSCs reside within the bone marrow stroma and they are typically retained in a quiescent state. Quiescence has a beneficial effect in the long-term survival and maintenance of BM-MSCs due to lower production of reactive oxygen species (ROS), which damage the mitochondrial and nuclear DNA as well as proteins. Therefore, establishing a low-cycling cell rate minimizes ROS production through the electron transport complex (ETC), preserving genome integrity and cell survival (Rossi et al., 2008; Suda et al., 2011). In addition to DNA-damage-induced cell death, excessive ROS production forces BM-MSCs to exit quiescence and promotes stem cell differentiation, which eventually leads to stem cell exhaustion (Chen et al., 2008; Renault et al., 2009; Tothova et al., 2007).

Under specific conditions, for example when rapid proliferation, migration or differentiation is required, BM-MSCs respond to signals from their neighboring cells and the extracellular environment, they are activated and they undergo increased proliferation. Thus, BM-MSCs contribute to the maintenance of tissue homeostasis, in response to challenging environmental conditions, such as upon injury and inflammation, as well as during physiological development. Activated BM-MSCs rely heavily on glycolysis for energy production, as evidenced by the increased expression levels of glycolytic enzymes and the low expression levels of oxidative phosphorylation (OXPHOS)-related enzymes (Chen et al., 2008). In line with their transcriptomic profile, BM-MSCs display high rate of glycolysis and reduced rate of oxygen consumption (Pattappa et al., 2011). Although glycolysis is less efficient in ATP generation compared to complete glucose oxidation during the TCA cycle and OXPHOS, it enables rapid ATP synthesis independently of the presence of oxygen. Beyond its protective role against ROS-mediated oxidative damage and the fast supplementation of cells with high amounts of ATP, glycolysis in activated BM-MSCs offers one more advantage; it provides the metabolic precursors for nucleic acid, protein and lipid biogenesis, which are all required for biomass increase and proliferation (Lunt and Vander Heiden, 2011).

1.2.1 Stem cell differentiation is linked to lineage-specific metabolic changes

BM-MSC differentiation requires profound changes in the cellular energetic profile, which are summarized in **Figure 1.3**. Uncommitted progenitors are highly glycolytic and contain multiple mechanisms to efficiently suppress oxidative metabolism. By contrast, stem cell priming and lineage determination are usually associated with higher TCA cycle and OXPHOS activity. Up-regulation of mitochondrial biogenesis and stimulation of aerobic metabolism are common characteristics upon BM-MSC differentiation (Chen et al., 2008; Lunt and Vander Heiden, 2011; Pattappa et al., 2011; Renault et al., 2009; Zhang et al., 2013). Indeed, during BM-MSC differentiation to adipocytes and osteoblasts a complex and tightly coordinated cascade of several transcription factors, including the PPARγ and the RUNX2, which are the key-regulators of adipogenesis and osteogenesis respectively, co-operate to promote a metabolic switch from glycolysis to OXPHOS. In particular, in early stages of adipogenesis and osteogenesis the mitochondrial DNA (mtDNA) copy number, which is an indicator of the mitochondrial content, increases as a result of enhanced mitochondrial biogenesis. Mechanistically, this is achieved via activation of the mTORC1 protein, which in turn controls PGC-1α activity, to stimulate mitochondrial biogenesis and metabolism. Furthermore, in differentiating BM-MSCs, lactate secretion is significantly decreased compared to the uncommitted progenitors, while levels and activity of respiratory enzymes are significantly increased. Consistently, the structural and morphological conformation of mitochondria change; the cristae-rich mitochondria fuse to generate tubular, elongated mitochondria, which are connected to complex networks and are more efficient in ATP production (Pietilä et al., 2012; Sánchez-Aragó et al., 2013). Notably, the shift in energy metabolism from glycolysis to mitochondrial respiration is accompanied by an increase in ROS levels, which were recently found to favor adipogenesis (Tormos et al., 2011). By contrast, ROS production is maintained at low levels during osteogenesis. Unlike adipocytes, osteoblasts are extremely vulnerable to ROS-induced DNA and protein damage; thus, they contain high levels of several antioxidant enzymes, including CAT, GPx and SOD, which enhance the antioxidant defense system of the differentiating cells to prevent ROS accumulation (Chen et al., 2008). Indeed, treatment of human BM-MSCs with H_2O_2 resulted in reduced osteogenesis and impaired maturation of murine pre-

osteoblasts to mature osteocytes. Interestingly, ascorbic acid, whose presence in the culture media is indispensable for *in vitro* osteogenesis, is an important cellular antioxidant that increases the cellular capacity to cope with the ROS-induced oxidative stress (Bielski et al., 1975; Buettner and Moseley, 1993).

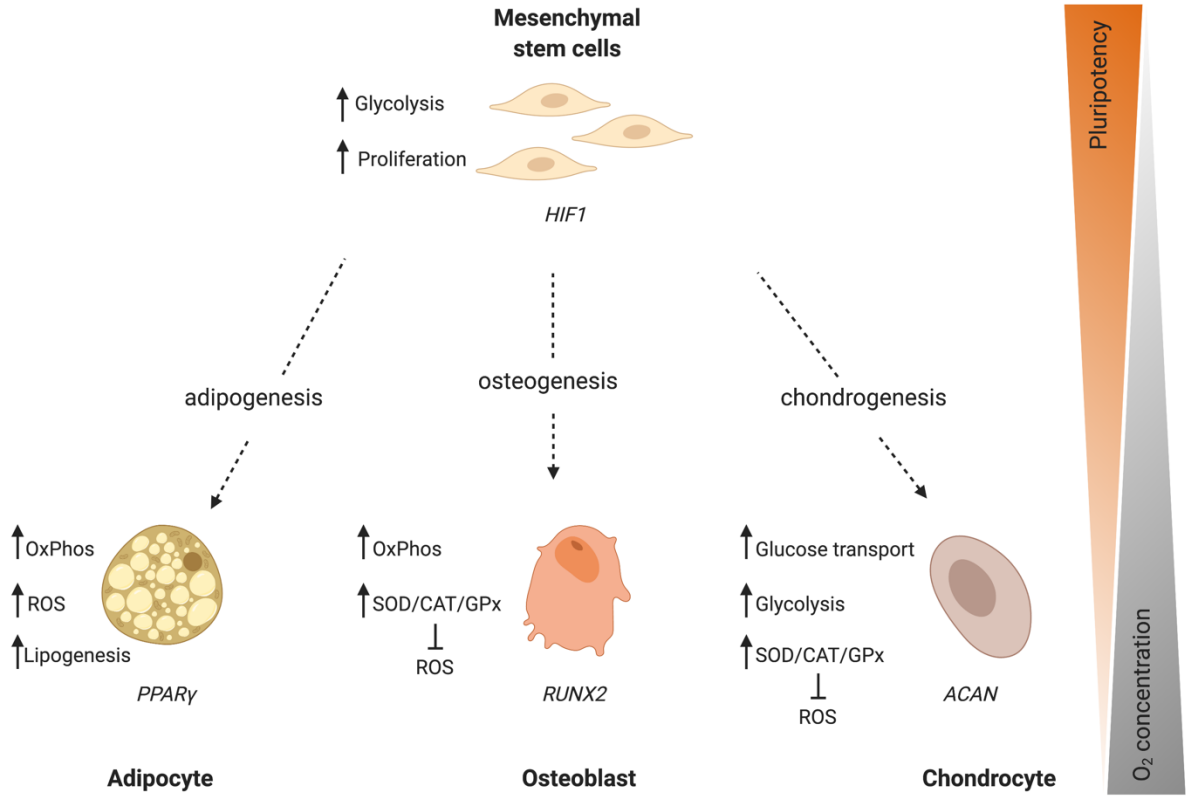

Figure 1.3. **Metabolic characteristics of uncommitted and differentiated BM-MSCs and major transcription factors driving lineage determination.** Quiescent BM-MSCs display low metabolic rates and contain reduced ROS levels. Upon injury and inflammation as well as during organogenesis quiescent BM-MSCs are activated and undergo proliferation. Proliferating BM-MSCs rely on glycolysis to generate energy. These cells undergo self-renewal and/or differentiation. During adipogenesis and osteogenesis mitochondrial respiration and OXPHOS are up-regulated, whereas chondrogenic differentiation relies on glucose metabolism and requires activation of anti-oxidant mechanisms to prevent ROS accumulation. Uppercase letters, below each cell type, indicate the key-regulators of differentiation towards each respective cell type. Pie-charts represent the relative contribution of glycolysis (yellow) and OXPHOS (blue) in ATP generation. Figure obtained from Pouikli and Tessarz (Pouikli and Tessarz, 2021).

Reduced tolerance to ROS levels and enhanced activity of glutathione peroxidases are also characteristics of differentiating BM-MSCs to chondroblasts. In order to efficiently deal with the oxidative stress, mitochondrial respiration and activity remain

suppressed upon induction of chondrogenic differentiation (Pattappa et al., 2011). By contrast, the glycolytic flux is maintained at high levels in chondrocytes and efficient chondrogenic differentiation requires increased glycolysis (Nishida et al., 2013). Thus, ample supply of glucose is indispensable for the energy production in chondrocytes. This is achieved by expression of several glucose transporters; in fact, there is evidence that mature chondrocytes express at least six members of the GLUT/SLC2A family, which exhibit different kinetics and their efficiency changes based on the substrate concentration (Mobasheri et al., 2002). Therefore, the presence of various GLUT/SLC2A proteins in chondrocytes ensures that cells will efficiently take up glucose, even when there is limited amount available in the environment. Importantly, apart from ATP production, glucose in the developing chondroblasts provides precursors for the anabolic generation of complex macromolecules found in the cartilage extracellular matrix (ECM), such as various polysaccharides and proteoglycans (Otte, 1991). To this end, metabolism of glucose as well as of other hexose sugars contributes to the generation of structural components of the ECM, which is crucial for efficient differentiation and maintenance of chondrocytes.

How is glycolysis established in BM-MSCs and what drives the metabolic rewiring upon induction of differentiation? Is glycolysis an inherent characteristic of BM-MSCs dictated by their transcriptional profile or does it represent a metabolic adaptation to stimuli from their external environment?

1.2.2 The hypoxic BM-MSC niche is a key-regulator of stem cell function

BM-MSCs reside in a distinct bone compartment within the bone marrow stroma, usually referred to as ‘niche’. This specific microenvironment is characterized by the presence of other stem cell populations, such as hematopoietic stem cells (HSCs), and differentiated cells, including osteoblasts and adipocytes, which interact with the BM-MSCs via secretion of various paracrine factors, like cytokines (Lapidot and Kollet, 2002). In addition to the cellular components of the niche, the complex vascular network, the ECM and several signaling pathways, including the TFG-β, the IGF-1, the BMP and the WNT pathways, play a fundamental role in the regulation of BM-MSC physiology (Kfoury and Scadden, 2015; Wei and Frenette, 2018; Zhang et al., 2003).

One factor whose role in stem cell behavior has recently become the subject of increased scientific interest is the oxygen concentration. Typically, the mesenchymal stem cell niche in the bone marrow cavity is characterized by low oxygen tension, despite the high vascularization. In fact, hypoxia occurs due to increased cellular density and elevated oxygen consumption by the rapidly proliferating hematopoietic cells. Using two-photon phosphorescence lifetime microscopy to measure *in vivo* oxygen tension in the murine bone marrow, Spencer et al. found that the BM-MSC niche is extremely hypoxic and the oxygen concentration ranges from 1.3% to 4.2%, depending on the distance from the blood vessels (Spencer et al., 2014).

Several mechanisms have been shown to regulate stem cell adaptation to hypoxia, but the major pathway controlling cellular response to low oxygen levels involves a specific protein family, named hypoxia-inducible factors (HIFs). Wang and Semenza were the first to identify that cell response to hypoxia is - at least in part - mediated at the transcriptional level, via the HIF1 protein, which comprises the HIF1α and HIF1β subunits (Wang and Semenza, 1993). In the low-oxygen containing niche, the HIF1α subunit is stabilized and subsequently translocates to the nucleus, where it forms a complex with the constitutively expressed HIF1β, to control different aspects of stem cell behavior, including the energetic profile (Bertout et al., 2008; Majmundar et al., 2010; Semenza, 2012a, 2012b). For instance, hypoxia promotes the expression of glucose transporters, such as *Glut1* and *Glut4*, and of many glycolytic genes including the *Pfk1*, *Pgk1* and the *LdhA*, in a HIF1α-dependent manner. In parallel, HIF1α induces the expression of *Pdk1*, which phosphorylates and inhibits PDH; thus, it prevents pyruvate oxidation and entrance into the TCA cycle, suppressing OXPHOS (Kim et al., 2006). Consistently, when mitochondrial ROS levels are low, they stabilize HIF1α, facilitating further up-regulation of glycolysis (Chandel et al., 1998). This ROS-hypoxia interaction has been also confirmed in various other systems, whereby inhibition of mitochondrial ROS impaired HIF1 activity under low oxygen conditions (Brunelle et al., 2005; Guzy et al., 2005; Mansfield et al., 2005).

Despite the low oxygen levels in the physiological niche of BM-MSCs, standard cell culture practice involves *in vitro* cell expansion under high oxygen conditions. Interestingly, many studies have assessed the role of hypoxia in the maintenance of

pluripotency, by transferring high-oxygen-cultured BM-MSCs to low oxygen conditions. However, some of the results are controversial, mostly due to differences in the duration of hypoxia and the concentration of oxygen to which the cells were exposed. A recent review on this topic divides the effects of oxygen on stem cell biology based on the duration of cell culture under hypoxic conditions (Buravkova et al., 2014); although both short-term (up to 72 hours) and permanent (1-3 weeks) exposure of BM-MSCs to low oxygen increases anaerobic glycolysis through HIF1 stabilization, the impact on proliferation and differentiation varies between the two categories. Acute, temporary exposure to hypoxia activates the NF-kB signaling cascade and induces ROS-mediated cell death. Under these conditions ROS levels increase due to reduced CAT expression (Peterson et al., 2011). Thus, short-term switch to hypoxia is a stress factor to BM-MSCs. By contrast, many reports have shown that constant propagation of BM-MSCs under hypoxic conditions has a beneficial effect both on stem cell viability and proliferation (Basciano et al., 2011; Fehrer et al., 2007; Santos et al., 2009). This positive impact on self-renewal is mediated at the transcriptional level, whereby permanent cell expansion in an oxygen-limited environment up-regulates the expression of stemness genes, such as *Oct-4*, *Sox2*, *Ssea-4*, *Stro-1* and *Nanog*. Importantly, beyond its role in establishing pluripotency, OCT-4 binds to promoters of glycolytic genes, further inducing their expression. Notably, BM-MSCs cultured under high oxygen conditions (commonly referred to as normoxia), and forced to utilize OXPHOS, are still able to proliferate and to form colonies. However, normoxia results in oxidative stress-induced senescence, whereas enhanced ROS levels activate stem cell differentiation (Pattappa et al., 2013). Therefore, glycolysis in BM-MSCs is not only a metabolic adaptation to the hypoxic bone marrow niche, but also an active mechanism to balance stem cell survival, proliferation and commitment.

Under normal conditions, the niche maintains BM-MSCs in a quiescent state and activation of self-renewal prevents depletion of their population. Activated BM-MSCs serve as a feeder layer for the bone marrow-residing HSCs and generate signals, such as cytokines, required for their proliferation and differentiation. (Majumdar et al., 2000). At this physiological state, adipogenesis and osteogenesis in the bone marrow are balanced, ensuring successful development of bone and adipose tissue and

hematopoiesis (Sugimura and Li, 2010). Importantly, the bone marrow niche displays a specific cellular organization that reflects the oxygen availability at each site and participates in the regulation of stem cell fate decisions (Miura, 2006). Undifferentiated progenitors reside deep in the bone marrow cavity, away from the blood vessels, in a low oxygen environment (Kubota et al., 2008; Lord et al., 1975). At this hypoxic position, BM-MSCs are fully committed to utilize glycolysis. In line with this, ECM deposition and cartilage development limits the oxygen availability, favoring glycolysis in chondrocytes. By contrast, lineage commitment to adipocytes and osteoblasts requires metabolic redirection from anaerobic glycolysis to mitochondrial respiration, as discussed above. Therefore, differentiating BM-MSCs migrate closer to the blood vessels, whereby there is sufficient oxygen concentration to support oxidative metabolism (Acar et al., 2015).

Beyond their critical role in energy production and anabolic generation of cellular macromolecules, metabolites impact stem cell identity via regulation of gene expression (Ito and Suda, 2014).

1.2.3 Metabolic input on the epigenetic regulation of differentiation

Chromatin describes the macromolecular complex of proteins and DNA that can be found in the nucleus of every eukaryotic cell. It provides the scaffold for packaging the entire genetic material, facilitating its compaction and protecting DNA. The core of chromatin consists of the nucleosome. Research during the last decades has revealed that post-translational modifications on histones, which are the protein components of nucleosomes, and on DNA itself regulate gene expression and allow time- and tissue-controlled read-out of the genetic information (Tessarz and Kouzarides, 2014; Greenberg and Bourc'his, 2019). These studies have highlighted the importance of chromatin architecture and dynamics during physiological development as well as upon tumorigenesis (Perino and Veenstra, 2016; Zhao and Shilatifard, 2019).

Given that stem cells share the same genetic information with somatic cells, their epigenome and the associated transcriptional signature distinguish them from their differentiated counterparts. Importantly, the characteristic epigenetic profile of stem

cells reflects their wide developmental potential. During the last years, the molecular mechanisms via which changes in the chromatin landscape control stem cell fate decisions have been the subject of intense scientific research, both in embryonic stem cells (ESCs) as well as in various adult stem cell populations. Among the various pathways which shape the epigenetic landscape and the chromatin architecture, metabolism is considered as a potent means to control the epigenome. More precisely, it is now well-accepted that metabolism and epigenetics are tightly connected and interact in a reciprocal manner (Dai et al., 2020; Etchegaray and Mostoslavsky, 2016; Kaelin and McKnight, 2013; Li et al., 2018; Lu and Thompson, 2012; Reid et al., 2017; Sutendra et al., 2014); on one hand, expression of several metabolic genes is subjected to epigenetic regulation. On the other hand, metabolism influences chromatin states via metabolites that act as substrates and/or co-factors for DNA- and histone-modifying enzymes. This metabolism-chromatin crosstalk is implicated in a variety of physiological contexts, including BM-MSC fate transitions. The most extensively studied examples of mito-nuclear communication both during organismal development as well as within the context of BM-MSC fate determination, focus on the impact of metabolism on the establishment of “canonical” epigenetic modifications, such as histone acetylation and DNA and histone methylation. By contrast, the role of metabolism on the dynamics of novel, emerging epigenetic marks, such as histone lactylation and histone succinylation, is currently under investigation (**Figure 1.4**).

Metabolism regulates histone acetylation

Histone acetylation refers to the deposition of acetyl-groups on histones by histone acetyltransferases (HATs). Histone acetylation is usually associated with active gene transcription since it weakens the contact between DNA and histones (Tessarz and Kouzarides, 2014). In mammals, mitochondria-produced acetyl-CoA is the major donor of the acetyl-group, needed for the acetylation of histones and non-histone proteins (Sivanand et al., 2018). Histone acetylation is a dynamic and reversible modification; removal of the acetylation marks from histones is mediated via histone deacetylase enzymes (HDAC).

BM-MSC stemness requires enhanced levels of global H3K9 acetylation and H3K14 acetylation that facilitate expression of core pluripotency genes, such as *Oct-4* and *Sox2* (Li et al., 2011). By contrast, during osteogenic differentiation changes in the histone H3 acetylation pattern lead to down-regulation of self-renewal genes and increased expression of the *Alp* and *Runx2* osteogenic regulators (Li et al., 2011). Interestingly, Tan and colleagues demonstrated that H3K9 acetylation, a mark associated with active gene transcription, is globally reduced during osteogenesis (Tan et al., 2009), whereas it is more abundant specifically on the promoters of the osteogenic genes *Osx* and *Oc*, favoring osteogenesis (Lee et al., 2006). Likewise, during chondrogenesis, H3K9 acetylation is increased on the promoters of the chondrogenesis-involved genes *Col2a1* and *Acan*, enabling efficient lineage commitment (Herlofsen et al., 2013). Interestingly, these changes in the histone acetylation pattern are in accordance with alterations of the cellular bioenergetic profile and reflect the fluctuations in the intracellular acetyl-CoA concentration.

Another connection between histone acetylation and metabolism is mediated through class III HDACs, commonly referred to as sirtuins, which require NAD^+ as an essential cofactor; thus, they couple their activity to the cellular energetic status (Cantó et al., 2015; Ryall, 2012). Given that cell fate commitment is accompanied by a metabolic transition from the NAD^+-consuming glycolysis to OXPHOS, the concomitant changes in the NAD^+/NADH ratio impact the transcriptional output and subsequently the stem cell identity.

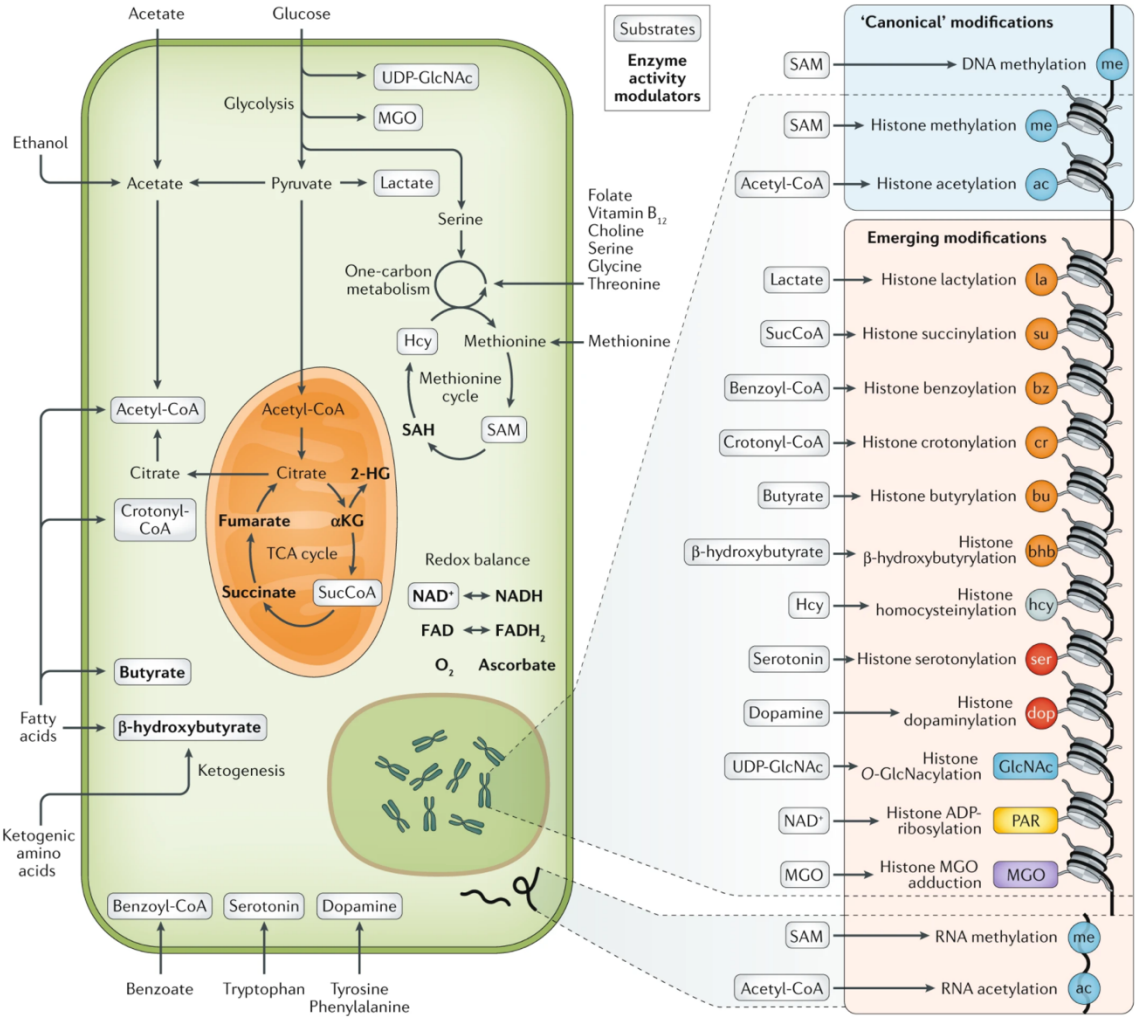

Figure 1.4. Metabolism-chromatin interplay. Metabolites serve as substrates and co-factors for epigenetic modifications, whereas metabolic enzymes regulate the activity of epigenetic writers and erasers. Figure obtained from Dai et al. (Dai et al., 2020)

For instance, up-regulation of SIRT1 facilitates osteoblast development, through silencing the *Sost* gene, an inhibitor of bone formation, and the adipogenic *Pparγ* and *Foxo1* genes (Cohen-Kfir et al., 2011; Tseng et al., 2011). Therefore, SIRT1 plays a fundamental role in maintaining a balance between adipogenic and osteogenic differentiation of BM-MSCs. Apart from regulating lineage specification, sirtuins are also involved in the oxidative stress response and redox homeostasis. In particular, it was shown that human BM-MSCs deficient for SIRT6, that plays a major role in redox homeostasis via activation of *Nrf2*, exhibit enhanced H3K56 acetylation. In the absence of SIRT6, RNAP II cannot bind to the promoters of NRF2-target genes to stimulate their expression, linking metabolism to oxidative stress induced-senescence (Pan et al., 2016). Hence, metabolic pathways that maintain an elevated NAD^+/NADH

ratio contribute to BM-MSC fate decisions by modulating the activity of epigenetic enzymes involved in the deposition and removal of acetylation marks from histones.

Metabolism regulates DNA and histone methylation

DNA methylation on gene promoters is associated with transcriptional repression and it takes place mostly at CpG islands in the mammalian genome. The effect of histone methylation on gene transcription depends on the methylated residue, the developmental stage and the cell type (Berger, 2007). S-adenosyl-methionine (SAM) functions as the donor of methyl groups for DNA and histone methylation reactions (Locasale, 2013). During the methionine cycle (MET cycle), homocysteine is used to generate methionine, which is the SAM precursor. Of note, the MET cycle is intimately linked to the one-carbon cycle and the folate cycle, connecting amino acid metabolism to chromatin states (Su et al., 2016). Histone methyltransferases (HMTs) and DNA methyltransferases (DNMTs) transfer methyl groups from SAM to histones and DNA, respectively, producing S-adenosyl-homocysteine (SAH) as a byproduct. Interestingly, SAH inhibits the activity of HMTs and DNMTs (Zee et al., 2010). Therefore, changes in metabolism that influence the SAM/SAH ratio can strongly impact the histone and DNA methylation status, and thus the transcriptional output and the stem cell identity.

In general, excessive DNA and histone methylation have been associated with stem cell differentiation but the decision between adipogenesis and osteogenesis depends on the gene at which the modification is enriched, the gene region that is modified and the exact site where the modification occurs. For instance, the histone methyltransferase EZH2 is a positive regulator of adipogenesis and a negative regulator of osteogenesis. Enforced EZH2 expression establishes the gene-silencing H3K27 trimethylation (H3K27me3) mark on the *Runx2* promoter, inhibiting osteogenesis and favoring adipogenesis (Hemming et al., 2014). Thus, EZH2 acts as an epigenetic switch regulating stem cell fate determination. Similarly, several studies have reported that reduced levels of the transcription-activating H3K4 trimethylation (H3K4me3) mark impair osteogenesis (Bustos et al., 2017; Hassan et al., 2007; Wang et al., 2016). Interestingly, H3K4me3 is also required for efficient adipogenesis and mice expressing inactive forms of the mixed lineage leukemias (MLLs) H3K4

methyltransferases display low fat accumulation and defective adipogenesis (Lee et al., 2008).

DNA and histone demethylation are also linked to cellular metabolism and regulate stem cell fate transitions. The activity of the LSD1 histone demethylase depends on FAD levels, whereas the TET and the JmjC family of DNA and histone demethylases couple their activity to alpha-ketoglutarate (α-KG) levels. α-KG is a TCA cycle metabolite whose concentration is under the orchestrated control of consuming and anaplerotic reactions. Highlighting the interaction between metabolism, histone methylation and stem cell fate decisions, recent work demonstrated that low α-KG levels lead to reduced deposition of the H3K9 trimethylation (H3K9me3) mark and impaired differentiation capacity of BM-MSC into osteoblasts (Morganti et al., 2020). In line with this, the activity of the TET and JmjC enzymes is also regulated by α-KG antagonists, most of which are metabolic intermediates. In particular, 2-hydroxyglutarate (2-HD), succinate and fumarate exhibit structural similarities to α-KG and they compete for the binding site on the TET and JmjC enzymes (Kaelin and McKnight, 2013; Xu et al., 2011b). Therefore, the metabolic pathways that generate or consume these metabolites might alter the DNA and histone methylation profiles and influence stem cell potency. Interestingly, recent work from Lee and colleagues highlighted the importance of malate/ aspartate shuttle in the maintenance of glycolysis and the efficient osteoblast differentiation in calvarial stem cells (Lee et al., 2020).

These are just few examples that illustrate the tight connection between the cellular metabolic states and the epigenetic profile in the regulation of BM-MSC fate decisions. Importantly, findings from epigenetic studies in adult stem cell populations have also led to the discovery of drugs, usually small molecules and metabolites, which can redirect - and even reprogram - stem cells towards specific lineages. For instance, Kohyama *et al*. (Kohyama et al., 2001) showed that treatment of mature osteoblasts with 5-azacytidine (5-AzaC), a DNA methylation inhibitor, converts them to neural stem cells (NSCs), via alterations on their epigenome and their gene expression profile. Similarly, osteocytes treated with valproic acid, a histone deacetylase inhibitor, are able to re-differentiate to functional NSCs (Woodbury et al., 2002).

1.3 Mitochondrial-derived vesicles (MDVs) contribute to mitochondrial proteostasis

Mitochondria are complex, double membrane-bounded organelles, which function primarily as the “cellular powerhouse”, as discussed above (Roger et al., 2017; Zimorski et al., 2014). The outer mitochondrial membrane (OMM) surrounds the intermembrane space (IMS), whereas the inner mitochondrial membrane (IMM) encloses the mitochondrial matrix and forms invaginations, called cristae, where protein complexes of the respiratory chain are localized. Beyond their critical role in oxidative respiration and ATP production, mitochondria are involved in numerous cellular processes that are essential for cell viability, including the biosynthesis of lipids and amino acids, the enzymatic catalysis of central reactions in the urea cycle and the formation of heme and iron-sulfur clusters, while they also serve as signaling platforms to regulate apoptosis and inter-organelle communication (Giacomello et al., 2020; Pfanner et al., 2019; Prinz et al., 2020). To fulfill such a multifaceted role, mitochondria contain about 1,000 proteins in mice (Zhang et al., 2008) and approximately 1,500 proteins in humans (Morgenstern et al., 2017), whose synthesis, degradation and activity are strictly controlled.

Although mitochondria contain their own DNA (mtDNA), this encodes only a small fraction of the total mitochondrial proteome. In fact, ~99% of the mitochondrial proteins are encoded by the nuclear genome, are synthesized on cytosolic ribosomes as precursors, enter into mitochondria for further processing and translocalize to the destined mitochondrial compartment (Endo et al., 2011; Pfanner et al., 2019). Therefore, a sophisticated network of mechanisms is necessary to coordinate the expression of both genomes in order to avoid excessive amounts of unprocessed proteins, and to rapidly remodel mitochondria in response to the cellular energetic demands (Couvillion et al., 2016; Ott et al., 2016; Priesnitz and Becker, 2018; Suhm et al., 2018). Failure of these mechanisms might result in: (i) accumulation of damaged or misfolded proteins, stimulating ROS production (Song et al., 2014), (ii) impaired ATP production (Kim et al., 2013), (iii) release of cytochrome c and subsequent activation of apoptosis (Winklhofer, 2014), (iv) opening of the mitochondrial permeability transition pore (mPTP) leading to necrosis (Kim et al., 2007), and (v)

release of oxidized mitochondrial proteins and DNA to the cytosol, activating inflammation (Krysko et al., 2011).

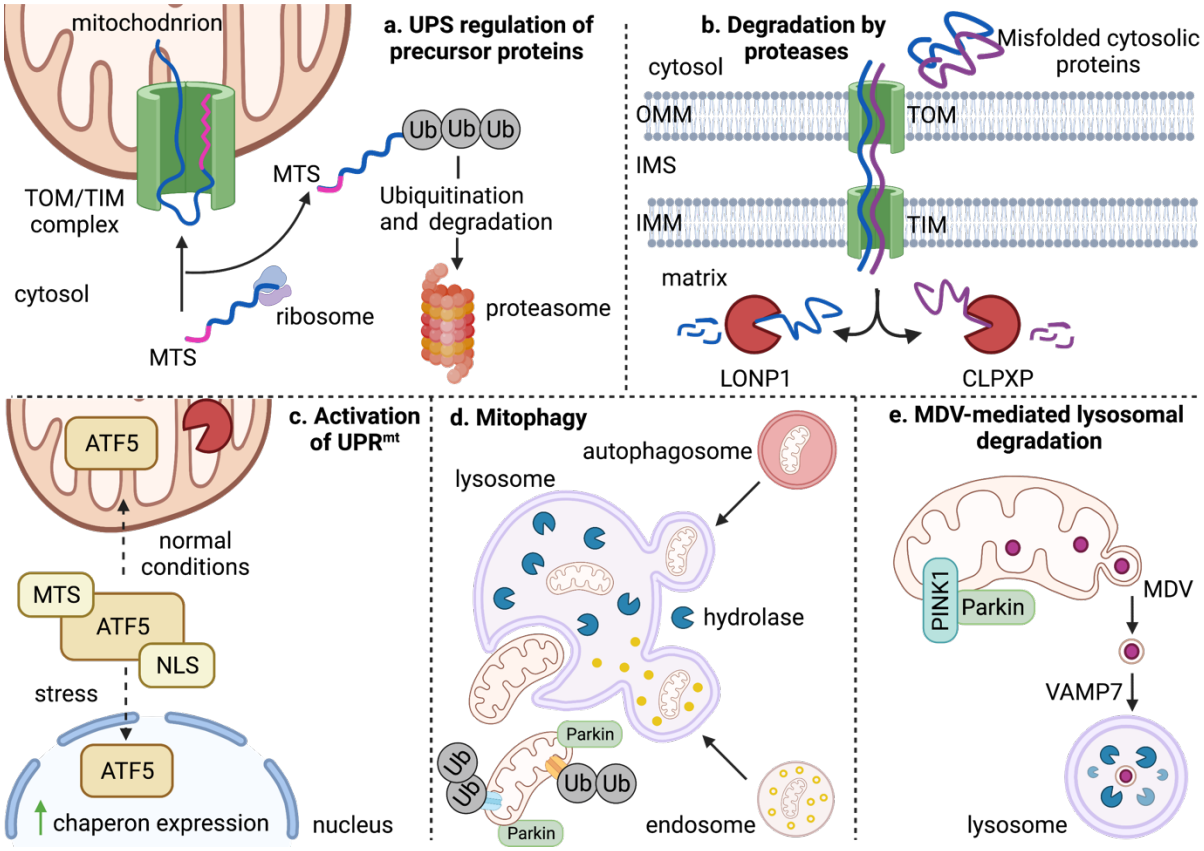

Figure 1.5. Mitochondrial quality control mechanisms. (**a**) Unfolded or damaged peptides targeted to mitochondria get degraded in the cytosol via the UPS pathway. (**b**) Mitochondrial proteases are responsible for the degradation of unfolded or oxidized proteins. (**c**) A retrograde signaling cascade between mitochondria and nucleus is activated during the UPR^{mt}, further promoting mitochondrial homeostasis. (**d**) Mitophagy is activated upon severe mitochondrial damage and removes the entire organelle. (**e**) Oxidized proteins can be removed from the mitochondria via mitochondrial-derived vesicles, which deliver them to lysosomes for degradation. MTS: mitochondrial targeting signal; NLS: nuclear localization signal. Figure modified from Quiles and Gustafasson (Quiles and Gustafsson, 2020).

Due to the broad consequences of mitochondrial dysfunction, the existence and proper activity of quality control mechanisms are vital to maintain both mitochondrial and organismal homeostasis. To minimize accumulation of unprocessed proteins and to prevent import of misfolded or damaged polypeptides, mitochondria rely on several

quality control mechanisms, which function in an orchestrated and tightly regulated manner (Quiles and Gustafsson, 2020; Sugiura et al., 2014) (**Figure 1.5**).

Nuclear DNA-encoded mitochondrial peptides are subjected to a constant turnover via the ubiquitin-proteasome system (UPS), which fine-tunes the amount of nuclear DNA- and mtDNA-encoded proteins within the mitochondria and ensures that only properly folded peptides get imported inside the organelles (**Figure 1.5a**). In the event of mito-nuclear protein imbalance or damage of mitochondrial peptides, a newly identified protein family, called Ubiquilins, stimulates the recruitment of an E3 ubiquitin ligase and their polyubiquitination (Itakura et al., 2016). The ubiquitinated peptides are then delivered to proteasome for degradation. Of note, several unfolded and oxidized OMM proteins are degraded via the same pathway. In this case, misfolded OMM proteins are extracted from the membrane, get ubiquitinated and transferred to the proteasome for degradation, via the cytosolic AAA-ATPase p97 (Fang et al., 2015; Hemion et al., 2014; Xu et al., 2011a). Therefore, the UPS comprises the first line of mitochondrial quality control.

Further surveillance of the mitochondrial proteome is achieved via the activity of mitochondrial proteases, which are also engaged in the mitochondrial quality control (**Figure 1.5b**). Proteins targeted to inner mitochondrial compartments are cleaved and processed by mitochondrial peptidases and chaperones, such as the MPP and mtHSP70 respectively, which allow them to fold correctly and acquire a proper conformation (Bender et al., 2011; Leonhard et al., 2000). Impaired activity of these enzymes activates the AAA proteases of the mitochondrial matrix, such as the CLPXP and LON proteins, as well as the i-AAA and m-AAA proteases that are responsible for the degradation of damaged proteins residing at the IMM, the IMS and the OMM.

When the levels of misfolded proteins outweigh the degradation capacity of the mitochondrial proteases, the mitochondrial unfolded protein response (UPR^{mt}) is activated (**Figure 1.5c**). The major regulator of the UPR^{mt} is ATF5, which contains both a mitochondrial target sequence and a nuclear localization signal. Thus, ATF5 translocates between these two organelles, in accordance to the cellular needs (Fiorese et al., 2016). Under normal conditions, ATF5 localizes to mitochondria, where

it is degraded by mitochondrial proteases. By contrast, under mitochondrial stress, ATF5 import into mitochondria is inhibited; thus, ATF5 translocates to the nucleus. There, it promotes the expression of mitochondrial chaperons and genes responsible for ROS detoxification, to promote mitochondrial health (Nargund et al., 2015).

The above-described mechanisms ensure that mitochondria reshape their proteome in response to stress and allow the cellular repair systems to become fully engaged in order to maintain mitochondrial proteostasis. However, in cases of more pronounced mitochondrial dysfunction, elimination of the entire organelle is required and selective mitochondrial degradation, called mitophagy, is activated by a mechanism involving the PINK1/PARKIN proteins (**Figure 1.5d**). In healthy mitochondria, PINK1 is imported into mitochondria, is cleaved by the PARL protease and is exported to the cytosol for proteasomal degradation (Jin et al., 2010; Yamano and Youle, 2013). However, mitochondrial defects leading to loss of membrane potential deactivate PARL. Therefore, PINK1 is either trapped in the import channel or it accumulates on the OMM, where it stimulates recruitment of the E3 ubiquitin ligase, PARKIN. Parkin ubiquitinates OMM proteins, marking the entire mitochondrion for degradation (Pickles et al., 2018).

A relatively novel mechanism which contributes to the mitochondrial quality control involves mitochondrial-derived vesicles (MDVs) (**Figure 1.5e**). MDVs bud off mitochondria, engulf oxidized proteins and lipids and transfer the damaged cargo to lysosomes for degradation, in a PINK1/Parkin-dependent manner (Soubannier et al., 2012a, 2012b). This pathway operates prior to activation of mitophagy, to prevent total mitochondrial degradation. Interestingly, beyond their role in mitochondrial proteostasis, Matheoud and colleagues showed that a subset of MDVs functions in mitochondrial antigen presentation following heat stress or exposure to lipopolysaccharides (LPS) (Matheoud et al., 2016), whereas Neuspiel and colleagues showed that MAPL-containing MDVs deliver their cargo to peroxisomes, most likely to participate in peroxisome biogenesis and division (Braschi et al., 2010; Neuspiel et al., 2008).

1.3.1 Morphological and functional properties of MDVs

MDVs are small, punctate, single- or double-membrane structures which bud off mitochondria and transfer aberrant proteins and lipids to the late endosome/lysosome compartment for degradation. Single membrane vesicles contain OMM proteins, whereas the double-membraned organelles incorporate also matrix and IMS components. While a comprehensive understanding of the mechanisms governing MDV formation and trafficking is still lacking, it is known that MDVs have a defined size of 60-150 nm and exhibit high cargo specificity (Sugiura et al., 2014). One of the best-described stimuli for MDV formation is mitochondrial oxidative stress. However, the nature of the stress impacts the identity of incorporated cargo. For example, Soubanier and colleagues showed that upon xanthine oxidase/xanthine treatment, which is an exogenous ROS source, MDVs contained the OMM pore protein VDAC, which was absent from the MDVs that were formed upon induction of mitochondrial stress by the complex III inhibitor Antimycin A (Soubannier et al., 2012b). Of note, these MDVs carried the complex III subunit core2 and findings of this study led to two major conclusions regarding the functional properties of MDVs:

i) MDVs exhibit high cargo selectivity carrying distinct classes of oxidized proteins and lipids, based on the trigger of the mitochondrial stress.

ii) MDVs generated upon mild mitochondrial stress are highly enriched in oxidized proteins and lipids, suggesting that they serve as an alternative mechanism to selectively extract oxidized components, preceding activation of mitophagy.

These data propose that potentially all mitochondrial proteins could be incorporated into MDVs, when oxidized. Furthermore, supporting their role in the maintenance of mitochondrial integrity prior to mitophagy, it was shown that MDV generation occurs within few hours after induction of mitochondrial stress, in contrast to activation of mitophagy which requires longer periods of time (McLelland et al., 2014). Thus, MDVs function as another mitochondrial quality control mechanism, which is kinetically faster than mitophagy.

1.3.2 Mechanisms of MDVs formation and trafficking

Although our knowledge on the exact mechanisms that facilitate membrane curvature, incorporation of the oxidized cargo and budding off mitochondria is currently limited, it has been shown that MDV formation is independent of the mitochondrial fission machinery. Indeed, loss of mitochondrial membrane potential triggers MDV formation even upon silencing the DRP1 fission protein (McLelland et al., 2014; Neuspiel et al., 2008; Soubannier et al., 2012a). By contrast, it has been demonstrated in several studies that generation of MDVs requires PINK1 and PARKIN, which are also involved in mitophagy, as discussed above. According to the recently proposed model for MDV formation (Sugiura et al., 2014) (**Figure 1.6**), mild mitochondrial stress leads to accumulation of oxidized proteins at a single import channel, which impairs proper entrance and folding of various proteins, such as PINK1. PARKIN recruitment and ubiquitination activity in response to PINK1 misfolding is crucial for the generation of MDVs (McLelland et al., 2014). Following PARKIN-mediated ubiquitination, unidentified factors facilitate initial bending of the membrane and scission of the MDVs. However, upon profound mitochondrial damage, where several mitochondrial import channels are blocked by protein aggregates, the mechanism might switch from local removal of a certain “patch” to a general elimination of the entire organelle via mitophagy, explaining the central role of PINK1 in both processes. This model suggests that the dysfunction of a single import channel serves as the important local trigger for the initiation of the MDV formation. In line with this, mitochondrial import channels are located at specific sites, where the inner and the outer mitochondrial membranes are in close proximity, explaining why some MDVs are double-membraned, containing both OMM and IMM proteins (Sugiura et al., 2014). Single membrane MDVs contain exclusively OMM components, most commonly the TOMM20 protein, and are depleted of the matrix PDH protein. These MDVs do not require the PINK1/PARKIN machinery for their formation, further confirming that defects in the import channel act as the first stimulus for the generation of a specific subpopulation of MDVs and that distinct mechanisms might be involved in the generation of each MDV subset.

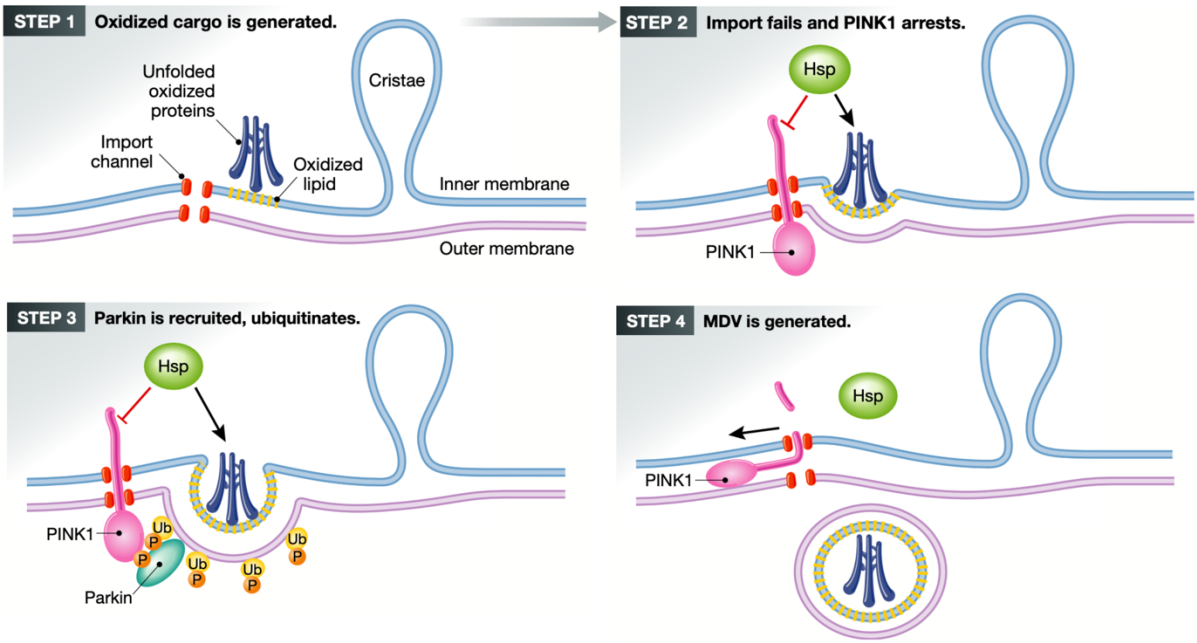

Figure 1.6. Current model for MDV formation. Dysfunction of the import channel due to aggregation of oxidized proteins and lipids, leads to PINK1 accumulation and recruitment of PARKIN at the OMM. PARKIN ubiquitinates OMM proteins and unknown factors are involved in membrane bending, cargo incorporation and scission of the MDV. Figure obtained from Sugiura et al. (Sugiura et al., 2014)

The precise mechanisms of MDV trafficking remain largely unknown but it is highly likely that components of the endocytic pathway are required for MDV delivery to their target organelles. For example, recent studies showed that the retromer complex is implicated not only in the formation and fission of MDVs, but also in the delivery of peroxisome-destined vesicles to their subcellular destination (Braschi et al., 2010; Cullen and Korswagen, 2012; Seaman, 2012). Furthermore, it has been shown that PARKIN is also involved in MDV transport, which is in line with its previously described role in various vesicular trafficking pathways (Fallon et al., 2006; Yamano et al., 2018). For instance, a recent study demonstrated that PARKIN interacts with TOLLIP, which is a major coordinator of the endosomal compartment, facilitating MDV-lysosomal docking (Ryan et al., 2020). Interestingly, a subset of PINK1/PARKIN-dependent MDVs require the formation of a complex between the STX17 and the VAMP7 proteins, which mediates their delivery and fusion with the lysosomes (McLelland et al., 2016). Thus, it is clear that distinct MDV classes utilize different trafficking routes and fusion machineries to reach their destined organelles and to release their cargo. Further research will shed more light on the mechanisms governing MDV biogenesis, cargo selection, vesicular transport and inter-organelle fusion.

1.4 The BM-MSC differentiation balance in ageing and age associated bone-diseases

Ageing is accompanied by a general decline in the organismal function and several mechanisms are known to contribute to the progression of ageing, including changes in the cellular energetic profile, epigenetic modifications and loss of proteostasis (López-Otín et al., 2013). For instance, mitochondrial dysfunction has been identified as one hallmark of organismal ageing that is also involved in stem cell ageing (López-Otín et al., 2013); indeed, upon ageing the mutation load of mtDNA increases, due to higher ROS levels and impaired function of the DNA damage repair mechanisms and the UPR^{mt} (Jesus et al., 2013; Merkwirth et al., 2016; Moskalev et al., 2013). This enhances further ROS production, which triggers stem cell commitment and oxidative stress-induced apoptosis, as discussed above. Furthermore, it has been reported that ageing reduces the NAD^+/NADH ratio (Gomes et al., 2013; Yoshino et al., 2011; Zhang et al., 2016), which is required to sustain the glycolytic flux in uncommitted stem cells. Given the importance of glycolysis in providing quiescent and proliferating BM-MSCs with ATP and macromolecules, maintenance of the BM-MSC pool could be heavily affected by age-induced fluctuations in NAD^+ levels. In this regard, nutrient sensing and the downstream signaling cascade, which encompasses the mTOR, AMPK and sirtuins, are also deregulated upon ageing and impact the stem cell function (Houtkooper et al., 2010).

Similar to metabolism, epigenetic regulation of gene expression is altered upon ageing, affecting BM-MSC fate decisions. For instance, it has been shown that aged BM-MSCs display lower expression of HDACs and polycomb-group proteins in comparison to their younger counterparts. This promotes loss of the H3K9me3 mark, which is associated with heterochromatin organization, and eventually leads to stem cell senescence (Jung et al., 2010). Moreover, the osteogenic regulators RUNX2 and homeobox A (HOXA) were found to be hypermethylated in human BM-MSCs isolated from old donors, in comparison to those from young donors. This leads to decreased gene expression and impaired osteogenesis, which is rescued after treatment with the DNMT1 inhibitor 5-AzaC (Bork et al., 2010; Wang et al., 2020a). Furthermore, age-dependent changes in the mitochondrial function and metabolism, as those described

above, impact deposition and removal of specific DNA and histone modifications, via alterations in the levels of the involved metabolites.

Skewed adipogenic differentiation at the expense of osteogenesis together with reduced responsiveness to tissue injury and dysregulated proliferation are commonly observed in BM-MSCs upon ageing (**Figure 1.7**). Such perturbations in the stem cell function result in accumulation of fat, loss of the bone mineral density and reduction of the bone mass. This phenotype has been associated with higher risk of osteoporosis and osteoarthritis and increased likelihood for bone fractures in the elderly (Kim et al., 2012; Zhou et al., 2008). Today, the so-called “fat theory of osteoporosis” is supported both by results from cell-based models as well as from *in vivo* studies.

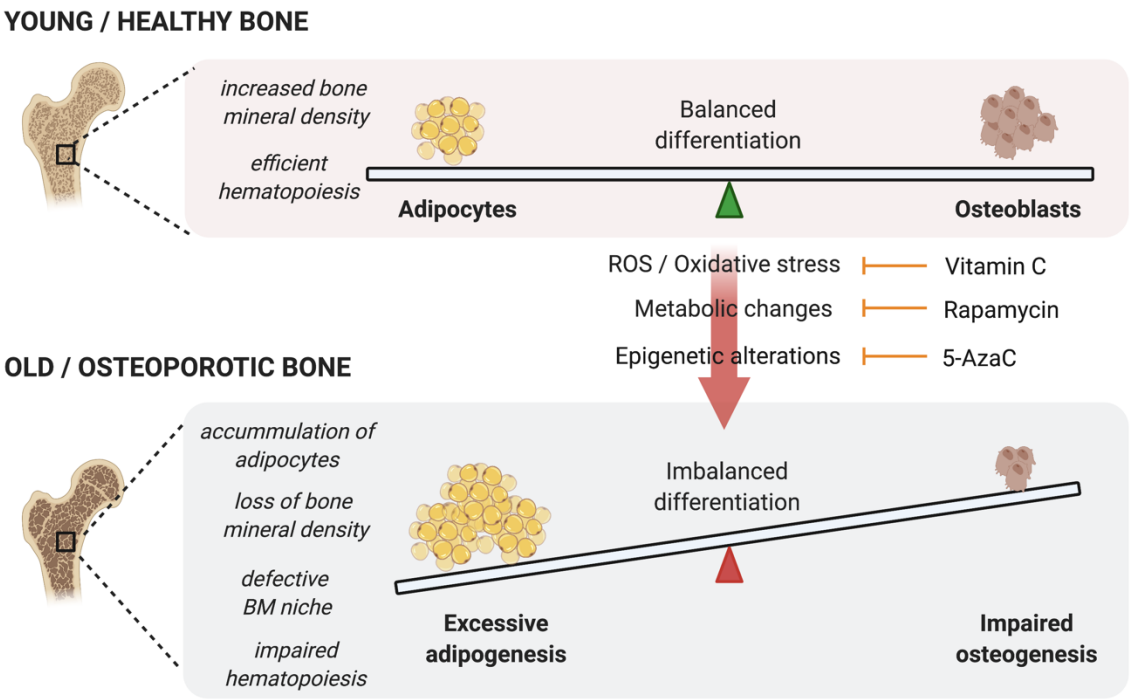

Figure 1.7. Changes in the adipogenesis-osteogenesis differentiation balance upon ageing and osteoporosis. Age-associated changes in metabolism, chromatin and ROS levels lead to imbalanced differentiation of BM-MSCs to adipocytes at the expense of osteoblasts. This causes loss of bone mineral density and marrow adiposity, which impairs bone development and hematopoiesis. Treatment with rapamycin, 5-AzaC and vitamin C rescues some of the ageing-induced changes in metabolism, histone modifications and ROS levels, respectively, re-establishing a balanced adipogenesis and osteogenesis. Figure obtained from Pouikli and Tessarz (Pouikli and Tessarz, 2021).

Indeed, studies comparing the differentiation capacity of BM-MSCs derived from healthy donors and osteoporotic patients revealed that osteoporotic cells exhibited higher lineage commitment into adipocytes, which was accompanied by reduced osteogenesis. In line with this, mice deficient for the PPARγ adipogenic regulator displayed increased bone mass and enhanced osteogenesis, whereas deletion of the osteogenic regulator RUNX2 induced spontaneous differentiation of stem cells to adipocytes. In agreement to these findings, *in vivo* studies using proton magnetic resonance (^{1}H-MRS) showed that in the osteoporotic bone marrow there is significant accumulation of adipocytes, which is associated with decreased bone mineral density. Of note, similar changes in the balance between adipogenic and osteogenic commitment of BM-MSCs have been linked not only to bone metabolic diseases but also to other pathological conditions such as diabetes, cancer and various syndromes characterized by impaired hematopoiesis (Ambrosi et al., 2017; Man and Man; Moerman et al., 2004). The precisely defined structure of the bone-marrow microenvironment together with the release of soluble factors from the residing cells play a fundamental role in HSC homing and hematopoiesis, as discussed above; hence, the age-associated excessive adipogenesis that leads to occupancy of the bone-marrow niche by adipocytes, disrupts the niche organization, alters the secretory profile of the bone-marrow cells and impairs hematopoiesis (Ambrosi et al., 2017; Naveiras et al., 2009).

BM-MSCs have recently emerged as attractive candidates for various therapeutic applications due to their unique immunomodulatory properties, which allow them to escape recognition from the immune system and to modulate the activity of immune cells (reviewed in (Weiss and Dahlke, 2019)). In addition to their immunosuppressive function, BM-MSCs promote hematopoiesis, since they have been shown to support hematopoietic stem cell engraftment in co-transplantation experiments (Derakhshani et al., 2019; Masuda et al., 2009; Noort et al., 2002). Lastly, due to their enhanced self-renewal and multi-lineage differentiation capacities (Seita and Weissman, 2010; Weissman et al., 2001), BM-MSCs have been used successfully in the regeneration of various tissues and organs, including the bone, cartilage, muscle, skin, heart, liver, cornea and trachea. There are now ~800 complete or ongoing BM-MSC-based clinical studies, further evaluating their therapeutic potential (Ayala-Cuellar et al., 2019).

Focusing on the use of BM-MSCs in the treatment of bone diseases, such as osteoarthritis, osteoporosis, and osteogenesis imperfecta disorders, it is known that these diseases are all characterized by decreased bone mineral density, mostly due to impaired BM-MSC osteogenesis. Mechanistically, it was demonstrated that this occurs partly due to imbalanced occupancy of histone marks on osteogenic and adipogenic genes. For instance, Jing and colleagues found that EZH2 occupancy and thus H3K27me3 abundance is higher on the *Wnt* promoters of osteoporotic mice, inhibiting osteogenesis (Jing et al., 2016). Likewise, low TET1 and TET2 levels increase DNA methylation on promoters of osteogenic genes and inhibit their expression, leading to the development of an osteopenic phenotype (Yang et al., 2018a).

Therefore, it is evident that careful interventions in the metabolism-chromatin axis might represent a potential target to alter stem cell fate decisions, rejuvenate aged BM-MSCs *in vitro* and maintain the balance between stem cell proliferation and differentiation. Given the role of stem cells in tissue homeostasis and regenerative medicine, such approaches will considerably improve the efficiency of stem cell-based therapies and ameliorate the adverse phenotypes of ageing and ageing-associated bone diseases.

1.5 The mitochondrial citrate carrier in physiology and disease

Mitochondrial carriers, encoded by members of the *Slc25* gene family, are membrane-embedded proteins catalyzing the transport of solutes across the mitochondrial membrane compartments. Although the OMM is highly permeable to small molecules and metabolites, allowing their translocation via its pores, the IMM represents a physiological barrier in the free diffusion of solutes. Therefore, mitochondrial carriers facilitate the intracellular flux of metabolites, providing a link between mitochondria and the cytosol (Palmieri, 2013). As such, their activity in the regulation of energy metabolism is of paramount importance.

The mitochondrial citrate carrier (CiC), also known as citrate transporter protein (CTP), is an inner mitochondrial membrane protein, encoded in the nucleus by the *Slc25a1* gene. This gene is located on chromosome 22q11.2, spreads over 2.8 kbp and consists of eight exons and seven introns (Iacobazzi et al., 1997). *Slc25a1* encodes a protein of 298 amino acids, which contains six transmembrane helices. The mature protein contains several internal targeting sequences and is preceded by a positively charged pre-sequence, of 13 amino acids. Despite the similarities of the pre-sequence with the mitochondrial target signals of known mitochondrial proteins (*i.e.*, positive charge, amphipathy, α-helix structure etc.) (Roise and Schatz, 1988), it was shown that the pre-sequence is not required for the proper mitochondrial localization of CiC. Instead, it serves as a chaperone, increasing CiC solubility and improving mitochondrial import competence (Zara et al., 2003, 2005).

Historically, CiC was firstly discovered in the liver by Palmieri and colleaugues and since then several researchers have purified and reconstituted CiC from hepatic mitochondria of various organisms (Bisaccia et al., 1989; Claeys and Azzi, 1989; Genchi et al., 1999; Kaplan et al., 1995; Zara et al., 1996). Expression of *Slc25a1* is high in metabolically active organs such as the liver, kidney and pancreas, in accordance with its well-described role in the regulation of cell metabolism (Huizing et al., 1998). Functionally, CiC mediates export of mitochondrial citrate or isocitrate to the cytosol, in exchange for malate (**Figure 1.8**). Cytosolic citrate is involved in several

cellular processes, including: (i) allosteric regulation of metabolic enzymes, (ii) fatty acid and sterol biosynthesis, after cleavage to acetyl-CoA, and (iii) epigenetic regulation of gene transcription. Notably, CiC is the only known mitochondrial transporter for citrate, highlighting the critical role of its activity in cellular physiology.

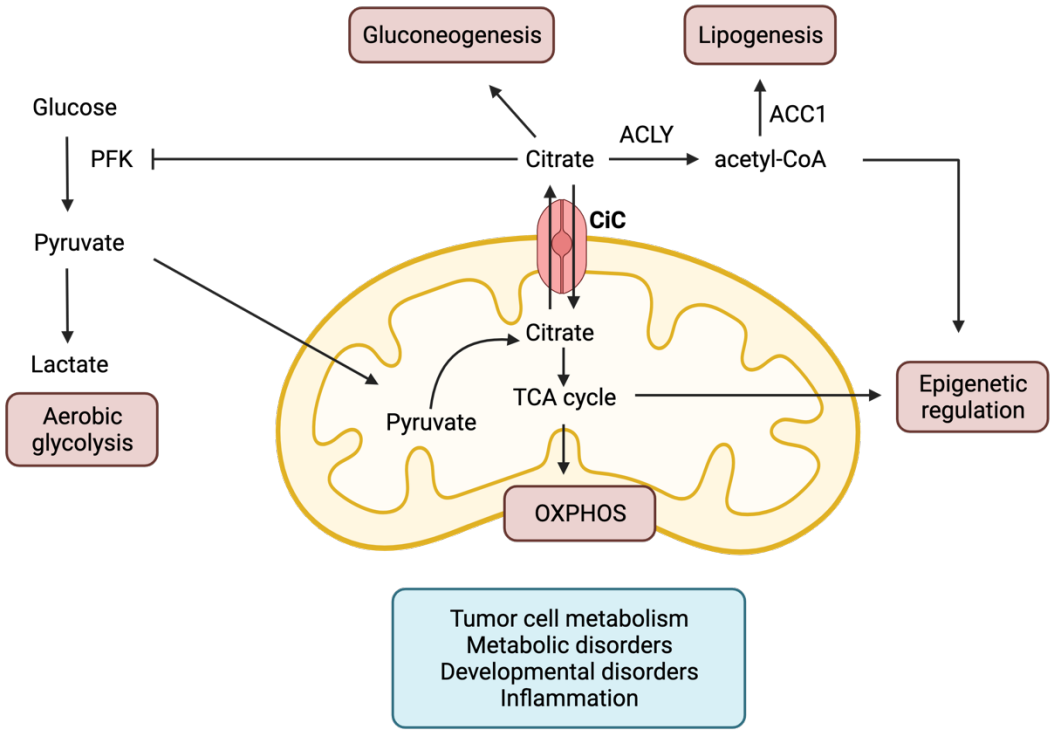

Figure 1.8. Summary of the CiC activities. CiC regulates several metabolic pathways, including glycolysis, OXPHOS, lipogenesis and gluconeogenesis. Moreover, it controls the levels of epigenetic-related metabolites, influencing the epigenetic landscape. Through these functions it participates in various physiological and pathological processes, such as tumor metabolism, developmental disorders and inflammation. Figure modified from Mosaoa et al. (Mosaoa et al., 2021).

1.5.1 Role of CiC in cell physiology

The best-described function of CiC is the regulation of the cytosolic and mitochondrial pools of citrate. As discussed above, CiC functions as an antiporter, exporting mitochondrial citrate and importing cytosolic malate. In the cytosol, citrate regulates the activity of several metabolic enzymes involved in glycolysis, lipogenesis and gluconeogenesis, including the rate-limiting glycolytic enzyme PFK1, which is inhibited by citrate binding, and the ACC1 which is activated upon citrate binding (Chesney,

2006). The allosteric inhibition of PFK1 and glycolysis by citrate, is of particular importance in the context of tumors, where it slows down aberrant proliferation of cancer cells (Yalcin et al., 2009). In addition to its allosteric regulatory role, cytosolic citrate serves as a precursor for lipogenesis. Indeed, cytosolic citrate is cleaved to acetyl-CoA, which is directly used to fuel lipid biogenesis. Additionally, acetyl-CoA is the only known donor of the acetyl-group for acetylation of cytosolic and nuclear proteins.

Currently, there is mounting evidence suggesting that CiC induces a proinflammatory program in macrophages. During inflammation, cells undergo a rapid metabolic rewiring, consisting mainly of a downregulation of OXPHOS and upregulation of glycolysis that stimulates the production of inflammatory mediators. The transcription rate of *Slc25a1* is induced in monocytes in response to inflammation (Infantino et al., 2011, 2014). CiC induction under these conditions leads to increased synthesis of prostaglandin E2 (PGE2), inducible nitric oxide synthase (iNOS) and ROS, which enhance the cellular inflammatory response. Importantly, their levels are decreased upon inhibition of CiC activity (Infantino et al., 2014).

Moreover, CiC is reported to regulate insulin secretion. Indeed, a regulatory role of CiC in human-ejaculated spermatozoa has been demonstrated by Cappello and colleagues, who showed that incubation of spermatic cells with the CiC inhibitor BTA significantly inhibits glucose-stimulated insulin secretion and impacts sperm motility (Cappello et al., 2012). This role of CiC has been also confirmed in pancreatic β cells (Joseph et al., 2006).

An understudied role of CiC involves its function in the chromatin regulation. Mutations in *Slc25a1* lead to DNA instability that, in turn, induces chromosome breaks (Morciano et al., 2009). More specifically, mutations in *Sea*, the *fly* ortholog of the human *Slc25a1*, impair citrate transport from mitochondria to the cytosol. Interestingly, inhibition of *Sea* expression results in extensive chromosome breakage in mitotic cells and induces an ATR-dependent cell cycle arrest, associated with a dramatic reduction in global histone acetylation levels. Notably, this effect is conserved in humans, whereby loss of *Slc25a1* in primary fibroblasts results in chromosome breaks and

histone acetylation defects, suggesting an evolutionary conserved role for Sea/CiC in the regulation of chromosome integrity (Morciano et al., 2009). Moreover, CiC can indirectly impact the epigenetic profile and the chromatin landscape, via alterations in the abundance of epigenetic-related metabolites, such as α-KG, succinate and 2-hydroxyglutarate (2-HG; Palmieri et al., 2020). Therefore, CiC provides an intriguing and unexpected link between intermediary metabolism and epigenetic control of the genome stability and the chromatin landscape.

1.5.2 Regulation of *Slc25a1* expression and CiC activity

Given the multifaceted role of CiC and the different biological processes in which citrate is involved, it is not surprising that a complex regulatory network controls *Slc25a1* expression levels and CiC activity.

Several mechanisms through which CiC activity is engaged in cells under physiological and pathological conditions act at the transcriptomic level. Structural and functional analysis of the human *Slc25a1* promoter region revealed the various regulatory factors which control *Slc25a1* expression. More precisely, it was shown that insulin upregulates and fatty acids suppress *Slc25a1* transcription, through SREBP1 (Infantino et al., 2007). Consistently, expression levels of CiC are regulated systemically by the levels of circulating glucose, being repressed by a low-glucose diet and strongly induced by high-glucose diet (Mosaoa et al., 2021). Among the transcription factors which were found to regulate *Slc25a1* transcription, FOXA1 acts as a strong gene activator in liver and pancreatic cells, binding to FOXA sites on CiC regulatory regions (Iacobazzi et al., 2009a). In addition, demethylation of the proximal promoter and establishment of histone H3 acetylation mark enhance binding of the stimulatory protein SP1 on *Slc25a1* promoter and favor gene transcription (Iacobazzi et al., 2008). By contrast, *Slc25a1* promoter contains a silencer region where ZNF224 binds, inhibiting CiC expression (Iacobazzi et al., 2009b). Reflecting the central role of CiC in inflammation, NF-κB and STAT1 stimulate *Slc25a1* expression, in response to tumor necrosis factor α (TNF-α) and interferon γ (IFN-γ) (Infantino et al., 2014).

Regarding the post-transcriptional regulation of CiC activity, Kaplan and colleagues showed first that the cellular nutritional and hormonal status impact CiC activity. Indeed, they observed that CiC isolated from diabetic-type 1 rats displayed lower activity in comparison to that of healthy controls and treatment of diabetic rats with insulin reverted the impaired CiC function (Kaplan et al., 1991a, 1991b). Apart from insulin, the thyroid hormone triiodothyronine (T3) controls CiC activity, as revealed by experiments with hepatic mitochondria from hyperthyroid rats (Paradies and Ruggiero, 1990). Furthermore, research studies uncovered that starvation not only reduces *Slc25a1* expression, as discussed above, but also inhibits CiC activity, post-transcriptionally. In fact, it is speculated that starvation enhances CiC degradation, through a not-yet identified mechanism (Siculella et al., 2002).

Despite the considerable progress in the understanding of mechanisms regulating CiC function, further research will shed light on the exact molecular pathways via which CiC activity and expression differs among species, tissues, and metabolic states.

1.5.3 Implication of CiC in disease and cancer

CiC is found at the center of the cellular metabolic crossroads. Therefore, it is not surprising that loss of CiC function is pathogenic, with mutations or mono-allelic deletions of the *Slc25a1* gene linked to a wide and heterogeneous spectrum of developmental disorders, cancer and ageing (Palmieri and Monné, 2016) (**Figure 1.8**).

Various *Slc25a1* missense or truncating mutations, spanning throughout the gene coding region, have been implicated in the development of neuromuscular and neurometabolic diseases, such as the D-2- and L-2-hydroxyglutaric aciduria (D-2-HGA), which shows autosomal recessive inheritance and causes developmental delays, hypotonia and seizures (Eguchi et al., 2018; Nota et al., 2013; Prasun et al., 2014). Mechanistically, loss of CiC activity results in accumulation of the D-2-hydroxyglutarate (D-2-HG) and the L-2-hydroxyglutarate (L-2-HG) metabolites. The current model of the disease proposes that, following disruption of CiC-mediated citrate export, cytosolic citrate levels are significantly reduced. This leads to loss of the inhibitory feedback loop on PFK1 and further upregulation of glycolysis (Chesney,

2006). On one hand, glycolysis-produced pyruvate is converted to lactate, resulting in lactic acidosis. On the other hand, pyruvate enters mitochondria, where it is converted to citrate/isocitrate. Due to lack of the CiC export activity, mitochondrial citrate is converted to downstream TCA cycle intermediates, including α-KG, succinate, fumarate and malate, which accumulate and get secreted in urine (Nota et al., 2013).

Furthermore, CiC activity has been studied by several groups in various cancer types. In breast cancer, *Slc25a1* mRNA levels are increased and inhibition of CiC function reduces the tumor size *in vivo* and the proliferation *in vitro*, most likely through changes in histone acetylation, mitochondrial function and ROS production (Catalina-Rodriguez et al., 2012). Consistently, in colorectal cancer, the expression levels of CiC are upregulated by PGC-1α and correlate with enhanced OXPHOS, TCA cycle flux and *de novo* lipogenesis (Bhalla et al., 2011). Similarly, liver and prostate cancer cell lines exhibit increased CiC activity, whose inhibition results in reduced cell viability (Liu et al., 2010; Mitra et al., 2014). These studies demonstrate that CiC is essential for the growth and proliferation of different cancer types and underscore the importance of developing CiC inhibitors as potential anti-cancer drugs.

Moreover, nonalcoholic fatty liver disease (NAFLD) and its evolution to inflammatory steatohepatitis (NASH) are the most common causes of chronic liver damage. The mitochondrial CiC has been proposed to play an important role in disease pathogenesis, via regulation of lipid metabolism. In particular, CiC rewires the lipogenic pathway and upregulates the expression of gluconeogenic genes, in a PGC-1α-dependent manner (Kaplan et al., 1982). Inhibition of CiC activity suppresses the lipid anabolic program and prevents the evolution of steatosis. Thus, CiC represents a potential novel therapeutic target for NAFLD (Tan et al., 2020).

Finally, alterations of CiC activity occur also in autoimmune disorders such as rheumatoid arthritis and Bechet's disease and in Down syndrome, whereas microdeletions of the chromosomal locus where *Slc25a1* is located are associated to DiGeorge syndrome, velo-cardio-facial syndrome and a subtype of schizophrenia (Maynard et al., 2008). In addition to its role in disease development, CiC seems to be

involved in ageing, since mutations in the *Indy* gene, which is the fly homologue of *Slc25a1*, promote lifespan (Rogina et al., 2000).

In conclusion, although some aspects of the CiC activities and mode of action have been elucidated, further investigation is required to fully understand CiC role, especially within the context of the disease pathophysiology.

1.6 Research aims of the thesis

Explore how the age-induced changes on the epigenome regulate the stem cell differentiation potential

Stem cell exhaustion is one of the key drivers of ageing (López-Otín et al., 2013), as discussed above. Loss of the proliferation ability of aged BM-MSCs and impaired differentiation towards osteoblasts and chondroblasts have been associated to ageing and are implicated in the development and progression of several bone quality-related diseases, including osteoarthritis and osteoporosis. Although the severe consequences of these conditions are very common in the population, with one in three women (and one in five men) above the age of fifty suffering a broken bone due to osteoporosis (Sözen et al., 2017), the precise molecular mechanisms leading to reduced bone density and increased risk for bone fractures upon ageing have not been fully understood. Given that the epigenome regulates stem cell fate decisions and undergoes dramatic alterations upon ageing, the first aim of this thesis is to investigate how age-induced alterations on the chromatin accessibility and the histone acetylation profile govern BM-MSC fate decisions, favoring adipogenesis at the expense of osteogenesis and bone development.

Study the metabolic impact on the chromatin landscape upon ageing

Metabolism fulfills multiple functions required both for cell viability and for tissue and organismal homeostasis. Importantly, beyond ATP generation and biosynthesis of complex macromolecules, metabolism produces several intermediate metabolites whose role in the regulation of the activity of epigenetic writers, erasers and readers has been extensively studied during the last years. This establishes a tight mito-nuclear communication which influences stem cell identity and activity. Thus, the second aim of this thesis is to investigate the metabolism-chromatin crosstalk both in young individuals as well as upon ageing and to study its impact on BM-MSC fate and function.

Investigate the role of oxygen in the metabolism-chromatin-stem cell fate axis

Mammalian cell culture represents a milestone in biomedical research and the conditions under which cells are expanded *in vitro*, such as the media composition, need to be precisely controlled. However, one of the parameters whose role in cell physiology and function is often neglected during cell culture routine is the oxygen concentration. In particular, oxygen levels within the mammalian body are significantly lower compared to the atmospheric oxygen concentration; yet standard tissue culture practice involves isolation of cells from their hypoxic niche and *in vitro* expansion under high oxygen. Given that oxygen impacts BM-MSC behaviour, mostly by altering the cellular energetic profile as discussed above, such shifts in the oxygen tension might have a profound effect on stem cell activity. Hence, the third aim of this thesis is to characterize the oxygen-induced changes in the mito-nuclear communication and the BM-MSC fate decisions.

Chapter 2

Materials and Methods

2.1 Materials

Table 1. Cell culture reagents, growth media, antibiotics and drugs.

Name	Supplier	Cat. number
Bafilomycin A1	Enzo	BML-CM110-0100
Beta-glycerophosphate	Sigma Aldrich	G9422
BTA	Sigma Aldrich	B4201
Collagenase	Sigma Aldrich	C9407
Dexamethasone	Sigma Aldrich	D4902
DMEM+GlutaMax medium	Gibco	61965
DPBS	Gibco	14190
E64d	LKT Laboratories	E0003
FBS	Gibco	10500-064
HBSS	Gibco	14025-092
HEPES	Gibco	15630-056
IBMX	Sigma Aldrich	15879
Indomethacin	Sigma Aldrich	17378
Insulin	Sigma Aldrich	16634
ITS	Sigma Aldrich	I1884
L-ascorbic acid	Sigma Aldrich	A8960
L-proline	Sigma Aldrich	P5607
MEM Alpha medium+GlutaMax (α-MEM)	Gibco	32561-037
Penicillin/Streptomycin	Gibco	15140-122
Polybrene	Santa Cruz	sc-134220
Puromycin	Gibco	A11138
Sodium acetate	Invitrogen	AM9740
Sodium butyrate	Sigma Aldrich	156-54-7
Sodium pyruvate	Gibco	11360

TGF-β3	Sigma Aldrich	SAB4502957
0.05% Trypsin-EDTA	Gibco	25300-054

Table 2. Antibodies used for FACS analysis.

Antibody	Supplier	Cat. Number
CD140a (PDGFRα)	eBioscience	17-1401-81
CD29-PE	eBioscience	12-0291-81
CD31-APC	eBioscience	17-0311-80
CD34-FITC	eBioscience	11-0341-81
CD45-PE	Life Technologies	A16325
Sca-1-FITC	eBioscience	11-5981-85
Terr-119-PE	eBioscience	12-5291-82
7AAD	ThermoFisher	A1310

Table 3. Antibodies used for Western Blot.

Antibody	Supplier	Cat. Number
ACC1	ProteinTech	21923-1-AP
ACLY	ProteinTech	15421-1-AP
ACS	Cell Signaling	3658T
CBP	Cell Signaling	7389S
Citrate Carrier	abcam	99168
FAS	Cell Signaling	3189S
GCN5	ProteinTech	14983-1-AP
LAMP2	EMD Millipore	ABL-93
LONP1	Sigma Aldrich	HPA002192
OPA1	BD Biosciences	612606
PARL	Sigma Aldrich	AV44851

PGAM5	Sigma Aldrich	HPA036978
STARD7	ProteinTech	15689-1-AP
YME1L	ProteinTech	11510-1-AP
β-actin	Santa Cruz	sc-47778
anti-mouse IgG HRP-linked	Cell Signaling	7076S
anti-rabbit IgG HRP-linked	Cell Signaling	7074S

Table 4. Antibodies used for Immunofluorescence and CUT&RUN-seq.

Antibody	Supplier	Cat. Number
acetyl-Lysine	Cell Signaling	9441S
Citrate Carrier	ProteinTech	15235
H3 acetylation	Active Motif	39139
H3K27ac	Active Motif	39133
H3K27me3	Active Motif	39155
H4acetylation	EMD Millipore	06866
Histone H3	Cell Signaling	14269
Histone H4	abcam	31830
PDH1	abcam	110333
SREBP1	Santa Cruz Biotechnology	365513
γH2AX	EMD Millipore	05636
anti-mouse TOMM20	Sigma Aldrich	WH0009804M1
anti-rabbit TOMM20	Sigma Aldrich	HPA011562
anti-mouse Alexa Fluor 488	ThermoFischer	A11001
anti-rabbit Alexa Fluor 594	ThermoFischer	A11012
anti-mouse Alexa Fluor 568	ThermoFischer	A11031
anti-mouse IgG1 Alexa Fluor 488	ThermoFischer	A21121
anti-mouse IgG2 Alexa Fluor 647	ThermoFischer	A21241

Chemicals

Chemicals used in this study were purchased from the companies Sigma Aldrich (Steinheim, Germany), ROTH (Karlsruhe, Germany), Roche (Mannheim, Germany), Life Technologies (Darmstadt, Germany) and Thermo Scientific (Waltham, USA). Plastic and glassware equipment was ordered from Sarstedt (Nümbrecht, Germany), Greiner (Pressig, Germany) and VWR International (Darmstadt, Germany).

Commercial kits

- BCA protein assay kit (SERVA, 39228.01)
- CyQuant Cell Proliferation assay kit (Invitrogen, C7026)
- Direct-zol RNA miniprep kit (Zymo Research, R2052)
- DNA clean&concentrator kit (Zymo Research, D4013)
- Maxima H Minus Reverse Transcriptase (Thermo Scientific, EP0752)
- NEBNext Ultra II Directional RNA Library Prep Kit for Illumina (BioLabs, E7760S)
- SeaHorse MitoStress kit (Agilent, 103010)

Electronic equipment

- Balance (Sartorius, Göttingen, Germany)
- Benchtop pH meter (VWR, Darmstadt, Germany)
- Centrifuge Mega Star 1.6R (VWR, Darmstadt, Germany)
- Centrifuge Pico21 and Fresco21 (Thermo Scientific, Waltham, USA)
- CO_2 cell incubator (Binder, Crailsheim, Germany)
- DiaMag Rotator (Diagenode, Liege, Belgium)
- Freezer -80°C (VWR, Darmstadt, Germany)
- Freezer -20°C (Liebheer, Bulle, Germany)
- Fridge 4°C (Liebheer, Bulle, Germany)
- Gel electrophoresis system (Bio Rad, Munich, Grermany)
- Hypoxia hood (COY, Michigan, USA)
- Ice machine (Scotsman, Mailand, Italy)
- Led Illuminator BL star16 (Biometra, Jena, Germany)
- Microwave (Severin, Sundern, Germany)
- Nanodrop (Implen, Munich, Germany)

- Qubit (Thermo Scientific, Waltham, USA)
- Rocking platform (VWR, Darmstadt, Germany)
- Roller 6 basic (IKA, Königswinter, Germany)
- TC automated cell counter (Bio Rad, Munich, Grermany)
- Thermal cycler T100 (Bio Rad, Munich, Grermany)
- Thermomixer basic (CellMedia, Zeitz, Germany)
- Vortex 2 genie (Scientific Industries, New York, USA)
- Water bath VWB18 (VWR, Darmstadt, Germany)

Instruments

- Acquity iClass UPLC (Waters, Massachusetts, USA)
- BD FACSAria IIu (BD biosciences, Heidelberg, Germany)
- BD FACSAria Fusion (BD biosciences, Heidelberg, Germany)
- BD FACSCanto II (BD biosciences, Heidelberg, Germany)
- CanonScan 9000F Mark II scanner (Canon, Ota City, Japan)
- Evos FL Auto 2 widefield microscope (Thermo Scientific, Waltham, USA)
- Film processor Curix60 (Agfa, Mortsel, Belgium)
- Illumina HiSeq 4000 III (Illumina, California, USA)
- JEM 2100 plus microscope (JEOL, Tokyo, Japan)
- Laser scanning confocal SP8-DLS microscope (Leica, Wetzlar, Germany)
- Laser scanning confocal SP8-X microscope (Leica, Wetzlar, Germany)
- UltraCut UCT (Leica, Wetzlar, Germany)
- LightCycler 96 instrument (Roche, Mannheim, Germany)
- Microplate Reader Infinite 200 Pro (Tecan, Bangkok, Thailand)
- SeaHorse XF96 extracellular Flux Analyzer (Agilent, California, USA)
- TapeStation 2200 (Agilent, California, USA)
- Vi-CELL MetaFLEX instrument (Beckman Coulter, California, USA)
- Xevo TQ-S triple quadrupole mass spectrometer (Waters, Massachusetts, USA)
- µCT scanner high resolution (SkyScan 1176, Bruker, Belgium)

2.2 Methods

2.2.1 Mouse husbandry, BM-MSC isolation and culture

Details about mouse strains and husbandry

C57BL/6 N mice were bred and cared for in the mouse facility of the Max Planck Institute for Biology of Ageing. Mice were kept at a relative humidity of 50 ± 5%, a room temperature (RT) of 22 ± 2 °C and a light/dark cycle of 12 hours (6 a.m. to 6 p.m., with a 15-minute twilight period). For the ageing experiments and profiling, I used exclusively wild-type male mice 3–4 months old (young cohort) and 18–22 months old (old cohort), a range commonly used in age-associated studies.

Ethical approval for all mouse work performed in this study was granted by the Landesamt für Natur, Umwelt und Verbraucherschutz (LANUV) of the federal state of North Rhine-Westphalia, Germany.

Details about human BM-MSCs

Bone marrow aspirates were obtained from patients undergoing a hemiarthroplasty or total hip arthroplasty at the University Hospital, Limerick, or the Midwestern Orthopaedic Hospital, Croom, Ireland. Ethical approval was obtained from the Health Service Executive and the University of Limerick and all patients gave their informed consent. Osteoporotic female patients were identified following the diagnosis of a femoral neck fragility fracture. Healthy female patients were identified following the diagnosis of a femoral neck fracture, where the mechanism of injury was considered sufficient to cause fracture. For details on the isolation procedure, please be referred to Corrigan et al. (Corrigan et al., 2019)

Endosteal BM-MSC isolation and cell culture

To isolate murine BM-MSCs from their endosteal niche, I followed a purification strategy based on a published protocol (Houlihan et al., 2012), and I adapted the isolation strategy to acquire sufficient cells for my experiments. In brief, young and old mice were sacrificed by cervical dislocation. Skin and muscles around the hind limbs were removed, the legs were cut above the pelvic joints and then placed in ice-cold

PBS, on ice. Tibias were then separated from femurs by dislocating the joints and the clean bones were placed back in ice-cold PBS. All the following steps were performed inside the hypoxia hood. Bones were crushed and cut into tiny pieces and bone chips were incubated for 75 minutes at 37°C, in α-MEM medium containing 0.2% w:v collagenase, shaking at 200 rpm. To stop the collagenase reaction, sample tubes with the bone chips were placed on ice and washed with α-MEM medium supplemented with 10% FBS and 1% penicillin/streptomycin (control α-MEM medium).

I modified the published protocol by culturing the bone fragments together with the released cells; this allows the outgrowth of more BM-MSCs from the bone *in vitro*, increasing the cell yield. Bone chips were transferred into T25 flasks and were cultured under humidified conditions in hypoxia (2% O_2, 5% CO_2, 37°C) or normoxia (21% O_2, 5% CO_2, 37°C). Cells were cultured in control α-MEM medium. On day 3 of cell culture the medium was changed, and on day 5 both the cells and the bone chips were passaged, using Trypsin-EDTA. On day 8 of the cell culture the bone chips were removed, and on day 12 I performed cell sorting using flow cytometry.

Fluorescence-activated cell sorting (FACS)

To obtain a purified BM-MSC population, I performed cell sorting by flow cytometry, using the 7AAD viability dye (1:500) and the following antibodies: Sca-1-FITC, CD140a-APC, CD45-PE and TERR-119-PE, all diluted 1:1000 in HBSS+ buffer. Details about the antibodies used for the FACS analysis can be found in **Table 2.** After harvesting, cells were washed with PBS and resuspended in HBSS+ buffer. Cells were incubated with the antibodies for 45 minutes on ice, were washed twice with HBSS+ buffer and were filtered through 35 um nylon mesh into 5 ml sample tubes.

Cell sorting was performed using the BD FACSAria IIu and the BD FACSAria Fusion instruments under low pressure sorting conditions (100 um nozzle and 20 psi sheath pressure). The CD45-/TERR-119-/CD140a+/Sca-1+ sorted population was collected into eppendorf tubes, containing 500 ul control α-MEM medium, at 4°C. Compensation was done using UltraComp compensation beads. Once sorted, BM-MSCs were centrifuged at 300 g for 10 minutes at 4°C. They were then resuspended in control α-

MEM medium. Cells were cultured under humidified conditions in hypoxia or normoxia, in T25 flasks and were cultured for 4-5 passages.

HBSS+ buffer
1x HBSS
0.01 M HEPES
2% FBS
1% Penicillin/Streptomycin

2.2.2 Molecular methods

Real-Time Quantitative Reverse Transcription (qRT)-PCR

Cells were lysed with QIAzol and the total RNA was extracted using an RNA extraction kit, following the manufacturer's protocol. This was followed by cDNA synthesis using Maxima^{TM} H Minus cDNA synthesis master mix, according to the manufacturer's instructions. Subsequent qRT-PCR analysis was performed with 10 ng of cDNA, using SYBR-Green chemistry on a LightCycler 96 instrument. Oligos were designed using Primer3 and Blast platforms. The primers used for each gene are listed in **Table 5**. Data were analyzed and further processed in Microsoft Excel and Prism GraphPad 8 software (version 8.4.2). Fold change in gene expression over control samples was calculated using the ΔΔCq method, where β-actin Cq values were used as internal control. All reactions were run in three technical replicates and averaged.

Table 5. Sequences of primers used for qRT-PCR analysis.

Gene name	Forward primer	Reverse Primer
Citrate Carrier	GGAGAGGACTATTGTGCGGTCT	CCCGTGGAAAAATCCTCGGTAC
Acan	CGTTGCAGACCAGGAGCAAT	CGGTCATGAAAGTGGCGGTA
Hk2	GTGGCTAGAGCTCGGGATC	TTTCCAGTCGCCCAACATCT
Pfk1	ACCGAATCCTGAGTAGCAAG	GTAGCCTCACAGACTGGTTC
Pgk1	GCGCCACCTTCTACTCCTCC	CTTCCATTTGTCACGTCCTG

Pgam1	ATCAGCAAGGATCGCAGGTA	TTCATTCCAGAAGGGCAGTG
β-actin	CTGCGCTGGTCGTCG	CGGTCATGAAAGTGGCGGTA

Measurement of mtDNA content

qRT-PCR analysis of mitochondrial DNA-encoded genes was used to estimate the mitochondrial DNA content. Cells were lysed with DNA lysis buffer and lysates were incubated with Proteinase K for 30 minutes at 55°C, rotating at 620 rpm on a Thermoshaker. Phenol was then added to the samples to denature proteins and after this step, an equal amount of chloroform was added to remove residual phenol. To precipitate DNA, the aqueous phase was collected again and samples were incubated overnight at -80°C with sodium acetate pH= 5.2 and 100% ethanol. Precipitated DNA was then washed with 70% ethanol for 20 minutes and after air-drying, it was resuspended in nuclease free ddH_2O.

qRT-PCR analysis of *Atp6* and *Cox1* mitochondrial DNA-encoded genes was performed using SYBR-Green chemistry with LightCycler 96 instrument, as described above. Data were analyzed and further processed in Microsoft Excel and Prism GraphPad 8 software (version 8.4.2). Fold change in gene expression over control samples was calculated using the ΔΔCq method and genomic β-actin Cq values were used for internal normalization. All reactions were run in three technical replicates and averaged. Oligos were designed as described above. The primers used for each gene are listed in **Table 6.**

Table 6. Sequences of primers used for qRT-PCR analysis of mtDNA-encoded genes.

Gene name	Forward primer	Reverse Primer
Atp6	GGCACCTTCACCAAAATCAC	CGGTTGTTGATTAGGCGTT
Cox-1	AGGTTGGTTCCTCGAATGTG	GCCTTTCAGGAATACCACGA

<u>DNA lysis buffer</u>

0.5% SDS

0.1 M NaCl

50 mM Tris, pH=8.0
2.5 mM EDTA, pH=8.0

MitoTracker staining

Cells were washed with PBS, harvested with Trypsin-EDTA and resuspended in the pre-warmed (37°C) staining solution, containing the MitoTracker Deep Red FM probe, diluted 1:15000 in α-MEM medium without FBS and phenol red. Cells were incubated with the staining solution for 30 minutes at 37°C. They were then washed twice with PBS, and centrifuged at 500 g for 5 minutes. In the end, they were resuspended in α-MEM medium without FBS and phenol red. After addition of DAPI, for dead-cell exclusion right before the measurement, cells were analyzed by flow cytometry. Data were collected using the FACS Diva software (version 9.0) and analyzed using the FlowJo software (version 10.0).

Staining solution
α-MEM medium
MitoTracker Deep Red FM probe, 1:15000 (Thermo Scientific, M22425)

Western Blot experiments

For all western blot experiments cells were harvested and lysed with RIPA buffer. For efficient lysis, cells were incubated with RIPA buffer for 30 minutes, at 4°C, rotating, and then centrifuged for 10 minutes at 6500 g, at 4°C. Protein concentration was determined using the BCA protein assay kit. 20-50 ug of total protein was loaded into each well and SDS-PAGE electrophoresis was performed at 150 V for ~45 minutes. This was followed by transfer to nitrocellulose membrane, using the Trans-Blot Turbo blotting apparatus and reagents. Protein transfer was confirmed by Ponceau S staining for 1-2 minutes. The membranes were then incubated with blocking buffer for 1 hour at RT and then with the indicated primary antibodies, diluted in antibody dilution buffer, overnight at 4°C. Following this step, membranes were washed three times with PBS, with each washing step lasting for 5 minutes, and were then incubated with the appropriate horseradish peroxidase (HRP)-conjugated secondary antibodies, diluted 1:10000 in antibody dilution buffer, for 1 hour at RT. After three 10-minute washing steps with PBS, the desired proteins were visualized by providing fresh HRP-substrate

solution and exposing the membranes for specific time periods to photographic film, using the Curix60 instrument.

RIPA buffer
150 mM NaCl
1% TritonX-100
0.5% sodium deoxycholate
0.1% SDS
50 mM Tris, pH=8.0
5 mM sodium butyrate
1x Protease Inhibitor Cocktail

Blocking buffer
5% non-fat dry milk
Tris-buffered saline-0.1% Tween20 (TBS-T)

Antibody dilution buffer
3% non-fat dry milk
Tris-buffered saline-0.1% Tween20 (TBS-T)

Immunofluorescence experiments

For immunofluorescence experiments 2,000 cells were seeded in glass-bottom 96-well plates and treated as indicated in each experiment. After treatments, cells were fixed for 15 minutes at 37°C with the fixation buffer. Samples were washed with PBS twice, permeabilized with 0.1% TritonX-100 in PBS for 10-15 minutes and blocked with the blocking buffer for 40 minutes at RT. Samples were then incubated with the indicated primary antibodies diluted 1:100-1:300 in the blocking buffer. Incubation with the primary antibodies was done overnight at 4°C. Following this step, samples were washed 3 times with PBS, with each washing step lasting for 10 minutes. Samples were then incubated with fluorophore-conjugated secondary antibodies, diluted 1:500 in the blocking buffer. Incubation with the secondary antibodies lasted for 45 minutes and during this period the samples were protected from light. After three 10-minute

washing steps with PBS, cells were mounted using the Roti-Mount FluorCare mounting medium, containing DAPI.

Fixation buffer
3.7% v/v formaldehyde in control α-MEM medium

Blocking buffer
5% BSA in PBS

For histone acetylation immunostaining experiments, cells were washed with PBS and were incubated for 10 minutes with the CSK buffer, on ice. They were then washed with ice-cold PBS and fixed for 20 minutes at RT with the fixation buffer. Following fixation, cells were washed 3 times with PBS and were then blocked with the blocking buffer, for 1 hour at RT. Cells were incubated with primary antibodies, diluted 1:100-1:500 in the blocking buffer. Incubation with the primary antibodies was done overnight, at 4°C. Samples were then washed 3 times with PBS and incubated with fluorophore-conjugated secondary antibodies, diluted 1:1000 in the blocking buffer, for 1 hour at RT, protected from light. After three 10 minute-washing steps with PBS, cells were mounted, as described above.

CSK buffer
10 mM PIPES, pH=6.8
100 mM NaCl
300 mM sucrose
3 mM $MgCl_2$
1 mM EDTA
0.5% Triton-X100

Fixation buffer
4% paraformaldehyde
2% sucrose
0.4 mM NaOH in ddH_2O
1x PBS

For triple immunostaining of MDVs, cells were fixed in fixation buffer for 20 minutes at 37°C. They were then washed 3 times with PBS and permeabilized with 0.1% Triton-X100 in PBS for 10 minutes. After 3 washing steps with PBS, they were blocked with the blocking buffer for 45 minutes at RT. Following blocking, cells were incubated with primary antibodies diluted 1:50 – 1:100 in the antibody dilution buffer. Incubation with the primary antibodies was done overnight at 4°C. Cells were then washed 5 times with PBS and incubated with fluorophore-conjugated secondary antibodies, diluted 1:1000 in the antibody dilution buffer, for 1 hour at RT, protected from light. After five 10-minute-washing steps with PBS, cells were mounted as described above.

Fixation buffer
6% paraformaldehyde in PBS

Blocking buffer
10% FBS in PBS

Antibody dilution buffer
5% FBS in PBS

Images of the immunofluorescent cells were acquired using 40x, 63x and 100x objective lenses on confocal SP8-X and SP8-DLS microscopes.

5-EU labeling

The 5-EU label was added to the cells, diluted in control α-MEM medium. After 7 hours of labeling with 1 mM 5-EU, cells were fixed in fixation buffer for 30 minutes at RT. For 5-EU detection, fixed cells were stained for 30 minutes at RT with the staining buffer. The samples were then rinsed several times with 0.5% TBS-TritonX-100 and then stained with DAPI; 30–40 stained cells per sample were imaged using the confocal SP8-X microscope with a 63x objective lens.

Fixation buffer
125 mM PIPES, pH=6.8
1 mM $MgCl_2$

10 mM EGTA
0.2% TritonX-100
3.7% formaldehyde

Staining buffer
100 mM Tris, pH= 8.5
1 mM $CuSO_4$
38.4 µM fluorescent azide 488
100 mM ascorbic acid added last from a 0.5 M stock

Nile Red staining

1 mM of the Nile Red dye was added to the cells, diluted in HBSS+ buffer. Cells were incubated with the dye for 15 minutes at 37°C. They were then washed with HBSS+ buffer and live cell imaging was performed using the confocal SP8-DLS microscope with a 40x objective lens.

Plasmid construction, generation of lentivirus and BM-MSCs transduction

Construct pLVX-Puromycin-CiC was generated by cloning the CiC cDNA sequence which is fused to the C-terminal FLAG epitope into a pLVX-Puromycin vector, between the XhoI and XbaI restriction sites. Lentivirus was generated by co-transfection of 293T cells with the empty pLVX-Puromycin vector or the pLVX-Puro-CiC-FLAG vector, along with the pMD2.G and psPAX2 packaging vectors. Specifically, 2.8,000,000 HEK cells were seeded in a 10-cm plate. The next day, a transfection mix containing 2xHBS, 2 M $CaCl_2$, 10 mg pLVX, 5.2 mg pMD2.G and 5.2 mg psPAX2 was incubated for 30 minutes at RT and subsequently added to the cells. After 16 hours, the medium was changed and fresh control DMEM medium was added to the cells. After 72 hours, the supernatant was collected, spun at 500 g for 5 minutes and filtered through a 0.45 µM filter.

The transfection medium consisted of virus:medium in 1:1 v:v ratio, along with 4 µg/ml polybrene, was used to transduce BM-MSCs. Medium was changed after 18 hours. 2 µg/ml puromycin was added after 72 hours to positively select the transduced cells.

Colony-Forming Unit (CFU) assay

To determine the efficiency by which BM-MSCs form colonies, 100 cells were seeded in a 6-well plate and cultured for 10-12 days, as described above. On the day of the experiment, cells were washed with PBS and stained with 1% v:v crystal violet in PBS for 5-10 minutes at RT. Cells were then washed thoroughly with ddH_2O for three times and visible colonies were counted. Images were acquired on Mark II scanner.

Proliferation assay

Cell proliferation was determined using the CyQuant Cell Proliferation assay kit, according to the manufacturer's protocol. In brief, 1,000 cells were seeded in 48-well plates and proliferation was assessed after 1, 3, 5 and 7 days of cell seeding. On the day of the experiment, cells were incubated in the CyQuant cell lysis buffer for 45 minutes at 37°C, protected from light. Fluorescence was measured at ~480 nm excitation wavelength and ~520 nm emission wavelength, using a microplate reader.

Differentiation assays

i) Differentiation to adipocytes. For adipogenesis, 2,000 cells were seeded in 96-well plates. Adipogenic differentiation was induced once cells reached confluency, by culturing them in adipogenic medium. For BTA treatment, 1 mM BTA was added in the control α-MEM medium for three days, prior to induction of differentiation.

Adipogenesis was confirmed by Oil Red O staining of adipocytes, performed 8-10 days after induction of adipogenesis. Cells were washed with PBS and fixed with 3.7% formaldehyde in control α-MEM media, for 30 minutes at RT. After fixation, cells were washed twice with ddH_2O and once with 60% isopropanol, with every washing step lasting for 5 minutes. Cells were then stained with Oil Red O staining solution for 15 minutes at RT. After staining, cells were washed four times with ddH_2O and images were acquired with a bright-field microscope, using the 20x objective lens.

Adipogenic medium

control α-MEM

1 uM dexamethasone

1 uM IBMX

10 ug/ml insulin

100 uM indomethacin

Oil Red O staining solution
Stock solution: 0.35% w:v Oil Red O in ddH_2O.
Staining solution: 60% v:v Oil Red O stock solution in ddH_2O.

ii) Differentiation to osteoblasts. For osteogenesis, 2,000 cells were seeded in 96-well plates. Osteogenesis was induced once cells reached confluency, by culturing them in osteogenic medium. For BTA treatment, 1 mM BTA was added in the control α-MEM medium, for three days prior to induction of differentiation. For acetate treatment, 5 mM of sodium acetate was added in the control α-MEM medium three days prior to the induction of differentiation.

Osteogenesis was confirmed by Alizarin Red S staining of osteoblasts, performed 12 days after induction of osteogenesis. Cells were washed once with PBS and fixed with 3.7% formaldehyde in control α-MEM media, for 30 minutes at RT. Fixation was followed by washing cells with ddH_2O. Cells were then incubated with the Alizarin Red S staining solution for 45 minutes, protected from light. After staining, cells were washed with ddH_2O and images were acquired with a bright-field microscope, using the 20x objective lens.

Osteogenic medium
control α-MEM
100 nM dexamethasone
10 mM beta-glycerophosphate
100 uM ascorbic acid

Alizarin Red S staining solution
2% w:v Alizarin Red S in ddH_2O

iii) Differentiation to chondrocytes. For chondrogenesis, 75,000 cells were seeded in 96-well plates with flat (control) or conical (differentiated) bottom. Chondrogenesis was induced once cells reached confluency, by culturing them in differentiation medium for

12-14 days. Osteogenesis was confirmed by extracting RNA and performing qRT-PCR analysis for the *Acan* osteogenic gene, as described above.

Chondrogenic medium
control DMEM medium
100 nM dexamethasone
1% ITS
10 uM ascorbic acid
1 mM sodium pyruvate
50 ug/ml proline
20 ng/ml TGF-β3

SeaHorse analysis of mitochondrial respiration and glycolytic activity

To determine the oxygen consumption rate (OCR), 96-well SeaHorse microplates were coated with 10% Gelatin - 90% Poly-L-Lysine solution for 1 hour at RT. 20,000 cells were seeded in each well and cells were incubated overnight at 37°C, in a humidified 5% CO_2 incubator, with control α-MEM medium. To measure endogenous fatty acid oxidation, on the day of the experiment, cells were treated with or without 100 uM etomoxir and incubated for 1 hour at 37°C, in a humidified 5% CO_2 incubator. They were then washed twice with the assay medium and incubated for 1 hour in a non-CO_2 - containing incubator, before loading into the XF Analyzer. To assess exogenous fatty acid oxidation, cells were incubated overnight with substrate-limited medium. On the day of the experiment cells were incubated with assay media for 1 hour in a non-CO_2 - containing incubator. BSA-Palmitate was added to the wells before running the assay.

Following measurements of resting respiration, cells were injected with 20 uM oligomycin (or 1.5 uM for the palmitate experiment), 5 uM FCCP (or 2 uM for the palmitate experiment) and 5 uM Rotenone/Antimycin (or 0.5 uM for the palmitate experiment). Each measurement was taken over a 2-minute-interval followed by 2-minute-mixing and 2-minute-incubation. Three measurements were taken for the resting OCR: after oligomycin, after FCCP and after Rotenone/Antimycin A treatment. Values were normalized to protein concentration using Bradford kit and were plotted

using the Wave software (version 2.4) and the Prism GraphPad 8 software (version 8.4.2).

Assay medium for endogenous fatty acid oxidation
XF-DMEM medium
10 mM Glucose
1 mM Sodium Pyruvate
2 mM L-Glutamine

Substrate-limited medium
DMEM without glucose and phenol red
0.5 mM Glucose
0.5 mM L-carnitine
1 mM Glutamax
1% FBS

Assay medium for exogenous fatty acid oxidation
substrate-limited medium
2 mM Glucose
0.5 mM L-carnitine

To determine extracellular acidification rate (ECAR), 96-well SeaHorse microplates were coated with 10% Gelatin - 90% Poly-L-Lysine solution for 1 hour at RT. 30,000 cells were seeded in each well and cells were incubated overnight at 37°C, in a humidified 5% CO_2 incubator, with control α-MEM medium. On the day of the experiment, cells were washed twice with the assay medium and incubated for 1 hour in a non-CO_2 - containing incubator, before loading into the XF Analyzer. Glycolytic activity was measured after injection with Glucose (10 um), Oligomycin (1 uM) and 2-DG (50 um). Each measurement was taken over a 2-minute-interval followed by 2-minute-mixing and 2-minute-incubation. Values were normalized to protein concentration using Bradford kit and were plotted using the Wave software (version 2.4) and the Prism GraphPad 8 software (version 8.4.2).

Assay medium for glycolysis
XF-DMEM medium
2 mM L-Glutamine

Measurement of glucose, lactate and pH

Measurement of glucose, lactate and pH in the media of BM-MSCs was performed using the Vi-CELL MetaFLEX instrument, according to manufacturer's instructions. All measurements were done in triplicates and averaged.

Measurement of bone quality parameters

To assess changes in the bone quality upon ageing, I dissected femurs from young and old mice and collected them in PBS. Bone density and bone volume were measured in the Phenotyping Core Facility at the Max Planck institute for Biology of Ageing by micro-computed tomography (uCT), as described in **Appendix A**.

Electron microscopy

Preparation of samples for electron microscopy and image acquisition were performed in CECAD Institute, as described in **Appendix B**.

Targeted liquid chromatography mass spectrometry (LC-MS) analysis

Metabolite extraction from each sample was performed using a mixture of prechilled (−20 °C) acetonitrile:methanol:water in ratio 40:40:20 v:v:v and protein concentration was used for normalization. Detection and measurement of the extracted metabolites were performed in the Metabolomic Core Facility at the Max Planck Institute for Biology of Ageing, as described in **Appendix C**.

2.2.3 Sequencing-based approaches and data analysis

Sequencing of all libraries was performed at the Cologne Center for Genomics (CCG) and data analysis was done by Dr. Parekh Swati at Max Planck Institute for Biology of Ageing, as described in **Appendix D**.

RNA-sequencing (RNA-seq)

Total RNA was isolated using an RNA extraction kit following the manufacturer's protocol. Once RNA quality and integrity were verified, RNA libraries were created using a NEBNext Ultra II Directional RNA Library Prep Kit.

Assay for Transposase Accessible Chromatin-sequencing (ATAC-seq)

ATAC-seq was performed on 50,000 cells per sample, as described previously (Buenrostro et al., 2013). In brief, cells were harvested, washed with PBS, resuspended in ice-cold lysis buffer and centrifuged for 10 minutes, at 500 g at 4°C. Nuclei were then incubated with the transposition reaction mix, for 30 minutes at 37°C, shaking at 250 rpm. DNA was purified using the DNA concentrator kit.

Following purification, 10 ul of the DNA fragments were amplified using the NEBnext PCR master mix and Nextera PCR primers, using the following PCR conditions: 72°C for 5 minutes; 98°C for 30 seconds; 98°C for 10 seconds; 63°C for 30 seconds; 72°C for 1 minute. Libraries were amplified for five cycles. DNA concentration of the libaries was measured using Qubit and library quality was assessed by running samples on the TapeStation.

Lysis buffer

10 mM Tris-CL, pH=7.4

10 mM NaCl

3 mM $MgCl_2$

0.1% NP-40

Transposition reaction mix

25 ul TD

2,5 ul TDE1

25,5 ul ddH_2O

CUT and RUN-sequencing (CUT&RUN-seq)

CUT&RUN was performed on 100,000 cells per sample, adapting a previously described protocol (Skene and Henikoff, 2017). In brief, Concanavalin A magnetic

beads were resuspended in binding buffer. Cells were washed twice with wash buffer and incubated with activated Concanavalin A beads for 10 minutes at RT. The cell-bead suspension was then resuspended in antibody buffer and incubated overnight at 4°C with the desired antibodies (antibody dilution 1:50). The cell-bead suspension was then washed twice with digitonin buffer and incubated with the EpiCypher CUTANA pAG-MNase, for 10 minutes, rotating. After two washing steps with digitonin buffer, samples were resuspended in digitonin buffer and 100 mM $CaCl_2$ was added to the tubes. Samples were incubated for 2 hours at 4°C, rotating. To stop the reaction, STOP buffer was added in each tube and samples were incubated at 37°C for 10 minutes at 500 rpm. After centrifugation, the liquid was collected, the DNA was purified using the DNA concentrator kit and the DNA was eluted in the elution buffer.

For library construction, first, DNA ends were blunted for 30 minutes at 20°C. DNA was then cleaned-up using Ampure XP beads and was next subjected to poly-A addition. Next, adapters were ligated to each sample by incubation for 15 minutes at RT and 15 minutes at 30°C. DNA samples were cleaned up by Ampure XP beads and libraries were amplified using the following PCR, conditions: 45 seconds at 98°C; 15 seconds at 98°C; 30 seconds at 63°C; 30 seconds at 72°C; 60 seconds at 72°C. Libraries were amplified for twelve cycles. DNA was cleaned up by Ampure XP beads and purified using the DNA concentrator kit. DNA concentration of the libaries was measured using Qubit and library quality was assessed by running samples on the TapeStation.

Binding buffer
20 mM HEPES, pH=7.9
10 mM KCl
1 mM $CaCl_2$
1 mM $MnCl_2$

Wash Buffer
20 mM HEPES, pH=7.5
150 mM NaCl
0.5 mM Spermidine
1x Protease Inhibitor

Digitonin Buffer
Wash Buffer
0.05% Digitonin

Antibody Buffer
Digitonin Buffer
2 mM EDTA

STOP Buffer
340 mM NaCl
20 mM EDTA
4 mM EGTA
0.02% Digitonin
50 ug/ml RNase A
50 ug/ml Glycogen

2.2.4 Microscopy image acquisition and processing

Bright-field images were acquired using the Evos FL Auto 2 microscope. Quantification of the Alizarin Red S and Nile Red staining were done in ImageJ64 software (version 10.2), quantifying 3-5 randomly selected fields per image. Measurement of intensity was done after making RGB stacks for each image and applying the same thresholds to all samples from each experiment. Immunofluorescent images were acquired using the confocal SP8-X and SP8-DLS microscopes. Images were acquired using the 40x, 63x and 100x objective lenses. All immunofluorescent images were processed identically in ImageJ and Fiji (version 2.1.0/1.53c); in particular, images are shown after background subtraction (rolling ball radius:50) and noise despeckle.

2.2.5 Quantification and statistical analysis

Except for the epigenome analyses, all other graphs were generated in GraphPad Prism 8 (version 8.2.4) software. For all bar graphs, results are shown as mean ± S.E.M. For quantification of images where more than 10 cells were taken into account,

distribution of data points is shown as violin plots, where the mean is indicated by a solid line and quartiles are indicated with dotted lines. I performed all sequencing experiments using n=2 biologically independent replicates. For all other experiments I used n=3 biologically independent replicates, unless otherwise stated. p-values for box plots of sequencing data were determined using a two-sided Wilcoxon test. In all other instances, statistical significance was determined using two-sided unpaired and paired t-test, unless otherwise specified, and the exact p-values are indicated on each plot. For boxplots, the lower and upper hinges correspond to the first and third quartiles (25th and 75th percentiles), while the middle line is median and the whiskers extend to 1.5 × interquartile range (IQR) from both lower and upper hinges. GO enrichment analysis was performed using Metascape (Zhou et al., 2019), which calculates p-values on the basis of a cumulative hypergeometric distribution. Model is drawn using BioRender.

Chapter 3

Results

Part I: Chromatin remodeling due to degradation of Citrate Carrier impairs osteogenesis of aged stem cells

3.1 Chromatin compaction and histone hypo-acetylation during BM-MSC ageing

3.1.1 Aged BM-MSCs exhibit skewed adipogenesis and impaired osteogenesis

To investigate the molecular link between chromatin, metabolism and stemness upon ageing, I isolated mesenchymal stem cells from the bone endosteum of young (~3-5 months old) and old (~18-22 months old) mice. For the isolation of BM-MSCs I followed a published protocol (Houlihan et al., 2012). In brief, after dissecting the hind limbs, bones were cut into tiny pieces and the bone fragments were incubated with collagenase, to facilitate bone digestion. The released cells were then seeded and cultured *in vitro*.

a

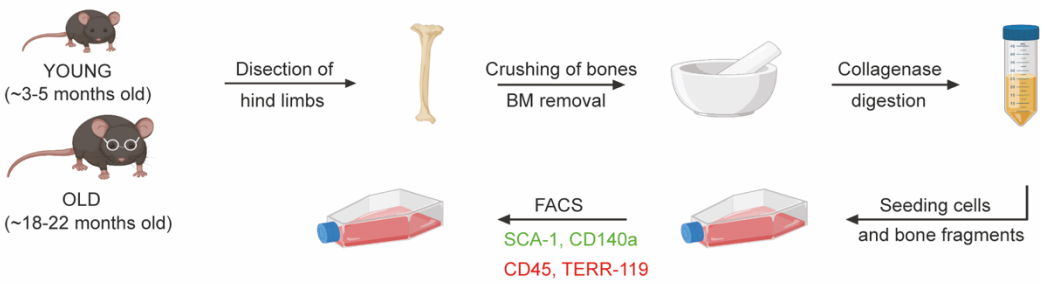

b

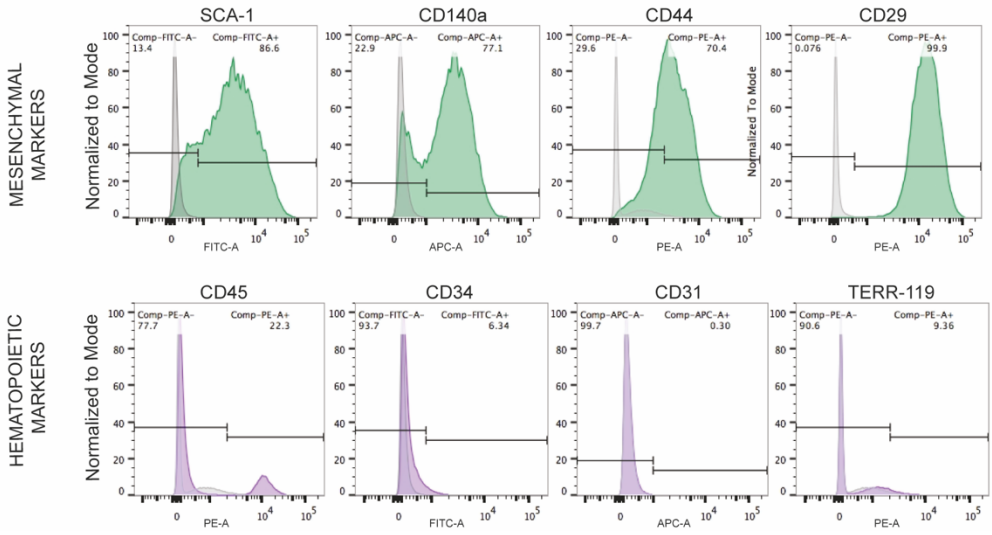

Figure 3.1. Isolation and characterization of BM-MSCs derived from the bone endosteum. (**a**) Schematic representation demonstrating the isolation protocol of bone marrow mesenchymal stem cells (BM-MSCs) from the back limbs of young (~3-5 months old) and old (~18-22 months old) mice. After collection of the limbs, clean bones were cut into small pieces, which were then treated with collagenase for 1 hour at 37°C. Cells and bone fragments were seeded in flasks and incubated for 10 days under 2% O_2. On day 10, I performed cell sorting using flow cytometry; I selected the CD45-/Ter-119-/Sca-1+/CD140a+ mesenchymal stem cell population. (**b**) Expression profile of BM-MSCs for mesenchymal (top) and hematopoietic (bottom) markers, as assessed by flow cytometry. The purified BM-MSC population is highly enriched in mesenchymal stem cell markers and depleted from hematopoietic stem cell markers.

This strategy purified a homogenous BM-MSC population, expressing high levels of the Sca-1 and CD140a BM-MSC markers. However, since only 500-1000 BM-MSCs per mouse could be isolated following this procedure, I modified this protocol by adding the possibility for outgrowth of more BM-MSCs from bones *in vitro*, before cell sorting (**Figure 3.1a**); this modification increased the number of the isolated BM-MSCs (~70,000 per mouse), which were devoid of hematopoietic markers, while expressing mesenchymal stem cell surface markers (**Figure 3.1b**). Taking into consideration the variability between individual mice, pooled cells obtained from three different animals were used in each biological replicate. Additionally, in order to maintain the oxygen concentration similar to that of their niche, purified BM-MSCs were cultured exclusively under 2% oxygen.

The isolated cells from both age groups maintained their characteristic mesenchymal marker expression profile even after four weeks in cell culture, as revealed by FACS analysis (**Figure 3.2a**). Interestingly, the FACS data were confirmed by RNA-seq analysis of young and aged cells, which showed that the isolated BM-MSCs from both age cohorts did not express hematopoietic markers, whereas they exhibited high expression levels of known mesenchymal stem cell markers (Pedemonte et al., 2007) (**Figures 3.2b-3.2c**). Importantly, the isolated cells possessed tri-lineage differentiation capacity, giving rise to adipocytes, osteoblasts and chondroblasts (**Figure 3.2d**).

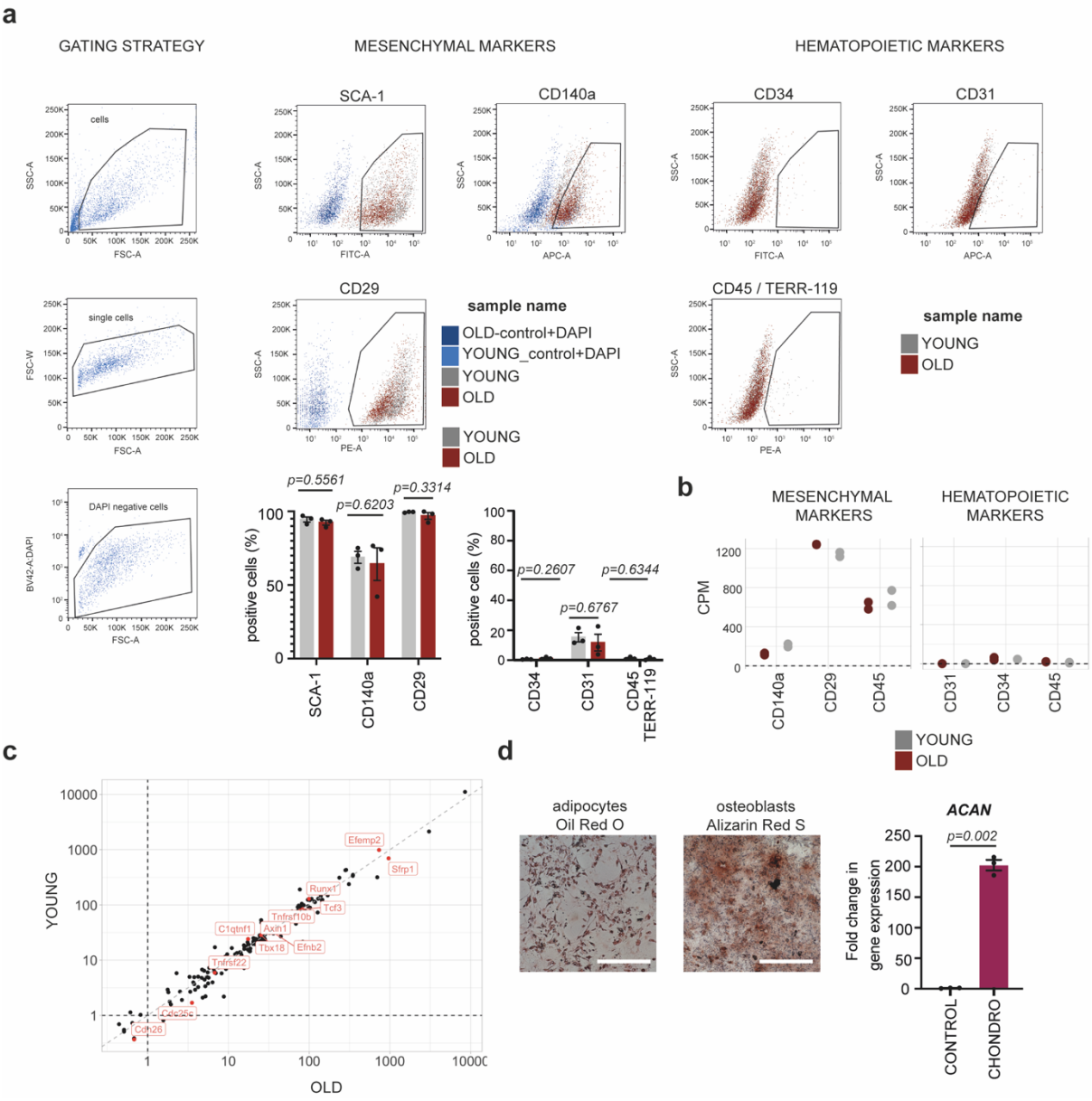

Figure 3.2. Maintenance of BM-MSC properties during *in vitro* culture. (**a**) Marker profile of BM-MSCs for mesenchymal and hematopoietic genes, as assessed by flow cytometry, using cells at passage 5 (~4 weeks in culture). (**b**) Validation of results shown in (**a**) by RNA-seq. Plotted here are the counts per million (CPM) values for each gene. (**c**) Correlation of the transcription levels of known BM-MSC-specific markers in young and aged BM-MSCs, using the RNA-seq dataset. The values are counts per million and both axes are scaled to log10. (**d**) Multilineage differentiation capacity of BM-MSCs. Representative images showing adipogenic and osteogenic differentiation, which were confirmed after Oil Red O and Alizarin Red S staining, respectively. Images were acquired 12 days after induction of differentiation. Scale bars, 500 um. Chondrogenic differentiation was confirmed by qRT-PCR analysis of the chondrogenic gene *Acan*, 14 days after induction of differentiation. *β-actin* was used as an internal control for normalization. CHONDRO: chondrocytes.

In vitro culture of BM-MSCs from young and aged mice revealed that aged BM-MSCs exhibited similar proliferation rate to young BM-MSCs, although they displayed lower colony forming capacity (**Figures 3.3a-3.3b**). Moreover, aged cells displayed skewed adipogenic differentiation at the expense of osteogenesis (**Figures 3.3c-3.3d**). The biased adipogenesis and impaired osteogenesis were in line with age-dependent changes in the transcriptome profile (**Figure 3.3e**) and are both well-described characteristics of aged BM-MSCs.

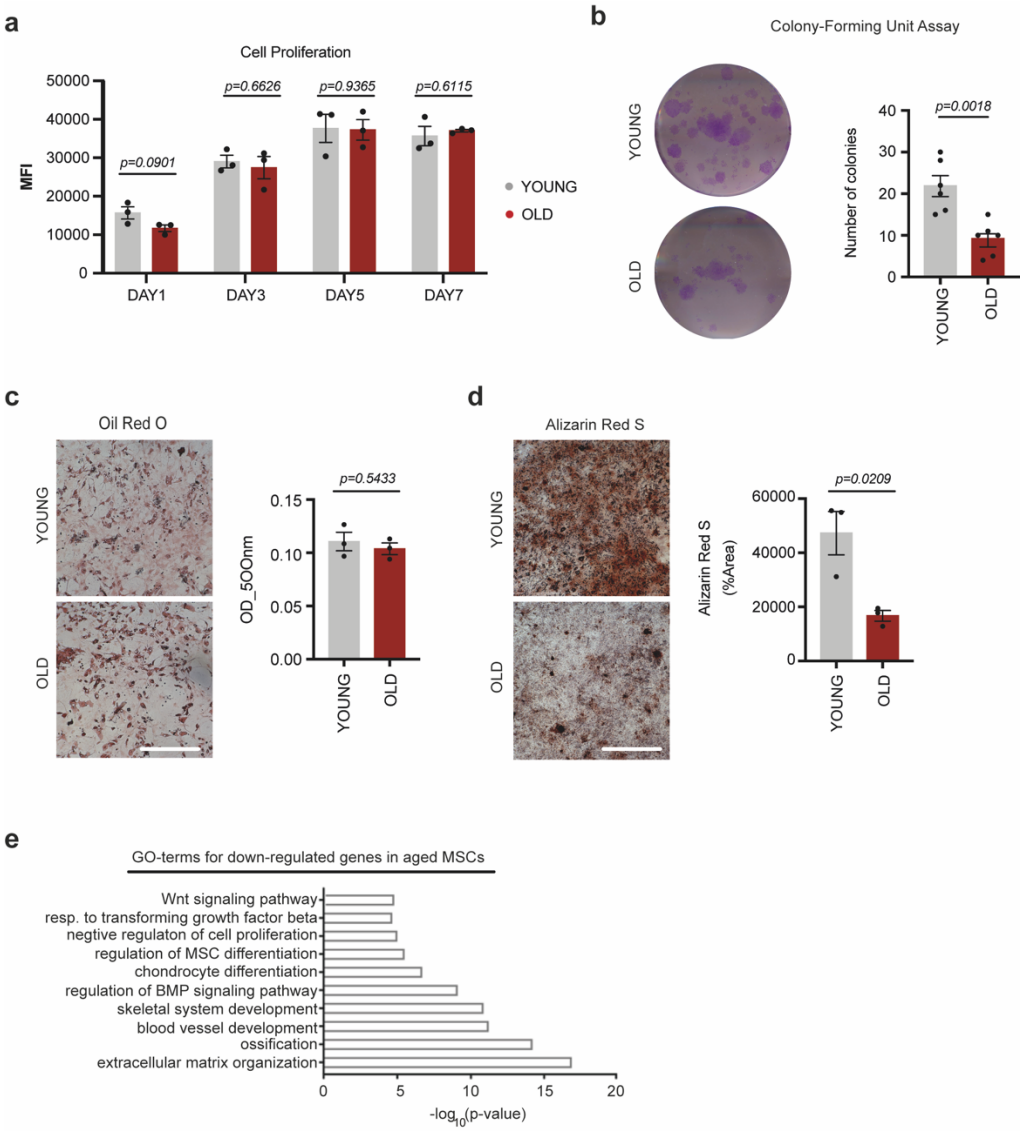

Figure 3.3. BM-MSCs lose their osteogenic capacity upon ageing. (**a**) Comparison of the proliferation rate of young and aged BM-MSCs, after 1,3,5, and 7 days in culture, using the CyQuANT NF Cell Proliferation Assay kit. (**b**) Representative images and quantification of Colony-Forming Unit assay for young and aged BM-MSCs, after culturing them for 10-14 days. n = 6 biologically independent

experiments. (**c**) Representative images and quantification after Oil Red O staining of young and aged cells, 9 days after induction of adipogenesis. (**d**) Representative images and quantification of Alizarin Red S staining of young and aged BM-MSCs, 12 days after induction of osteogenesis. (**e**) GO enrichment analysis for down-regulated genes upon ageing, identified by RNA-seq. n = 3 biologically independent replicates.
Scale bars in (**c**) and (**d**), 500 um.

Together, these data suggest that the purification and culture strategy enabled successful isolation of homogenous, multipotent BM-MSCs that maintained their typical properties *in vitro*. Notably, analysis of several bone quality-related parameters revealed a strong decrease of the bone quality in aged animals, particularly in the trabecular bone compartment, where BM-MSCs reside (**Figures 3.4a-3.4c**). These results confirmed the *in vitro* findings of lower osteogenic capacity upon ageing.

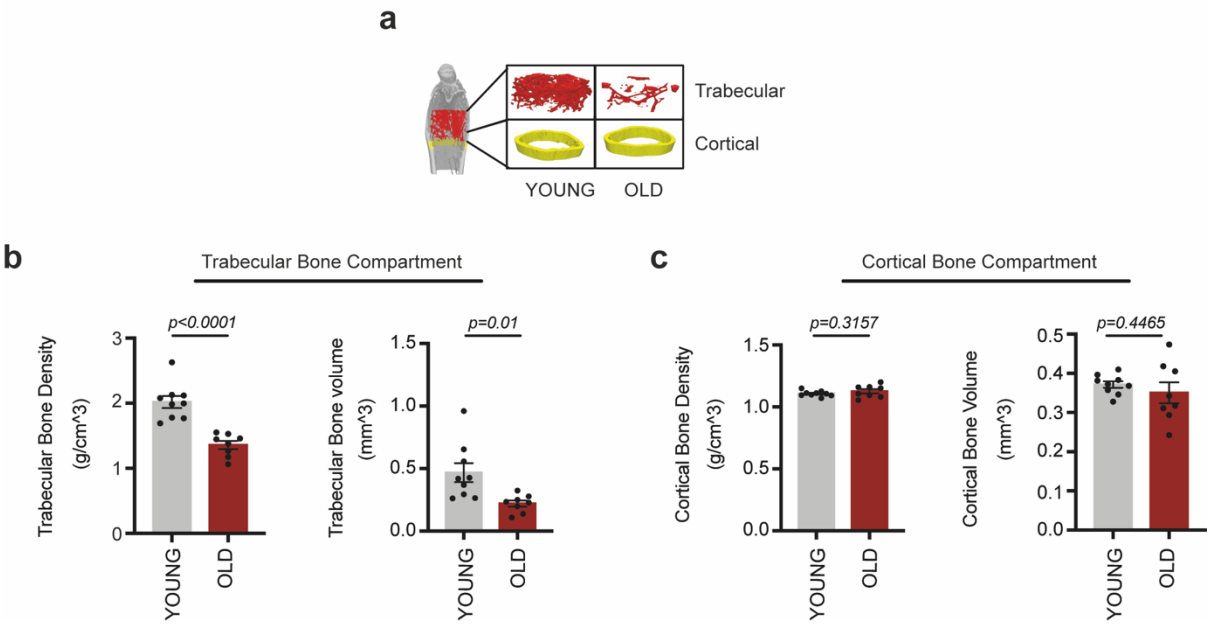

Figure 3.4. Loss of trabecular bone volume and density in aged mice. (**a**) Measurement of bone density and bone volume of the cortical and trabecular bone compartments from the femurs of young and old mice; n = 9 biologically independent experiments of young mice and n = 8 biological replicates of old mice.

3.1.2 Aged BM-MSCs display reduced chromatin accessibility

Using BM-MSCs isolated from young and old mice I sought to investigate the underlying epigenetic determinants of the age-associated loss of the osteogenic

differentiation capacity. Initially, I measured global chromatin accessibility by Assay for Transposase-Accessible Chromatin using sequencing (ATAC-seq) on young and aged BM-MSCs (**Figures 3.5a-3.5c**). As outlined in **Figure 3.5a**, this assay uses the hyperactive Tn5 transposase which recognizes and fragments the accessible, nucleosome-free DNA regions, while simultaneously adding adapters for high-throughput sequencing; thus, it monitors chromatin accessibility on a genome-wide scale (Buenrostro et al., 2013).

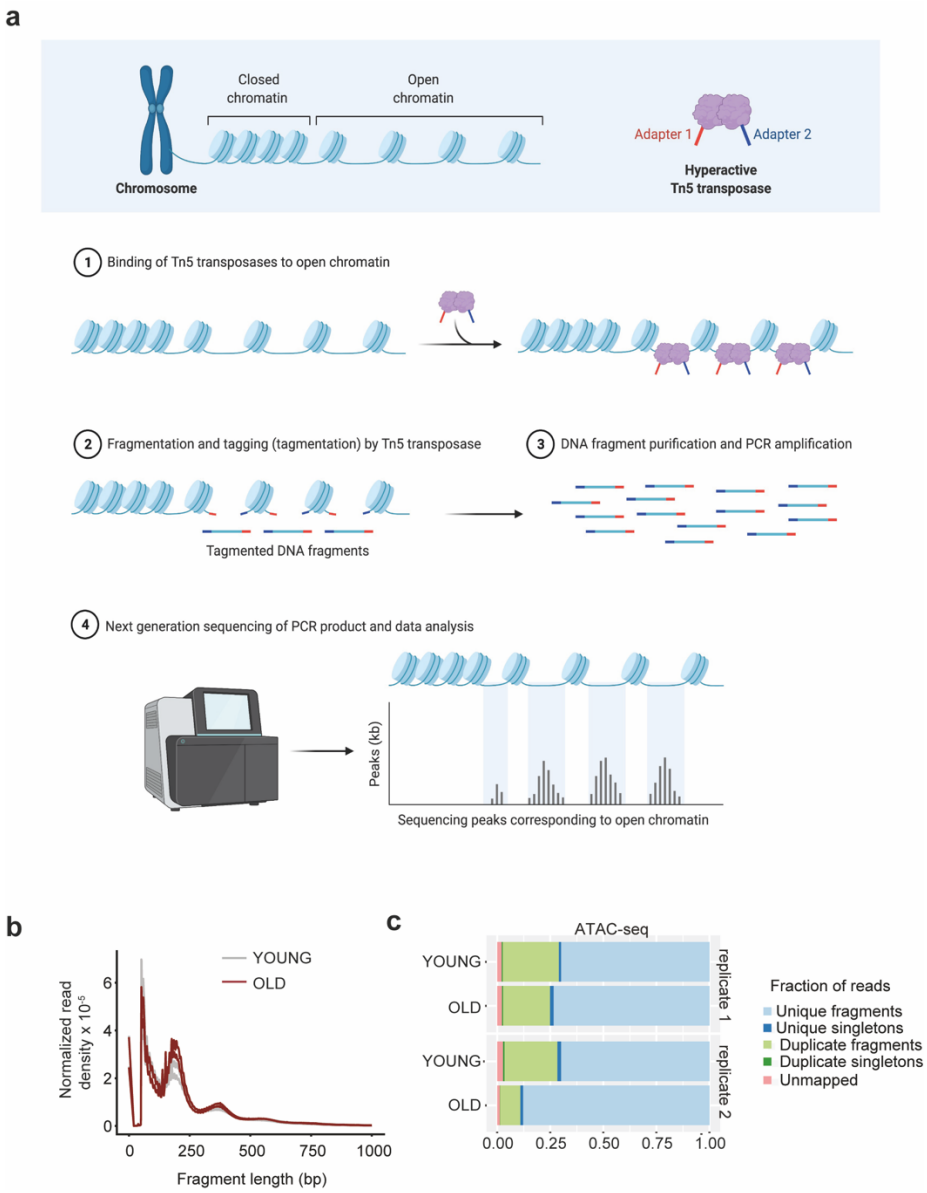

Figure 3.5. Quality control of ATAC-seq. (**a**) Workflow of ATAC-seq experiment. (**b**) Insert size distribution of each single ATAC-seq library. (**c**) Mapping statistics for each individual ATAC-seq library.

Upon ageing, ~14,750 sites in the genome changed significantly in accessibility status (FDR < 0.05). In particular, ~6,500 sites were more accessible in aged BM-MSCs, while ~8,250 sites became less accessible during ageing (**Figure 3.6a**). Surprisingly, aged BM-MSCs exhibited significantly reduced global chromatin accessibility (**Figure 3.6b**). This is opposite to what has been proposed for various organisms that display higher chromatin accessibility upon ageing, which is associated with aberrant gene transcription (Hu et al., 2014). To further analyze the age-dependent changes in the chromatin structure, accessibility over the transcription start site (TSS) was plotted as a metaplot (**Figure 3.6c**). This analysis revealed that the chromatin on gene promoters of aged cells became more compacted. This result was validated using NucleoATAC, an algorithm that allows the precise mapping of nucleosomes from ATAC-seq datasets (Schep et al., 2015). Plotting nucleosome occupancy over the TSS of all protein-coding genes confirmed that ageing led to higher nucleosome density at the promoter region (**Figure 3.6d**).

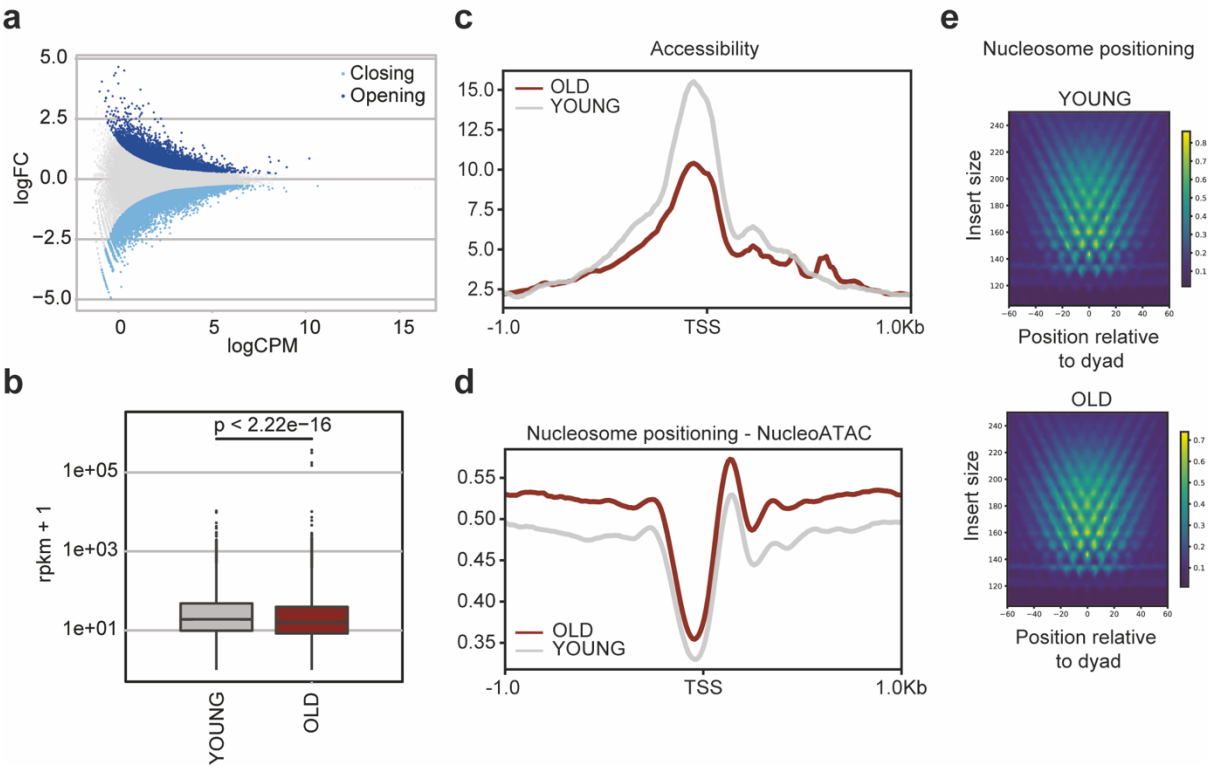

Figure 3.6. Chromatin compaction in aged BM-MSCs. (**a**) MA-plot showing opening and closing peaks with age, as determined by ATAC-seq. (**b**) Overall genome accessibility expressed as RPKM values measured by ATAC-seq. The y axis is scaled to log10 for visualization purposes. (**c**) Metaplot of ATAC-seq reads over the TSS of all protein-coding genes. (**d**) NucleoATAC metaplot to map the

position of all nucleosomes around the TSS of all protein-coding genes. (**e**) V-plots to characterize dyad position within the nucleosomes.

One major feature of the ageing epigenome is the increased nucleosome fuzziness (Hu et al., 2014), which suggests that the position of nucleosomes is not precisely determined and the nucleosomes are rather unstable. However, in the aged BM-MSC population the position of nucleosomes remained properly defined, indicating that only their abundance was affected during ageing (**Figure 3.6e**). Next, I investigated which genes changed promoter accessibility upon ageing. GO enrichment analysis for genes with altered accessibility profile revealed terms surrounding mesenchymal stem cell differentiation, signaling and cell-matrix adhesion processes (**Figure 3.7a**). Notably, these results were in line with the transcriptional changes observed by RNA-seq (**Figure 3.3e**) and there was a linear correlation between the transcriptomic changes and the alterations on the promoter accessibility profile (**Figure 3.7b**). Given that chromatin accessibility correlates with gene transcription, I then assessed whether the age-associated chromatin compaction promoted global reduction of transcription. Indeed, comparison of 5-EU incorporation between young and aged BM-MSCs, revealed that aged BM-MSCs exhibited lower global transcriptional rate compared to young BM-MSCs (**Figure 3.7c)**.

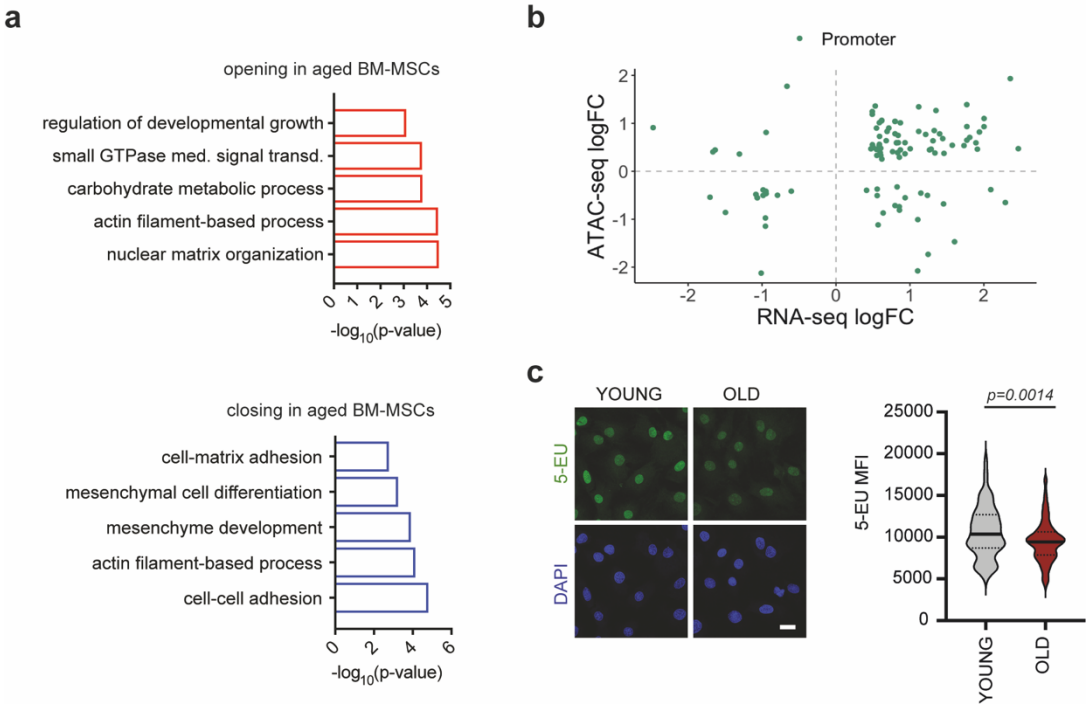

Figure 3.7. Reduced transcription rate in aged BM-MSCs. (**a**) GO enrichment analysis of opening and closing peaks upon ageing that were identified by ATAC-seq. GTPase-med. signal transd.: GTPase-mediated signal transduction (**b**) Correlation of ATAC-seq and RNA-seq data, where the log_2fold change (logFC) of genes differentially expressed in young and aged BM-MSCs and of their differentially accessible promoters is plotted. Only the significantly differentially expressed genes (adjusted p-value <= 0.05) after multiple testing corrections were taken into account. **(c)** Representative images and quantification of mean fluorescence intensity (MFI), after labeling young and aged cells with 1 mM 5-EU, for 7 hours. Nuclei were stained with DAPI. Scale bar, 25 um.

3.1.3 Lower histone acetylation correlates with chromatin compaction of aged BM-MSCs

These unexpected results of a strong decrease in chromatin accessibility and transcriptional rate upon ageing prompted me to further investigate the molecular underpinnings for the age-dependent changes in the chromatin architecture. Histone acetylation neutralizes the positive charge of the side-chain of histones and weakens the contact between histones and DNA (Tessarz and Kouzarides, 2014). Thus, it plays a fundamental role in the regulation of chromatin accessibility and gene expression. Therefore, I investigated whether alterations in the histone acetylation profile between young and aged BM-MSCs contributed to the observed changes in chromatin accessibility. Indeed, aged BM-MSCs contained significantly reduced levels of total histone H3 and histone H4 acetylation (**Figures 3.8a-3.8b**), suggesting that the loss of chromatin accessibility was largely influenced on the level of histone post-translational modifications.

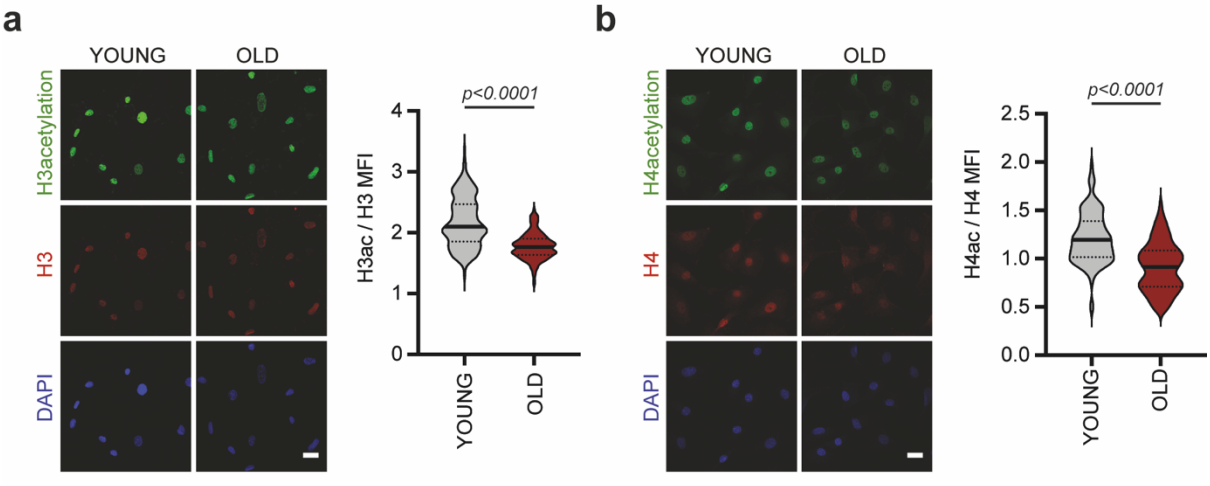

Figure 3.8. Lower histone acetylation in aged BM-MSCs. (**a)** Representative images and quantification of MFI after immunostaining against H3ac and H3 of young and aged cells. MFI of histone H3 was used as internal control, for normalization. Nuclei were stained with DAPI. (**b**) Representative images and quantification of MFI after immunostaining against H4ac and H4 of young and aged cells. MFI of histone H4 was used as internal control, for normalization. Nuclei were stained with DAPI. Scale bars, 25 um.

Together, these data suggest that ageing is accompanied by histone hypo-acetylation and decreased chromatin accessibility, leading to transcriptional changes that are responsible for the reduced osteogenic capacity of aged BM-MSCs.

3.2 Age-induced changes in the abundance of histone marks on lineage-defining genes

3.2.1 Ageing alters the abundance of H3K27 acetylation on lineage-specific genes

To investigate whether ageing was accompanied by changes in other functional elements on the epigenome, levels of H3K27 acetylation (H3K27ac), a mark associated with active enhancers and gene transcription, were analyzed by immunofluorescence. H3K27ac levels remained unchanged globally upon ageing (**Figure 3.9a**).

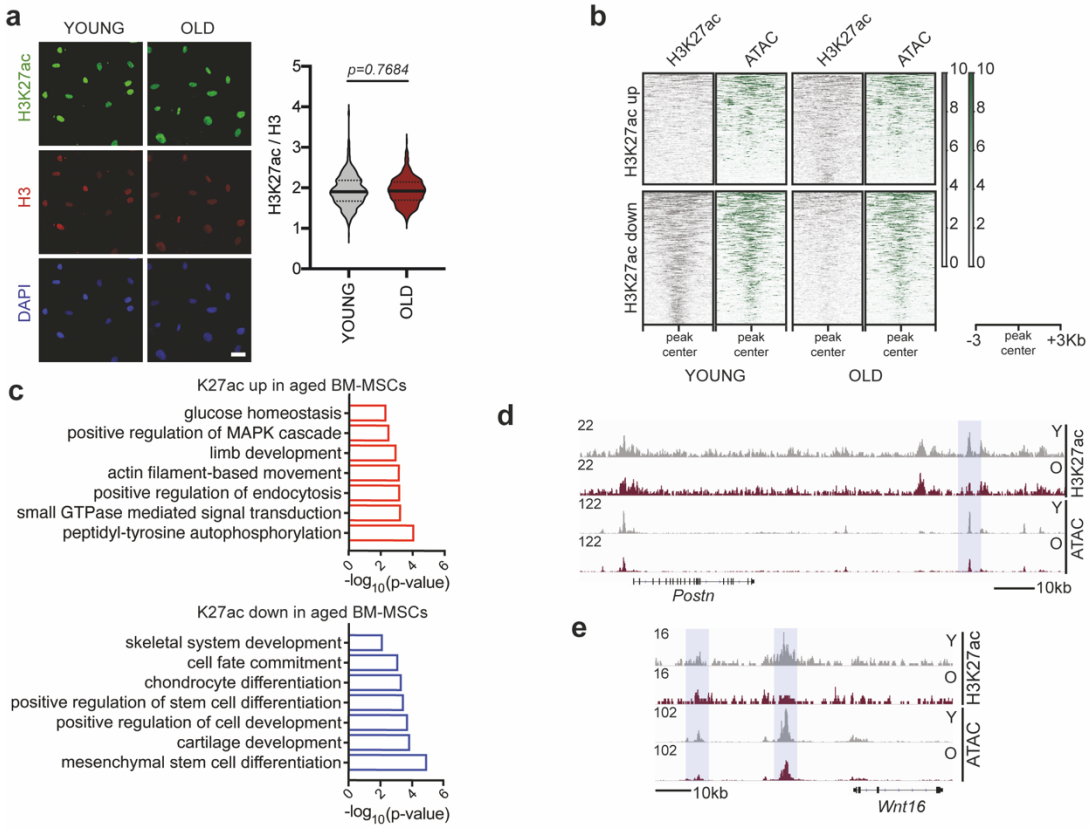

Figure 3.9. Altered abundance of H3K27ac on lineage-determining genes. (**a**) Representative images and quantification of MFI after immunostaining against H3K27ac and H3 of young and aged cells. MFI of H3 was used as an internal control for normalization. Nuclei were stained with DAPI. Scale bar, 25 um. (**b**) Heatmaps of regions that overlapped in H3K27ac and ATAC-seq datasets, representing potential enhancers. Plots were aligned to the peak center, ±3 kb. (**c**) GO enrichment analysis of gene promoters gaining and losing H3K27ac abundance upon ageing. (**d-e**) Integrative genomics viewer (IGV) snapshots showing H3K27ac read density and chromatin accessibility as assessed by ATAC-

seq, in young and aged BM-MSCs, near the *Postn* (**d**) and *Wnt16* (**e**) genes. Shaded regions demonstrate differences between young and aged BM-MSCs.

However, to identify if specific genomic loci displayed altered H3K27ac abundance upon ageing, I performed CUT&RUN-sequencing, using a H3K27ac-specific antibody. CUT&RUN-seq is an alternative for ChIP-seq that allows low cell number as input and precise quantification, using genomic spike-in for normalization. Intersection of the ATAC-seq data and the H3K27ac regions outside promoters identified potential gene enhancers (**Figure 3.9b**). Strikingly, potential enhancers losing H3K27ac abundance upon ageing were associated with genes encoding for transcripts involved in mesenchymal stem cell function and particularly in differentiation into chondrocytes and skeletal system development (**Figure 3.9c**). Examples of genes that lost chromatin accessibility and H3K27ac abundance on potential enhancers upon ageing are shown for *Wnt16* and *Postn*, which are involved in stem cell proliferation and osteogenesis, respectively (**Figures 3.9d-3.9e**). This indicates that the loss of enhancer marking by H3K27ac played a crucial role in the loss of the differentiation potential of aged BM-MSCs.

By contrast, regions that gained H3K27ac occupancy upon ageing were not associated with lineage-specific terms; instead, they were linked to genes encoding for transcripts involved mainly in glucose homeostasis and signaling (**Figures 3.9c**). To investigate whether this change had a functional impact on glucose metabolism, I next compared the glycolytic activity of young and aged BM-MSCs. Interestingly, aged BM-MSCs displayed lower levels of glucose uptake and lactate secretion and higher pH, indicating decreased glycolytic activity (**Figures 3.10a-3.10c**).

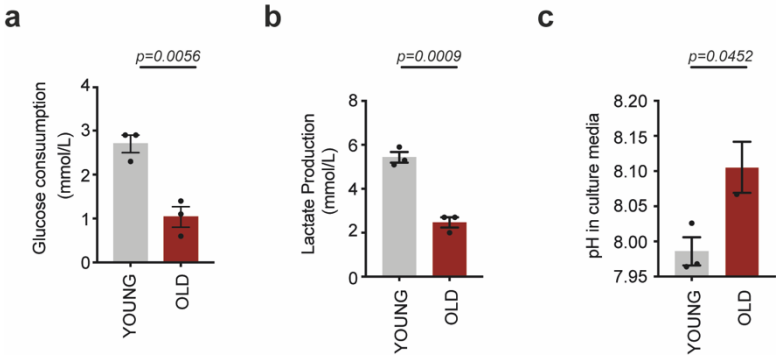

Figure 3.10. Age-associated changes in glucose metabolism. (**a**) Glucose consumption in young and aged BM-MSCs, measured using the Vi-Cell MetaFLEX instrument. (**b**) Lactate production measured in the media of young and aged BM-MSCs, as described in (**a**). (**c**) pH measured in the media of young and aged cells as described in (**a**).

3.2.2 Ageing alters the abundance of H3K27 tri-methylation on lineage-specific genes

Due to the age-dependent alterations in the H3K27ac occupancy and the increased chromatin compaction, I next sought to investigate whether H3K27 tri-methylation (H3K27me3) was altered upon ageing, too. Of note, this histone modification is associated with gene silencing. Indeed, a global increase in H3K27me3 levels upon ageing was observed (**Figure 3.11a**), supporting the previous findings of a chromatin state that is transcriptionally less permissive. To identify the precise genomic regions that exhibited an altered H3K27me3 status upon ageing, I performed CUT&RUN-seq, using a H3K27me3-specific antibody. While H3K27me3 occupancy close to gene promoters did not change between young and aged BM-MSCs, there was an increase in the H3K27me3 abundance across the gene bodies (**Figure 3.11b**). Interestingly, genes gaining H3K27me3 upon ageing were associated with Gene Ontology terms enriched for metabolic processes and cell adhesion terms, whereas those that lost H3K27me3 were strongly enriched for terms involved in neuronal differentiation (**Figure 3.11c**). Although there are some reports showing that BM-MSCs are capable of differentiating into neurons (Song et al., 2018; Karakaş et al., 2020), this is clearly not a mesenchymal lineage. However, the loss of H3K27me3 on these genes was only mild, as shown for the *Pax6* gene that regulates development of neuronal tissues (**Figure 3.11d**). Thus, silencing of neuronal genes was likely not strongly altered with age.

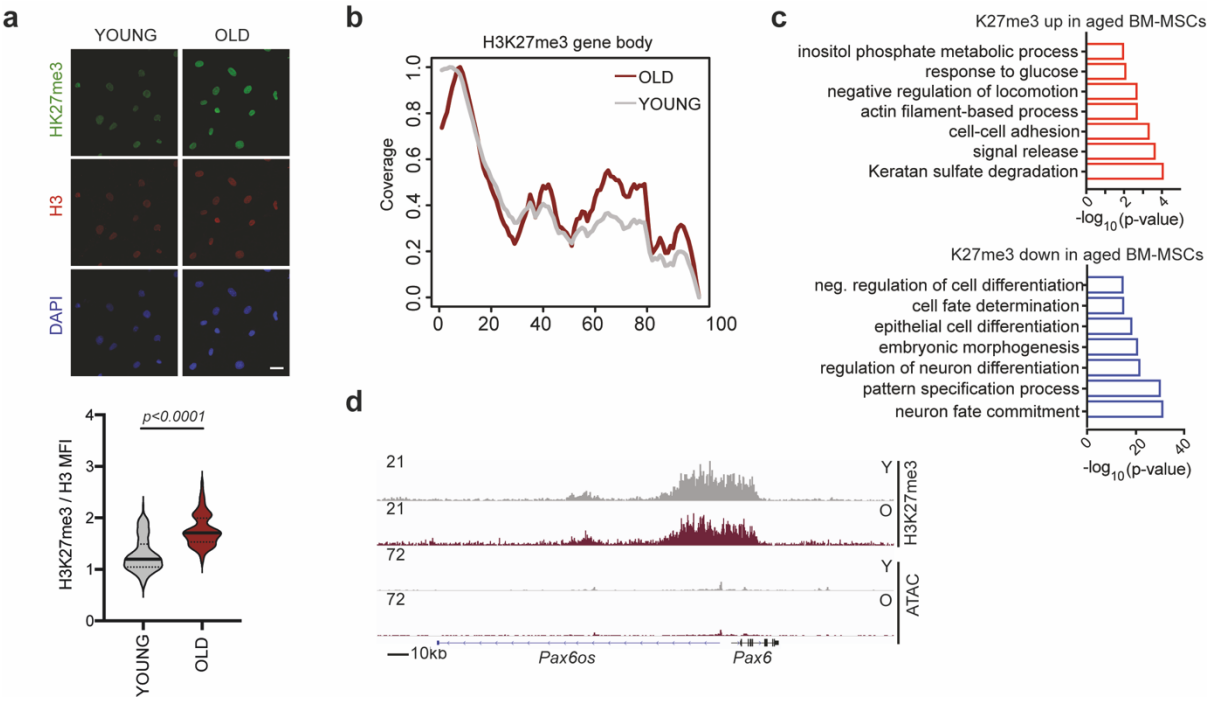

Figure 3.11. Age-associated changes in H3K27me3 abundance. (**a**) Representative images and quantification of MFI after immunostaining against H3K27me3 and histone H3 young and aged cells. MFI of H3 was used as an internal control for normalization. Nuclei were stained with DAPI. Scale bar, 25 um. (**b**) H3K27me3 enrichment density over the gene body of all protein-coding genes. (**c**) GO enrichment analysis of regions gaining and losing H3K27me3 abundance upon ageing. (**d**) Integrative genomics viewer (IGV) snapshots showing H3K27me3 read density and chromatin accessibility as assessed by ATAC-seq in young and aged BM-MSCs, near the *Pax6* gene.

3.3 Lower CiC levels lead to acetyl-CoA trapping inside mitochondria of aged cells

3.3.1 Lower lipid biogenesis in aged BM-MSCs results in acetyl-CoA accumulation

The loss of histone acetylation in aged BM-MSCs prompted me to explore how the histone acetylation profile was established in young and aged cells and whether other cellular processes were involved in this phenotype. To address this, I first compared the levels of the two major histone acetyltransferases (HATs), CBP and GCN5. Levels of both proteins remained stable upon ageing, suggesting that the age-dependent histone hypo-acetylation was not due to differential expression of these two enzymes (**Figure 3.12a**). Thus, I next focused on metabolism, since it is well described that various metabolic intermediates impact the establishment of DNA and histone modifications, via altering the activity of epigenetic enzymes. For instance, local availability of acetyl-CoA directly influences histone acetylation, independently of the enzymatic activity of HATs (Cai et al., 2011; Wellen et al., 2009). Comparison of acetyl-CoA levels in young and aged BM-MSCs revealed that aged cells contained higher acetyl-CoA levels (**Figure 3.12b**). This unexpected result was in contradiction to the lower histone acetylation observed in aged BM-MSCs and motivated me to further investigate where the higher acetyl-CoA levels originated from and what they were used for.

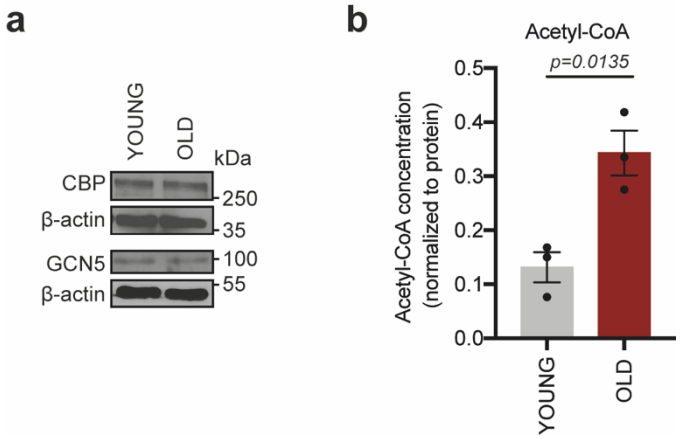

Figure 3.12. Discrepancy between the levels of acetyl-CoA and histone acetylation. (**a**) Representative immunoblots for CBP and GCN5 histone acetyl-transferases in young and aged BM-

MSCs. β-actin was used as loading control. n = 2 biologically independent experiments. (**b**) Comparison of acetyl-CoA levels in young and aged BM-MSCs.

Acetyl-CoA is a central metabolite that plays a fundamental role in lipid metabolism; it is generated through lipid catabolism during fatty acid oxidation (FAO), whereas it is consumed during lipogenesis (**Figure 3.13a**). Thus, I sought to determine whether age-induced changes in the lipid metabolism were responsible for the increased acetyl-CoA levels in aged BM-MSCs. To understand if the lipid content changed with age, cells were stained with Oil Red O to visualize neutral lipids. Aged BM-MSCs displayed a much weaker lipid staining, indicating that they contained fewer neutral lipids (**Figure 3.13b top**). Importantly, this phenotype was also confirmed by electron microscopy, revealing that aged cells exhibited a strong decrease in the amount of lipid droplets (LDs) compared to young BM-MSCs (**Figure 3.13b bottom**).

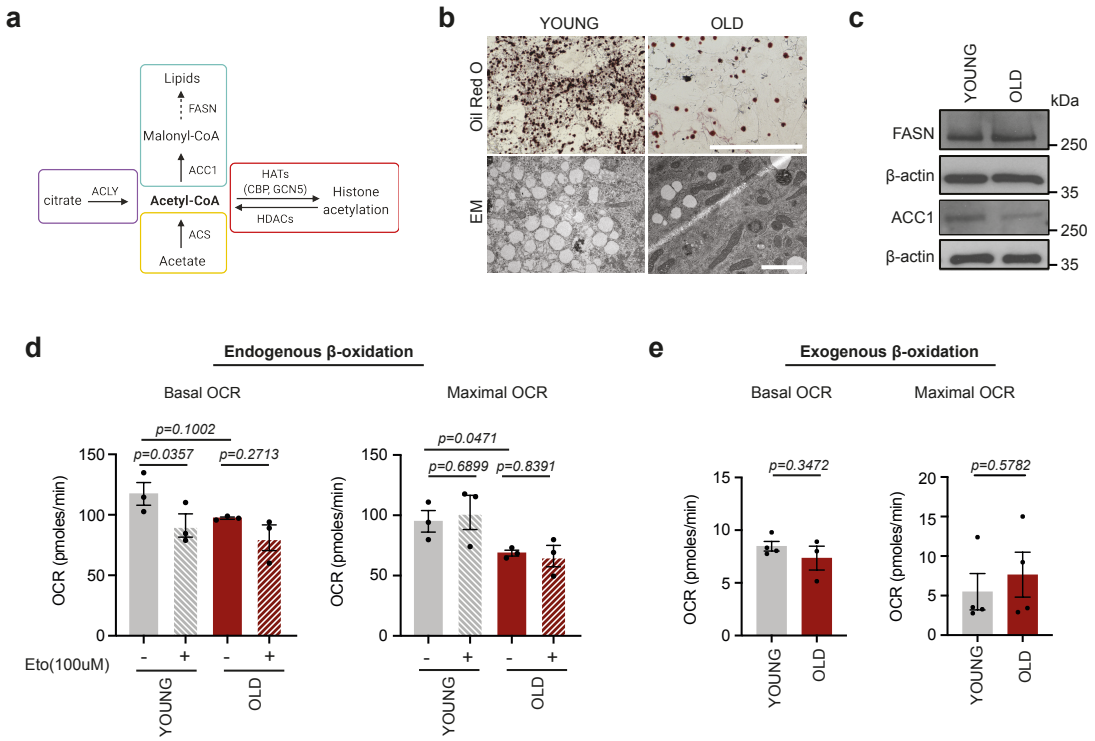

Figure 3.13. Lower lipid content in aged cells is due to impaired lipogenesis. (**a**) Schematic graph describing the different metabolic pathways generating and consuming acetyl-CoA and the associated key enzymes. (**b**) Representative images of lipid droplets. Images were acquired by bright filed microscope after Oil Red O staining (top) and by electron microscope (EM, bottom). Scale bar, 500 um in bright-field images and 2 um in EM images. (**c**) Representative immunoblots for FASN and ACC1 proteins. β-actin was used as loading control. (**d**) Basal (left) and maximal (right) oxygen consumption

rates (OCR) in young and aged BM-MSCs, treated with or without 100 uM Etomoxir for 1 hour, prior to the assay. (**e**) Basal (left) and maximal (right) OCR in young and aged BM-MSCs. Cells were incubated overnight with a substrate-limited medium. On the day of the assay, BSA-Palmitate was injected to cells. n = 4 biologically independent experiments in young and n = 3 biologically independent experiments in old.

The lower LD content could be explained either by lower fatty acid biosynthesis and/or increased lipid consumption through β-oxidation of fatty acids. To investigate whether any of these two mechanisms was altered in my system upon ageing, contributing to the observed loss of lipids and the acetyl-CoA accumulation in aged cells, I initially compared the levels of the key enzymes involved in *de novo* synthesis of fatty acids. Although FASN protein levels did not change upon ageing, levels of the ACC1 enzyme, that is important for the initiation of the fatty acid biosynthesis pathway, were strongly decreased in aged cells (**Figure 3.13c**). This finding suggested that acetyl-CoA was not used efficiently to generate *de novo* fatty acids which could explain why it accumulated in the aged BM-MSC. I next compared the rate of endogenous and exogenous β-oxidation in young and aged BM-MSCs. To assess changes in the endogenous β-oxidation rate, cells from both age groups were treated with etomoxir, an inhibitor of CPT-1, which is the rate-limiting enzyme in FAO. Mitochondrial respiration was measured following etomoxir treatment. Etomoxir treatment did not affect basal and maximal OCR in aged cells, suggesting that these cells did not rely more heavily on endogenous FAO compared to young BM-MSCs (**Figure 3.13d**). Next, I compared the exogenous β-oxidation rate in young and aged cells. For this, young and aged BM-MSCs were starved and were then supplemented with palmitate, which is used as the main energy source in starved cells. Comparison of basal and maximal OCR after palmitate supplementation revealed that there was no significant change between the two age groups (**Figure 3.13e**), suggesting that in aged BM-MSCs there was no higher activation of the FAO pathway, which could explain the increased acetyl-CoA levels.

3.3.2 Acetyl-CoA is trapped in the mitochondria of aged BM-MSCs due to low CiC levels

Since aged BM-MSCs contained higher levels of acetyl-CoA, one potential explanation for the reduced lipid biogenesis and histone acetylation could be a decrease in the cytosolic pool of acetyl-CoA. However, levels of ACLY and ACS enzymes, which are involved in the cytosolic/nuclear generation of acetyl-CoA (Cai et al., 2011; Mews et al., 2017), were stable upon ageing (**Figure 3.14a**). Hence, I speculated that aged BM-MSCs exhibited impaired acetyl-CoA export from the mitochondria to the cytosol. To test this hypothesis, I took into consideration the fact that mitochondrial proteins are hyper-acetylated in a non-enzymatic manner when acetyl-CoA concentration inside mitochondria is high (Hong et al., 2016; James et al., 2017). Thus, young and aged BM-MSCs were stained with an antibody against acetyl-Lysine, whereas TOMM20 was used in parallel, as a counterstain for mitochondria. Impressively, a strong, age-dependent change in the localization of the acetyl-Lysine signal, shifting from nuclear to mitochondrial, was observed upon ageing (**Figures 3.14b-3.14d**). These findings indicated that acetyl-CoA was indeed trapped inside mitochondria of aged BM-MSCs.

To explain why aged BM-MSCs showed such a compartmentalized localization of acetyl-CoA, I then focused on the protein that is responsible for the acetyl-CoA export from mitochondria to the cytosol. Citrate Carrier (CiC) resides in the inner mitochondrial membrane and functions as an antiporter; it imports malate from the cytosol into mitochondria and exports citrate (Gnoni et al., 2009). In the cytosol, citrate is converted into acetyl-CoA by ACLY. Importantly, a connection between CiC and histone acetylation has been demonstrated in *D. melanogaster* and in primary human fibroblasts (Morciano et al., 2009). Taking this into account, I speculated that down-regulation of CiC during ageing might result in lower cytosolic/nuclear levels of acetyl-CoA, explaining the observed decrease in histone acetylation and lipogenesis. Indeed, CiC protein levels were dramatically decreased in aged cells (**Figure 3.14e**), suggesting that BM-MSCs from old mice displayed impaired export of acetyl-CoA from mitochondria to the cytosol.

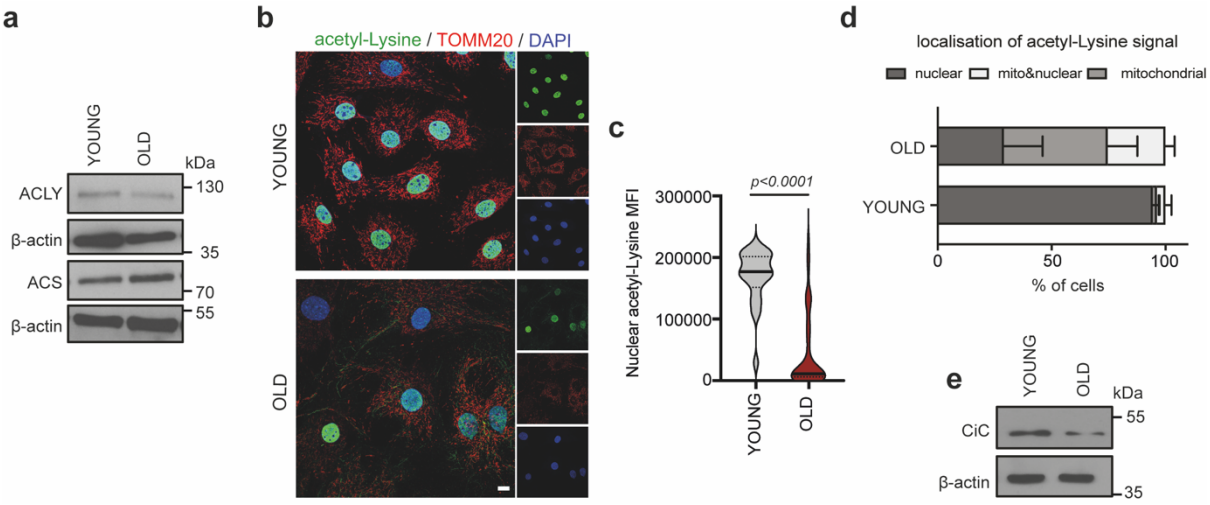

Figure 3.14. acetyl-CoA is trapped inside the mitochondria of aged cells. (**a**) Representative immunoblots for ACLY and ACS proteins. β-actin was used as a loading control. (**b-d**) Representative images after immunostaining against acetyl-Lysine and TOMM20 (**b**), quantification of nuclear acetyl-Lysine MFI in young and aged cells (**c**) and acetyl-Lysine signal localization after manual assignment into three categories: exclusively nuclear, exclusively mitochondrial and nuclear/mitochondrial (**d**). Nuclei were stained with DAPI. Scale bar, 10 um. (**e**) Representative immunoblot for CiC. β-actin was used as loading control.

Collectively, these results propose that the age-associated loss of CiC results in compartmentalized localization of acetyl-CoA within the mitochondria. Consequently, the cytosolic acetyl-CoA pool is limited, leading to lower histone acetylation and reduced lipogenesis in aged BM-MSCs.

3.4 Functional role of CiC in the regulation of osteogenesis

3.4.1 CiC inhibition leads to decreased histone acetylation and osteogenesis

The observation that acetyl-CoA was trapped within the mitochondria due to lower CiC levels in aged BM-MSCs, motivated me to explore whether CiC was indeed the mechanistic target linking mitochondrial acetyl-CoA to histone acetylation and osteogenesis. Initially, I used 1,2,3-benzene-tricarboxylic acid (BTA), a specific CiC inhibitor (Hlouschek et al., 2018; Kolukula et al., 2014) to modulate CiC activity in young BM-MSCs. Folllowing BTA treatment of young BM-MSCs, I analyzed the nuclear–mitochondrial localization of the acetyl-Lysine signal. Inhibition of CiC activity in young cells reduced levels of nuclear acetylation and redistributed the acetyl-Lysine signal inside mitochondria (**Figures 3.15a-3.15c**), mimicking the phenotype observed in aged cells. This result provided the first line of evidence that CiC is the mechanistic link between mitochondria and histone acetylation upon ageing.

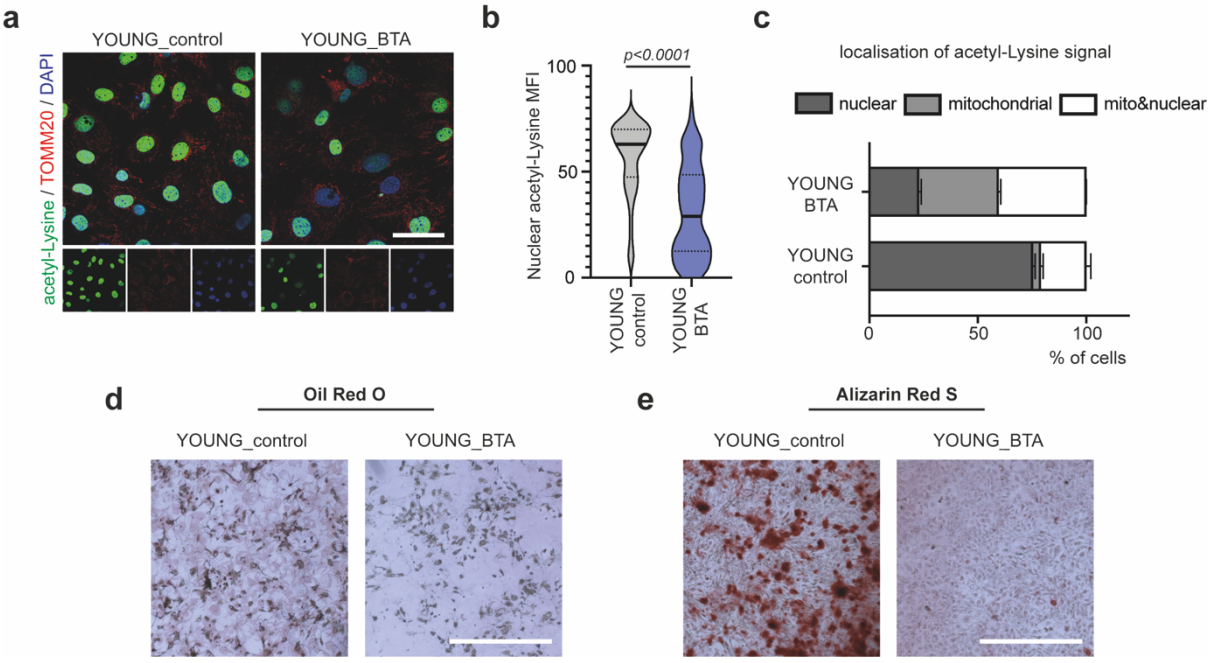

Figure 3.15. CiC inhibition impairs mitochondrial acetyl-CoA export and osteogenesis in young BM-MSCs. (**a-c**) Representative images after staining of control and BTA-treated young cells with acetyl-Lysine and TOMM20 antibodies (**a**), quantification of nuclear acetyl-Lysine MFI in control and BTA-treated cells (**b**), and assessment of the acetyl-Lysine signal localization after manual assignment into three categories, as described above (**c**). Nuclei were stained with DAPI. Scale bar, 50 um. (**d)**

Representative images after Oil Red O staining of young cells treated with or without 1 mM BTA for 3 days before induction of adipogenesis. Images were acquired 10 days after induction of adipogenesis. (**e**) Representative images after Alizarin Red S staining of young cells treated with or without 1 mM BTA for 3 days before induction of osteogenesis. Images were acquired 8 days after induction of osteogenesis. Scale bars in (**d**) and (**e**), 1 mm. p-values for (**c**) are 0.0248 (for nuclear), 0.0019 (for mitochondrial) and 0.0701 (for mito&nuclear).

Next, I sought to determine the biological consequences of the CiC-mediated mito-nuclear communication. The efficient differentiation of BM-MSCs towards the adipogenic and osteogenic lineages requires oxidative metabolism and a fully functional lipid biosynthesis pathway, including efficient export of the acetyl-CoA from mitochondria to the cytosol (Wellen et al., 2009). Therefore, I hypothesized that the decrease in CiC levels might contribute to the lower differentiation potential of aged BM-MSCs. To address this possibility, young cells were treated with BTA for three days, before induction of adipogenesis and osteogenesis. BTA-pretreated cells were able to differentiate into adipocytes, to the same extent as the control untreated cells, being only mildly affected by CiC inhibition (**Figure 3.15d**). In stark contrast, osteogenic differentiation was strongly decreased in BTA-pretreated cells (**Figure 3.15e**). This behavior of young BM-MSCs treated with BTA phenocopied that of the aged BM-MSCs, suggesting that CiC activity was required to maintain the osteogenic differentiation potential.

Together, impaired export of acetyl-CoA from mitochondria due to inhibition of CiC activity impacts histone acetylation and negatively affects the osteogenic differentiation capacity.

3.4.2 CiC overexpression rescues histone acetylation and osteogenesis in aged BM-MSCs

To further confirm that CiC linked histone acetylation to osteogenesis, through regulation of the acetyl-CoA localization, I then followed a genetic approach to manipulate CiC levels and I assessed how this impacts protein acetylation and osteogenesis. In particular, the FLAG-tagged-CiC was exogenously expressed in aged cells, using lentiviral transduction. Notably, overexpressed CiC localized properly

to mitochondria, as evidenced by FLAG-TOMM20 immunostaining (**Figure 3.16a**). Impressively, CiC overexpression in aged cells, redistributed the acetyl-Lysine signal to the nucleus, whereby the intensity of the signal was similar to that of the young cells (**Figures 3.16b-3.16d),** providing a direct link between CiC and histone acetylation levels. Furthermore, to confirm that the impaired acetyl-CoA export from mitochondria was responsible for the lower osteogenic differentiation of BM-MSCs from old mice, I compared the osteogenic differentiation capacity of control and transfected cells. Surprisingly, CiC overexpression rescued the osteogenic impairment of aged BM-MSCs (**Figure 3.16e**), highlighting the critical role of CiC in the regulation of osteogenesis.

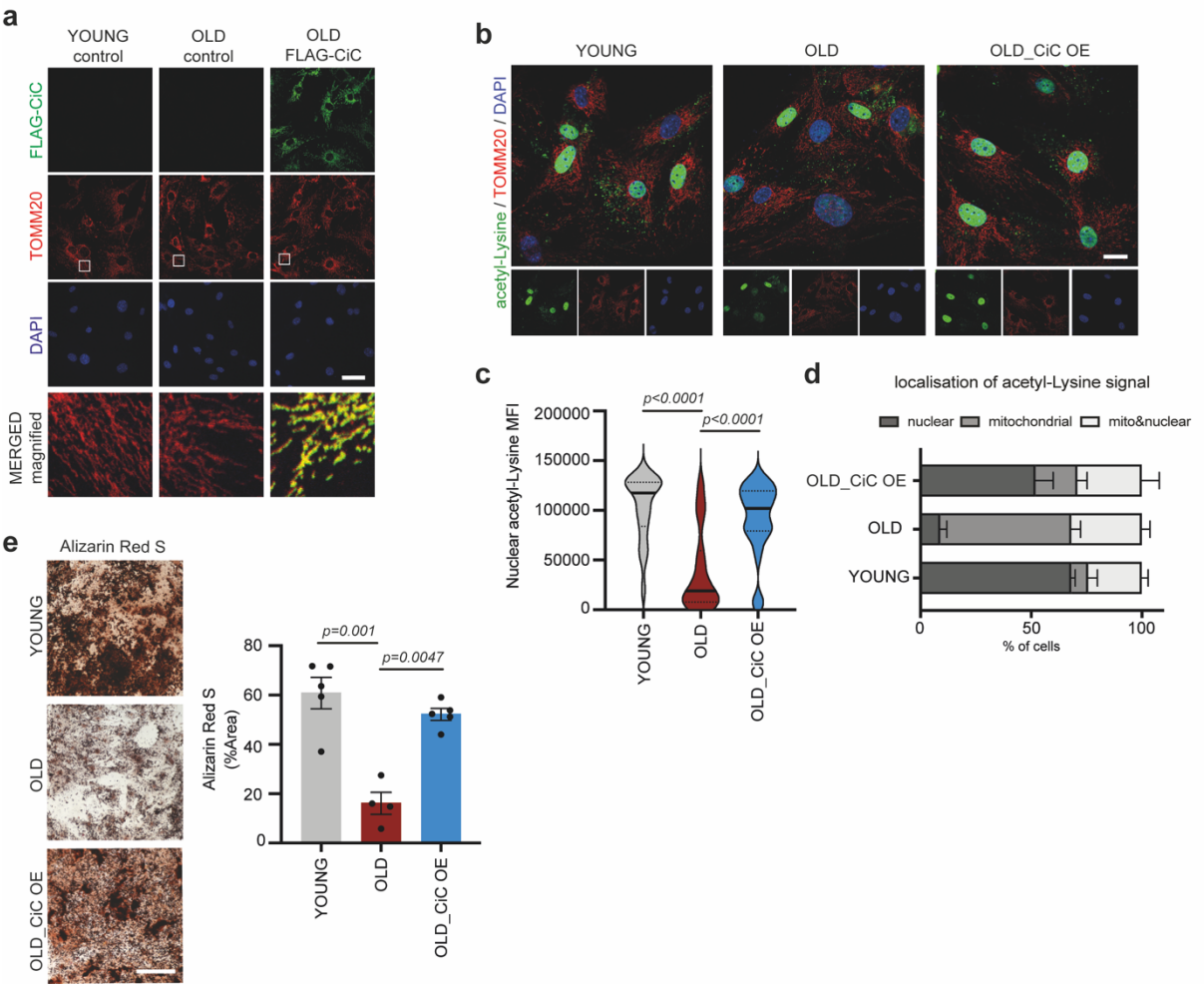

Figure 3.16. CiC OE restores nuclear acetyl-CoA localization and osteogenesis. (**a**) Representative images after staining control young and aged BM-MSCs and CiC-FLAG- expressing aged BM-MSCs, using an anti-FLAG antibody. TOMM20 was used as a counterstain for mitochondria, to confirm proper localization of the exogenously expressed CiC-FLAG protein, as shown in

magnification. Scale bar, 50 um. (**b-d**) Representative images after immunostaining against acetyl-Lysine and TOMM20 (**b**), quantification of nuclear acetyl-Lysine MFI in young cells, aged cells and CiC-over-expressing (CiC_OE) aged cells (**c**), and assessment of the acetyl-Lysine signal localization, as described above (**d**). Nuclei were stained with DAPI. Scale bar, 25 um. (**e**) Representative images and quantification after Alizarin Red S staining of young cells, aged cells and CiC-over-expressing (CiC_OE) aged cells. Images were acquired 12 days after induction of differentiation. Scale bar, 500 um.

In parallel, the CiC-histone acetylation-osteogenesis axis was validated in aged BM-MSCs using sodium acetate; cytosolic acetate can be converted to acetyl-CoA by ACS (Moussaieff et al., 2015), whose levels remained stable upon ageing, as shown above (**Figure 3.14a**). Therefore, acetate represents an exogenous source of acetyl-CoA and acetate supplementation would circumvent the impaired acetyl-CoA export from mitochondria to the cytosol. Similar to the genetic approach, acetate supplementation restored the levels of histone H3 acetylation in aged cells (**Figure 3.17a**). Functionally, acetate pre-treatment of aged cells for three days, before induction of differentiation, rescued the capacity of aged cells to give rise to osteoblasts (**Figure 3.17b**).

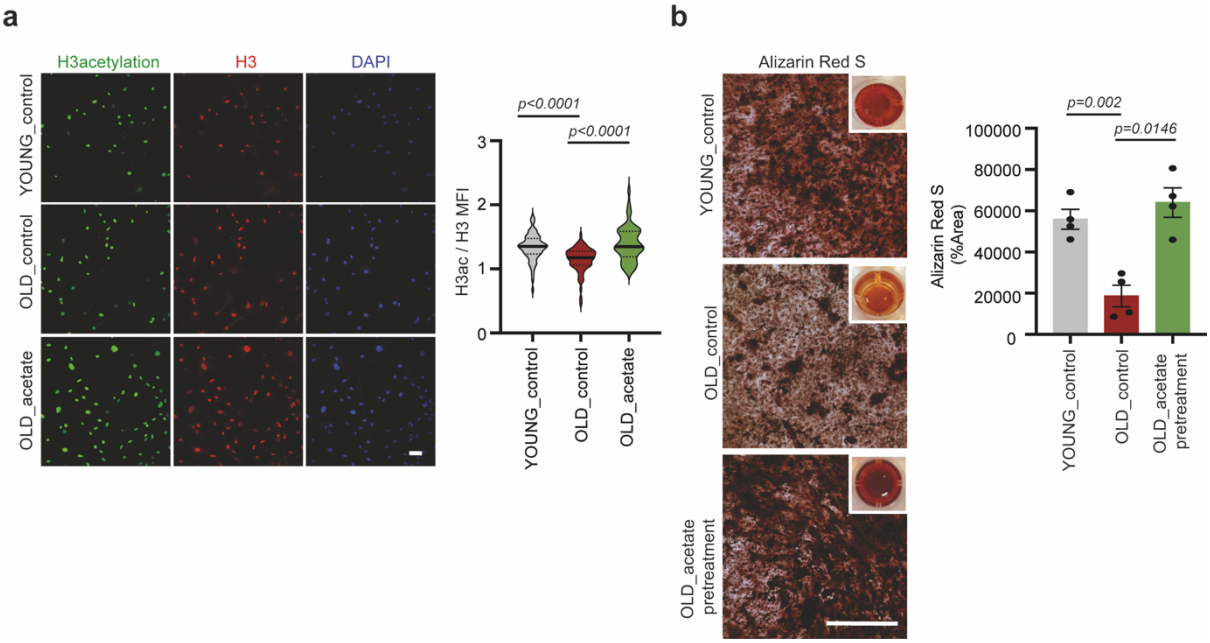

Figure 3.17. Acetate restores nuclear acetyl-CoA localization and improves osteogenesis of aged BM-MSCs. (**a**) Representative images and quantification of MFI after immunostaining against H3ac and H3 of young cells, control aged cells and aged cells treated with 5 mM sodium acetate for 3 days. MFI of H3 was used as an internal control, for normalization. Nuclei were stained with DAPI. Scale bar, 75 um. (**b**) Representative images and quantification after Alizarin Red S staining of young and aged BM-MSCs treated with or without 5 mM acetate for 3 days before induction of osteogenesis. Images were 12 days after induction of osteogenesis. Scale bar, 500 um.

Collectively, these data demonstrate that loss of CiC upon ageing is responsible for the reduction of histone acetylation and osteogenic differentiation potential, providing a mechanistic link between mitochondrial metabolism, histone acetylation and stem cell function upon stem cell ageing.

3.4.2 CiC shapes the chromatin landscape to promote osteogenesis

These findings indicate that CiC played a fundamental role in the regulation of histone acetylation and osteogenesis, with acetate-supplemented aged BM-MSCs presenting a reset histone acetylation profile and improved osteogenesis. Histone acetylation is a dynamic process that influences several chromatin-based processes, such as the DNA damage response. In fact, CiC and its role in the export of mitochondrial acetyl-CoA in the form of citrate, have been recently shown to impact the repair of DNA double strand breaks (Hlouschek et al., 2018). Therefore, it could not be excluded that the enhanced osteogenesis upon acetate supplementation was not due to re-establishment of the histone acetylation profile but rather due to increased DNA damage repair. To test this hypothesis, I compared DNA damage levels between young and aged cells before and after acetate treatment. Quantification of γH2AX foci, that is a marker of DNA damage, showed that there was no change between neither control young and aged cells nor between control and acetate-treated aged cells (**Figure 3.18a**), confirming that DNA repair mechanisms were not altered during acetate supplementation.

To gain more insight into the effects of acetate on histone acetylation on a global scale, CUT&RUN-seq was performed on young, old and acetate-treated-old BM-MSCs, using an antibody against histone H3 acetylation. Surprisingly, treatment with acetate was sufficient to restore histone H3 acetylation levels genome-wide, so that aged cells treated with acetate clustered closer to the young cells than to the untreated cells from the same age group (**Figure 3.18b**). In addition, acetate treatment restored the chromatin plasticity of aged cells, which exhibited increased histone H3 acetylation levels, compared to the control aged cells (**Figure 3.18c**). Furthermore, GO enrichment analysis for genes associated with promoter and enhancer regions that regained histone H3 acetylation abundance upon acetate supplementation revealed

terms surrounding skeletal and cartilage development (**Figure 3.18d**), such as the *Bmp2* and *Mdk1* genes (**Figure 3.18e**). These findings suggest that CiC-mediated export of acetyl-CoA from mitochondria to the cytosol is indispensable for histone acetylation and implicate the importance of chromatin accessibility in the osteogenic differentiation of BM-MSCs.

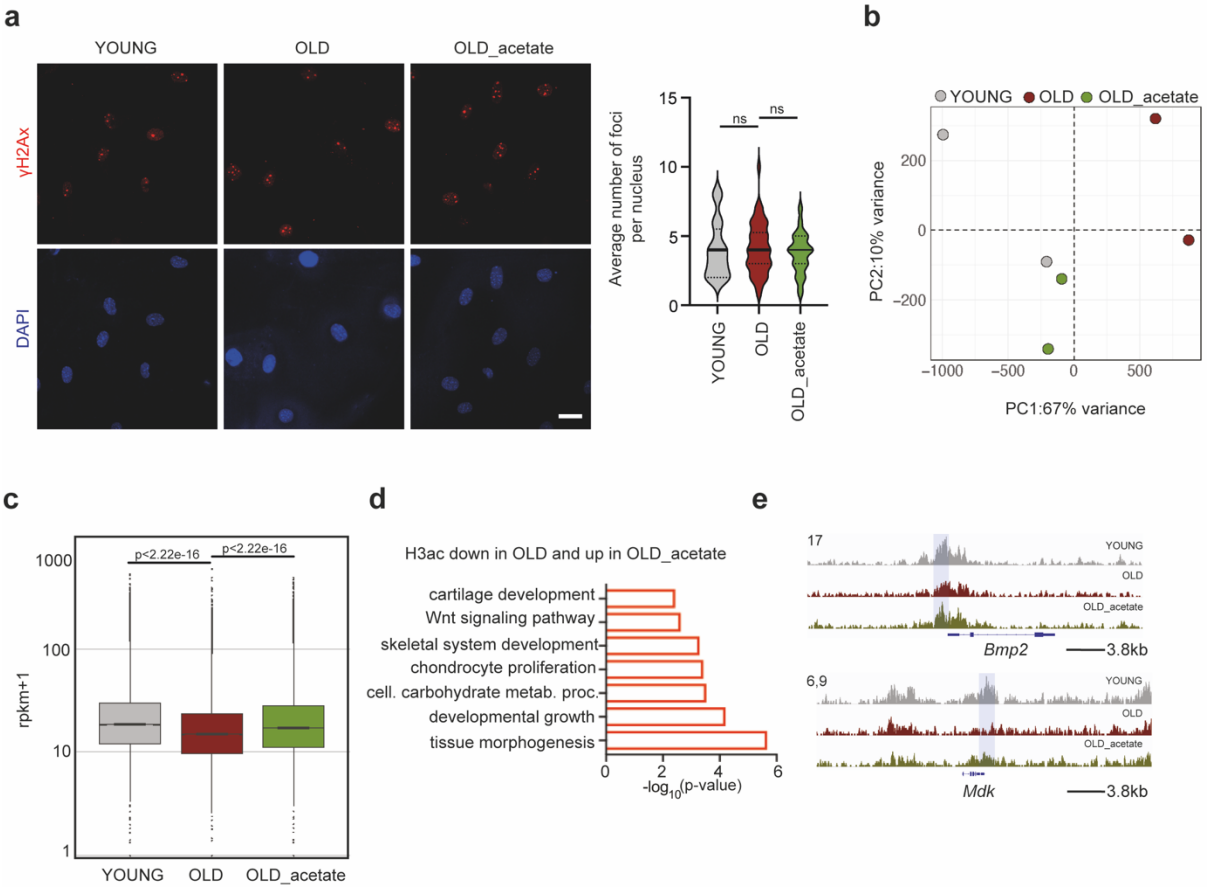

Figure 3.18. Acetate restores H3ac abundance on promoters of osteogenic genes. (**a**) Representative images and quantification of γH2AX foci. Nuclei were stained with DAPI. Scale bar, 25 um. (**b**) Principal component analysis (PCA) plot showing clustering of young, aged and acetate-treated aged cells, after CUT&RUN-seq using H3ac antibody. (**c**) Boxplot showing the peaks quantified as RPKM values in young, aged and acetate-treated aged cells, after CUT&RUN-seq using H3ac antibody. The y axis is scaled to log10 for visualization purposes. (**d**) GO enrrichment analysis of genes that regained promoter and enhancer H3ac abundance after acetate supplementation. Cell. carbohydrate metab. proc.: cellular carbohydrate metabolic process. (**e**) Integrative genomics viewer (IGV) snapshots showing H3ac read density in young, aged and acetate-treated aged BM-MSCs, near the *Bmp2* (top) and *Mdk1* (bottom) genes. Shaded regions demonstrate differences in young, old and acetate-treated old samples.

Taken together, impaired export of acetyl-CoA from mitochondria due to decreased levels of CiC underlies the observed age-dependent chromatin compaction and negatively impacts the osteogenic differentiation capacity of aged BM-MSCs. Strikingly, modifying CiC activity, either pharmacologically or genetically, in order to re-establish chromatin plasticity, is sufficient to rejuvenate aged BM-MSCs, with respect to their osteogenic differentiation potential.

3.5 MDV-lysosomal degradation of CiC in aged BM-MSCs

3.5.1 CiC regulation does not occur at the transcriptomic level

The data presented above unraveled the functional role of CiC in the regulation of stem cell fate decisions upon BM-MSC ageing. However, one intriguing question was why aged BM-MSCs contained lower CiC levels and how was CiC regulated upon ageing. The different mechanisms that control the abundance of a certain protein can be largely divided into those that occur at the transcriptomic level and those happening at the post-translational level. Hence, I sought to determine at which level CiC regulation occurred upon ageing. First, the expression of the *Slc25a1* gene, which encodes CiC, was analyzed by qRT-PCR; while there was considerable variation among the different samples and a tendency towards lower *Slc25a1* mRNA levels in aged BM-MSCs, this change was not significant (**Figure 3.19a**). Interestingly, this finding was also supported by the fact that chromatin features regulating *Slc25a1* expression, such as chromatin accessibility on the *Slc25a1* promoter region, did not change with age (**Figure 3.19b**). The absence of transcriptional regulation pointed towards a post-transcriptional and/or post-translational control of CiC levels. Therefore, I next focused on the different degradation pathways of proteins residing in the inner mitochondrial membrane.

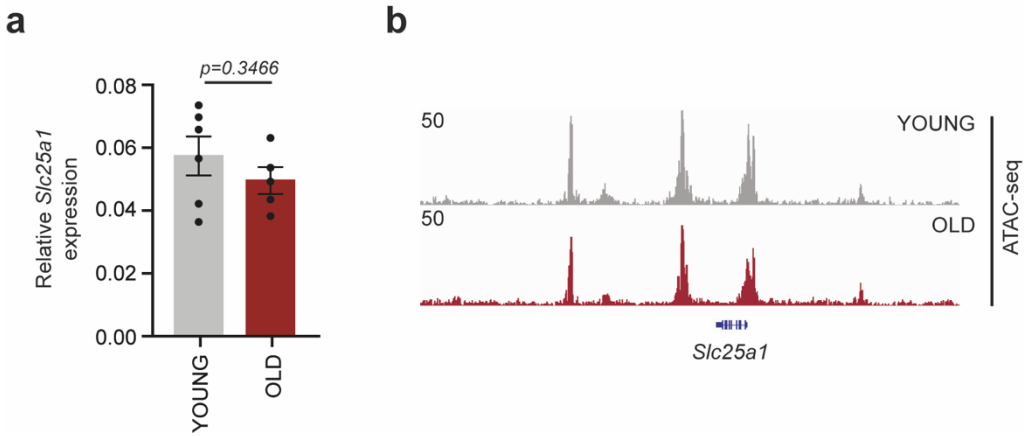

Figure 3.19. *Slc25a1* transcription remains stable upon ageing. (**a**) qRT-PCR analysis of *Slc25a1* gene, which encodes the Citrate Carrier. *β-actin* was used as an internal control for normalization. n = 6 biological replicates for young cells and n = 5 biological replicates for aged cells. (**b**) Integrative genomics viewer (IGV) snapshot showing chromatin accessibility assessed by ATAC-seq in young and aged BM-MSCs, near the *Slc25a1* gene.

3.5.2 CiC is degraded in the lysosomes in aged BM-MSCs

The most common mechanism via which mitochondrial proteins – and particularly those residing in the inner mitochondrial membrane – get degraded is by mitochondrial proteases. These enzymes participate in the degradation, processing and assembly of mitochondrial proteins, ensuring protein homeostasis that is vital for the mitochondrial function. Initially, I investigated whether mitochondrial proteases were responsible for the lower CiC levels in aged BM-MSCs. However, levels of several well-known mitochondrial proteases as well as of their targets (Deshwal et al., 2020) – which was used as a readout for their activity – remained stable upon ageing. This result suggested that the general activity of mitochondrial proteases did not change with age (**Figure 3.20a**) and that they were not responsible for the lower CiC levels. In support of this finding, CiC has not been yet identified as a target of any known mitochondrial protease in any known system.

Apart from mitochondrial proteases, two other mitochondrial quality control mechanisms regulate levels of mitochondrial proteins via targeted degradation: autophagy and lysosomal degradation. Therefore, I investigated if any of these two mechanisms was responsible for CiC degradation upon ageing. For this, BM-MSCs were treated with bafilomycin (BafA1), which is a well-known inhibitor of autophagy, or with E64d that blocks lysosomal activity. Analysis of CiC levels after treatment with these two compounds revealed that while BafA1 did not increase CiC levels in aged BM-MSCs, treatment with E64d restored levels of CiC in aged BM-MSCs (**Figure 3.20b**), suggesting that lysosomal activity was important for the degradation of CiC in aged cells. If that was indeed the case, CiC would get degraded in the active lysosomes of aged cells, whereas it would accumulate in these organelles after inhibition of their activity by E64d. To test this hypothesis, control and E64d-treated old cells were co-stained with antibodies against CiC and LAMP2, which is a lysosomal marker. Remarkably, levels of LAMP2 remained stable upon ageing, arguing that there was no total increase in the lysosomal activity and content (**Figure 3.20c**). CiC and LAMP2 co-localized to a greater extent in old E64d-treated cells, compared to the control old cells, confirming that in aged BM-MSCs CiC was degraded in the lysosomes (**Figure 3.20d**). Notably, although inhibition of the lysosomal activity in

aged cells restored CiC levels and resulted in accumulation of CiC in the lysosomes, E64d treatment of young cells did not affect CiC levels and localization (**Figures 3.20e-3.20f**), indicating that lysosomal degradation of CiC occurs specifically in aged BM-MSCs.

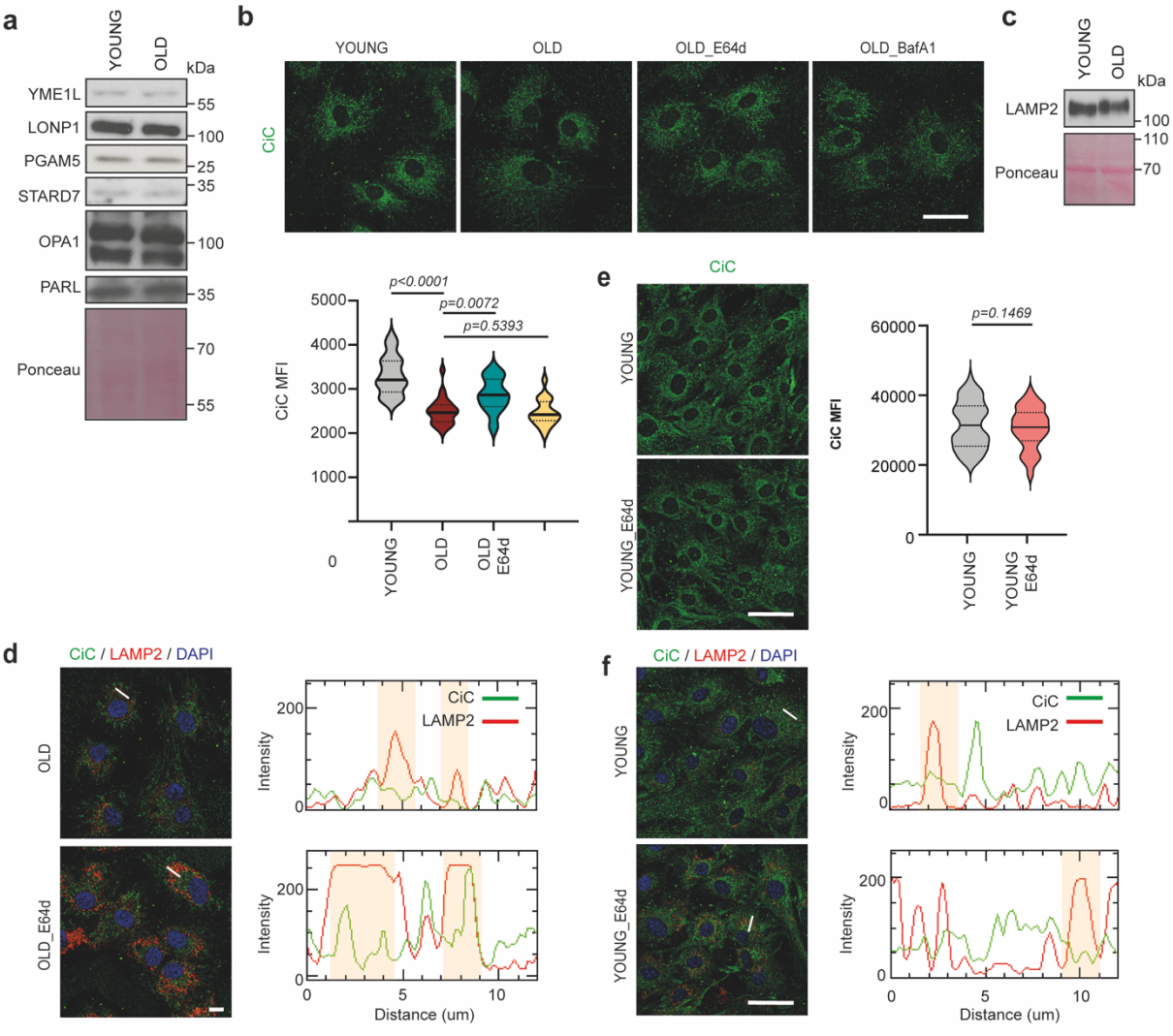

Figure 3.20. Lysosomal degradation of CiC in aged BM-MSCs. (**a**) Representative immunoblots for YMEL1, LONP1, PGAM5, STARD7, OPA1 and PARL proteins. Ponceau S was used as loading control. (**b**) Representative images after immunostaining against CiC and quantification of MFI in young and aged control cells, following indicating treatments. Nuclei were stained with DAPI. Scale bar, 10 um. (**c**) Representative immunoblot for LAMP2 in young and aged BM-MSCs. Ponceau S was used as loading control. (**d**) Representative images after immunostaining of cells from (**a**) against CiC and LAMP2 (right) and intensity plots of line scans showing the intensity of CiC (green line) and LAMP2 (red line); (left). Shaded regions highlight the CiC signal in areas with increased lysosomal intensity. Nuclei were stained with DAPI. Scale bar, 10 um. (**e**) Representative images after immunostaining against CiC and

quantification of MFI in young control and young E64d-treated cells. Nuclei were stained with DAPI. Scale bar, 50 um. (**f**) Representative images after immunostaining of cells from (**e)** against CiC and LAMP2 (right) and intensity plots of line scans, as described in (**d**); (left). Nuclei were stained with DAPI. Scale bar, 50 um.

3.5.3 Mitochondrial-derived vesicles deliver CiC to lysosomes for degradation in aged BM-MSCs

Lysosomal degradation of the inner mitochondrial membrane proteins has been described as one potential function of mitochondrial-derived vesicles (MDVs) (Soubannier et al., 2012a). Mitochondrial quality control via MDVs is believed to occur in mildly stressed mitochondria, as an initial stress response, to prevent total mitochondrial degradation through mitophagy. To address whether MDVs played a role in the mito-lysosomal transport of CiC, young and aged BM-MSCs were observed under the electron microscope; interestingly, I identified vesicles displaying the described characteristics for MDVs (Sugiura et al., 2014); in particular, double-membrane vesicles in close proximity or budding off mitochondria were easily detectable in aged BM-MSCs, while their abundance was much lower in young cells (**Figure 3.21a**). This finding suggested that CiC could indeed be degraded in aged BM-MSCs via the MDV-lysosomal pathway.

An increase in the MDV content also argued for an increase in mitochondrial stress levels in aged cells – a phenomenon that has been well documented over the last decades (López-Otín et al., 2013). However, stress levels should not exceed the level at which mitophagy would be activated to remove dysfunctional and damaged mitochondria. In line with this hypothesis, there was no major change in mitochondrial DNA content and mitochondrial membrane potential (**Figures 3.21b-3.21c**). By contrast, I observed an increase in mitochondrial fragmentation of aged cells both by electron microscopy and by TOMM20 immunostaining (**Figures 3.21d-3.21e**). This phenotype has been linked to mild mitochondrial stress (Willems et al., 2015; Wu et al., 2011). Given that aged cells fulfilled all known criteria for formation of MDVs, which were also detected under the electron microscope, I last sought to validate the cargo selectivity of the MDVs in aged BM-MSCs.

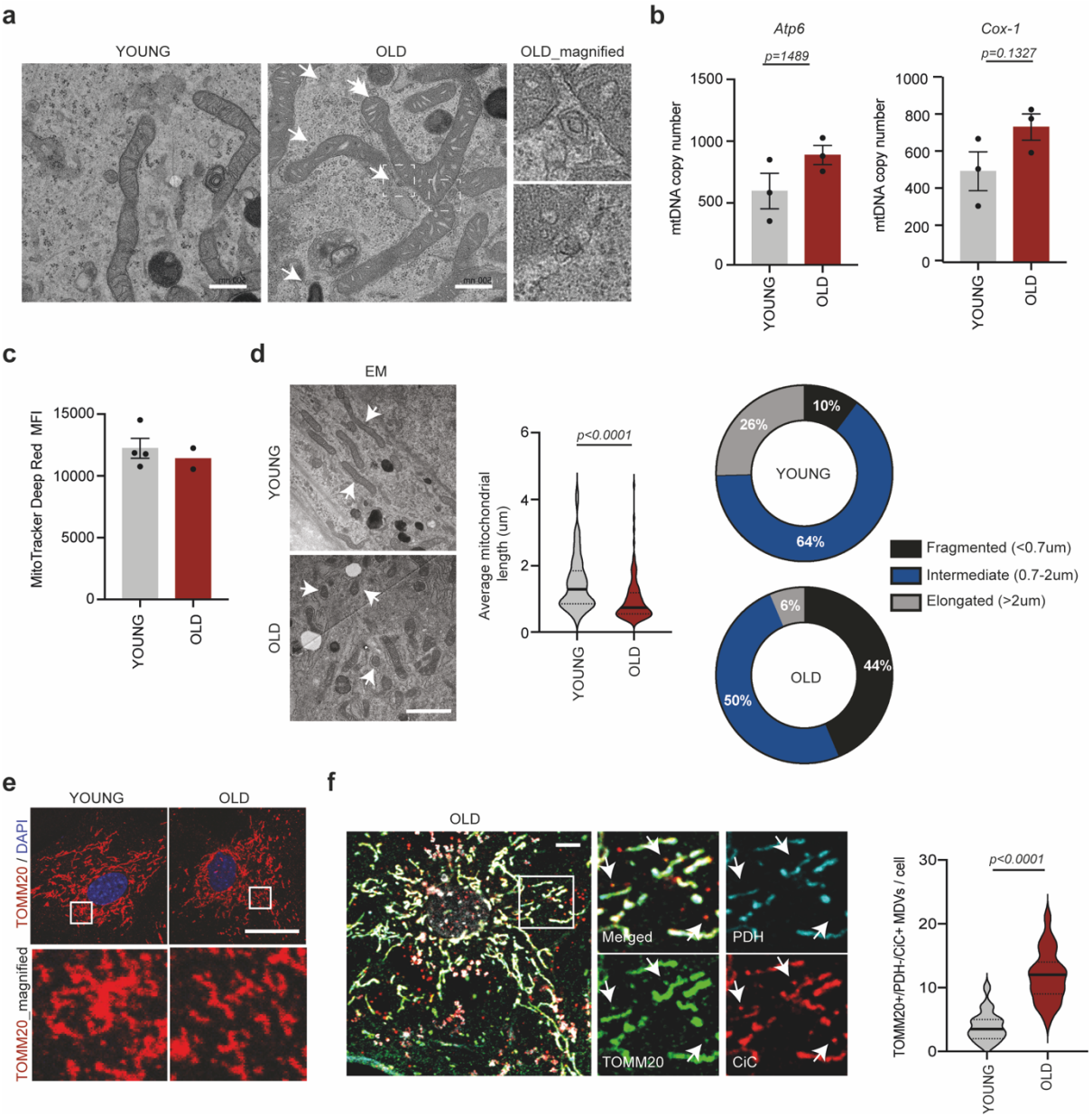

Figure 3.21. MDVs transfer CiC to lysosomes for degradation. (**a**) Representative images of MDVs highlighted with arrows, in young and aged cells and higher magnification of the areas in the boxes. Scale bars, 500 nm. (**b**) Quantification of mtDNA content in young and aged cells by qRT-PCR analysis of the mitochondrial DNA-encoded *Atp6* and *Cox-1* genes. Nuclear DNA-encoded *β-actin* expression levels were used as an internal control, for normalization. (**c**) MFI of young and aged cells after staining with MitoTracker Deep Red FM dye. n = 4 biologically independent replicates for young mice and n = 2 biologically independent replicates for old mice. (**d**) Representative images of mitochondria in young and aged BM-MSCs, analysis of the average mitochondrial length and manual classification of mitochondria into three categories: fragmented (length<0.7 um), intermediate (length:0.7-0.2 um) and elongated (length>0.2 um). Scale bar, 2 um. (**e**) Representative images after TOMM20 staining of young and aged cells. Nuclei were stained with DAPI. Higher magnification of areas within the box is shown in the panel below each image. Scale bar, 25 um. (**f**) Representative images after immunostaining

against TOMM20, CiC and PDH and higher magnification of the area in the box (left) and quantification of TOMM2+/PDH-/CiC+ MDVs (right). Nuclei were stained with DAPI. Scale bar, 8 um.

While we still lack a detailed understanding of the mechanisms driving MDV generation and cargo incorporation, MDVs are usually characterized by their proximity to mitochondria, their defined and uniform size of 70–150 nm and the presence or absence of specific mitochondrial membrane proteins. The two main classes of MDVs that have been best-characterized so far are TOMM20+/ PDH− and TOMM20−/PDH+ MDVs (Sugiura et al., 2014). Thus, aged cells were stained with antibodies against CiC, TOMM20 and PDH proteins. Of note, I did not observe PDH+/TOMM20− MDVs carrying CiC in any of the two age groups. However, aged BM-MSCs showed a strong increase in the number of CiC+/TOMM20+/PDH− MDVs compared to young cells. This indicated that in aged BM-MSCs, CiC was indeed incorporated exclusively into TOMM20+/PDH− MDVs (**Figure 3.21f**). The increase in CiC-containing MDVs correlated well with the enhanced lysosomal degradation of CiC, suggesting that CiC levels might indeed be regulated upon ageing via MDV-mediated lysosomal degradation.

In sum, these data demonstrate that the age-dependent decrease in CiC levels is a consequence of enhanced protein turnover, mediated via the mitochondrial quality control pathway that involves lysosomal degradation through MDVs. Collectively, these results provide a previously unknown physiological role for the MDVs and establish a tight, age-associated connection between mitochondrial quality control, chromatin and stem cell fate, whereby CiC acts as a critical mediator of the mito-nuclear communication.

3.6 The CiC–histone acetylation axis is conserved in human BM-MSCs

The reduction in the osteogenic differentiation potential upon ageing is a main contributor to the increased risk of osteoporosis with age (Phetfong et al., 2016). To test if the described pathway is also conserved in humans, I used human BM-MSCs derived from the bone marrow, upon hemiarthroplasty or total hip arthroplasty (Corrigan et al., 2019), and I analyzed CiC and histone acetylation levels. Similar to the observations in murine aged BM-MSCs, CiC levels were decreased in old individuals suffering from osteoporosis, compared to young healthy individuals (**Figure 3.22a**). As a consequence of lower CiC levels and decreased cytosolic acetyl-CoA, histone H3 acetylation levels were lower in the old individuals (**Figure 3.22b**). These data suggest that the CiC–histone acetylation link is conserved in humans, with age-dependent reduction in CiC levels resulting in decreased histone acetylation and lower chromatin plasticity.

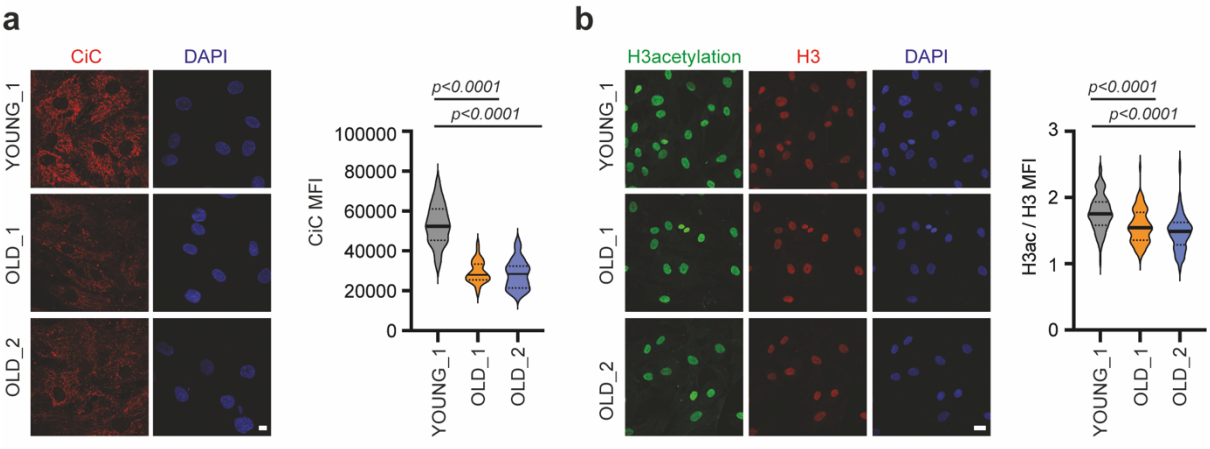

Figure 3.22. The CiC–histone acetylation-cell fate axis is conserved in human BM-MSCs. (**a**) Representative images and quantification of MFI after immunostaining against CiC of young and aged cells. Nuclei were stained with DAPI. Scale bar, 10 um. (**b**) Representative images and quantification of MFI after immunostaining against H3ac and H3 of young and aged cells. MFI of histone H3 was used as an internal control for normalization. Nuclei were stained with DAPI.
Scale bar, 25 um.

Part II: Citrate Carrier impacts the mito-nuclear communication and impairs osteogenesis in response to oxygen stress

3.7 Normoxia impairs osteogenesis via changes on the epigenome

3.7.1 Permanent osteogenesis defects upon exposure to normoxia

Given the critical role of oxygen in the regulation of energy metabolism, I next sought to explore how oxygen concentration impacts the metabolism-chromatin-stemness axis. For this, BM-MSCs were isolated from the bone marrow of young mice, following the process described above. Isolated and FACS-sorted BM-MSCs were then divided into two groups, of which one was cultured permanently under 2% O_2 (hereafter referred to also as hypoxia or low oxygen), whereas the other one was transferred to 21% O_2 (hereafter referred to also as normoxia or high oxygen), as outlined in **Figure 3.23**. Since short, acute exposure to normoxia is a stress factor for BM-MSCs (Peterson et al., 2011), I decided to describe the long-term effects of the oxygen-driven changes in BM-MSC biology. Therefore, the isolated BM-MSCs were cultured under these two different oxygen conditions for 7 days, before downstream analyses. During this 7-day-period, cells would have been adapted to the high oxygen environment, while the metabolic and epigenetic alterations would have been already established.

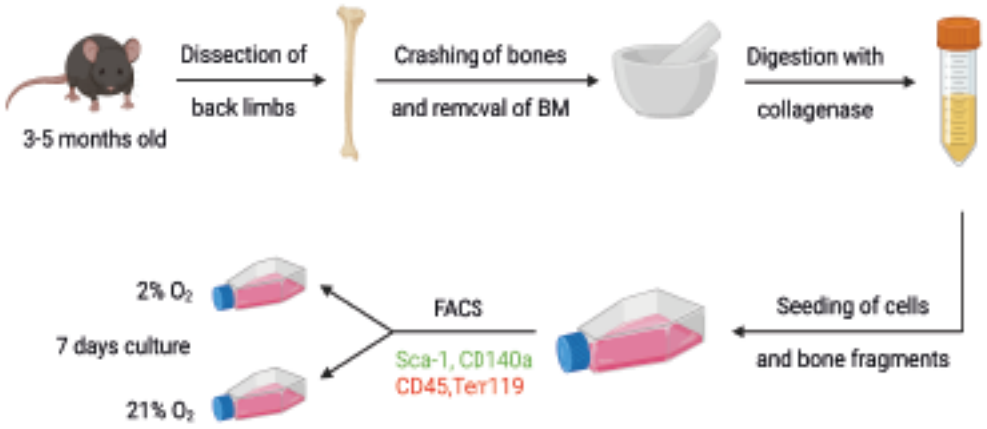

Figure 3.23. Isolation and culture scheme of BM-MSCs derived from the bone endosteum. Schematic representation demonstrating the isolation protocol and the culture conditions of BM-MSCs isolated from the back limbs of young (~3-5 months old) mice. After collection of the limbs, clean bones

were cut into small pieces, which were then treated with collagenase for 1 hour at 37°C. Cells and bone fragments were seeded in flasks and incubated for 10 days under 2% O_2. On day 10, I performed cell sorting using flow cytometry; I selected the CD45-/Ter-119-/Sca-1+/CD140a+ mesenchymal stem cell population. The isolated population was then split into two groups: one was transferred back to hypoxia, whereas the other one was shifted to normoxia. Cells were cultured under these conditions for 7 days.

It is known that low oxygen levels promote stem cell quiescence, while normoxic conditions stimulate lineage commitment (Basciano et al., 2011; Fehrer et al., 2007; Santos et al., 2009). However, the effects of long-term normoxia in the differentiation balance have not been conclusive and there are only limited mechanistic insights into the underlying molecular processes. Interestingly, I found that *in vitro* culture of BM-MSCs under high oxygen conditions did not influence their capacity to give rise to adipocytes, as revealed by Oil Red O staining of hypoxia- and normoxia-cultured cells, after induction of adipogenesis (**Figure 3.24a**). In stark contrast, normoxia-cultured cells exhibited a dramatic loss in the osteogenic differentiation capacity (**Figure 3.24b**), indicating that high oxygen levels shifted the differentiation balance, at the expense of osteogenesis. Impressively, the normoxia-induced defects in osteogenesis are permanent, since transferring normoxia-cultured cells back to hypoxia was not able to restore their osteogenic differentiation potential (**Figure 3.24c**). In line with the skewed adipogenic differentiation, analysis of the oxygen-driven changes in the transcriptome profile of BM-MSCs showed that cells cultured under high oxygen conditions displayed lower expression of genes involved in processes such as ossification and *Wnt* signaling (**Figure 3.24d**).

Together, these data revealed that switching BM-MSCs from hypoxia to normoxia affects dramatically their function, leading to permanent defects in osteogenesis, similar to the phenotype observed in aged BM-MSCs.

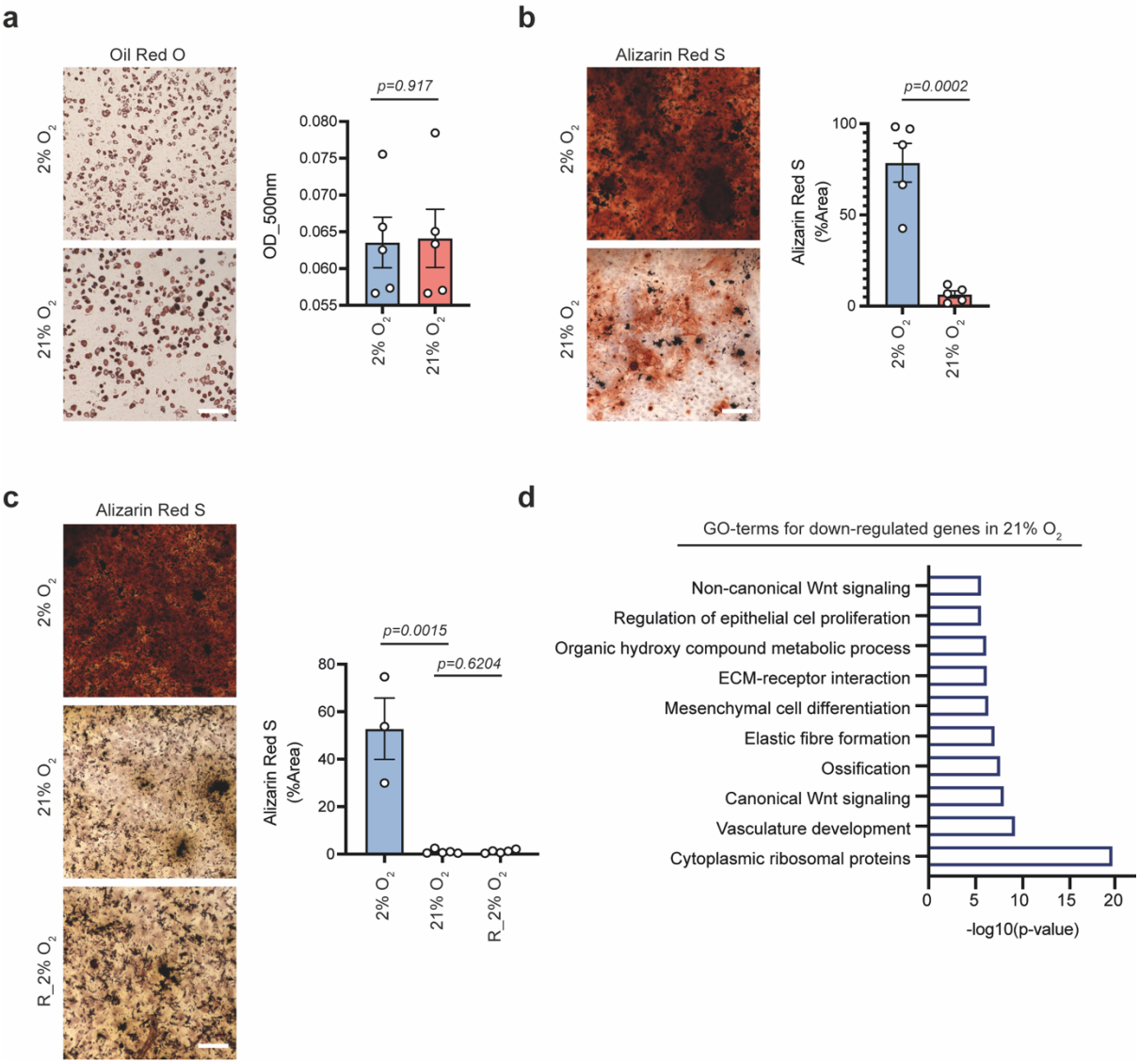

Figure 3.24. BM-MSCs lose their osteogenic capacity upon exposure to 21% O_2. (**a**) Representative images and quantification of Oil Red O Staining of hypoxia- and normoxia-cultured cells, 9 days after induction of adipogenesis. n=5 biologically independent replicates. (**b**) Representative images and quantification of Alizarin Red S staining of hypoxia- and normoxia-cultured cells, 12 days after induction of osteogenesis. n=5 biologically independent replicates. (**c**) Representative images and quantification of Alizarin Red S staining of hypoxic, normoxic and reversed hypoxic (R_2% O_2) cells, 12 days after induction of osteogenesis. Cells were exposed to 21% O_2 for 7 days and then moved back to 2% O_2, where osteogenesis was induced. (**d**) GO enrichment analysis for down-regulated genes upon exposure to normoxia, as identified by RNA-seq. n=3 biologically independent experiments. Scale bars, 500 um.

3.7.2 Normoxia leads to chromatin compaction

Since the normoxia-induced defects in BM-MSC osteogenic differentiation capacity were found to be dictated by the transcriptional output, I then sought to determine whether high oxygen levels impact the chromatin structure and the epigenetic landscape. ATAC-seq on hypoxia- and normoxia-cultured cells (**Figures 3.25a-3.25b**) revealed that switching BM-MSCs to normoxia led to profound chromatin re-arrangements. In particular, upon exposure to normoxia, ~23,537 sites changed significantly accessibility status (FDR <0.05); ~7,903 sites became more accessible whereas ~15,634 sites became more compact (**Figure 3.56c**), indicating that genome-wide, there were fewer accessible sites in the normoxia-cultured cells and suggesting that high oxygen promoted global chromatin compaction (**Figure 3.25d**).

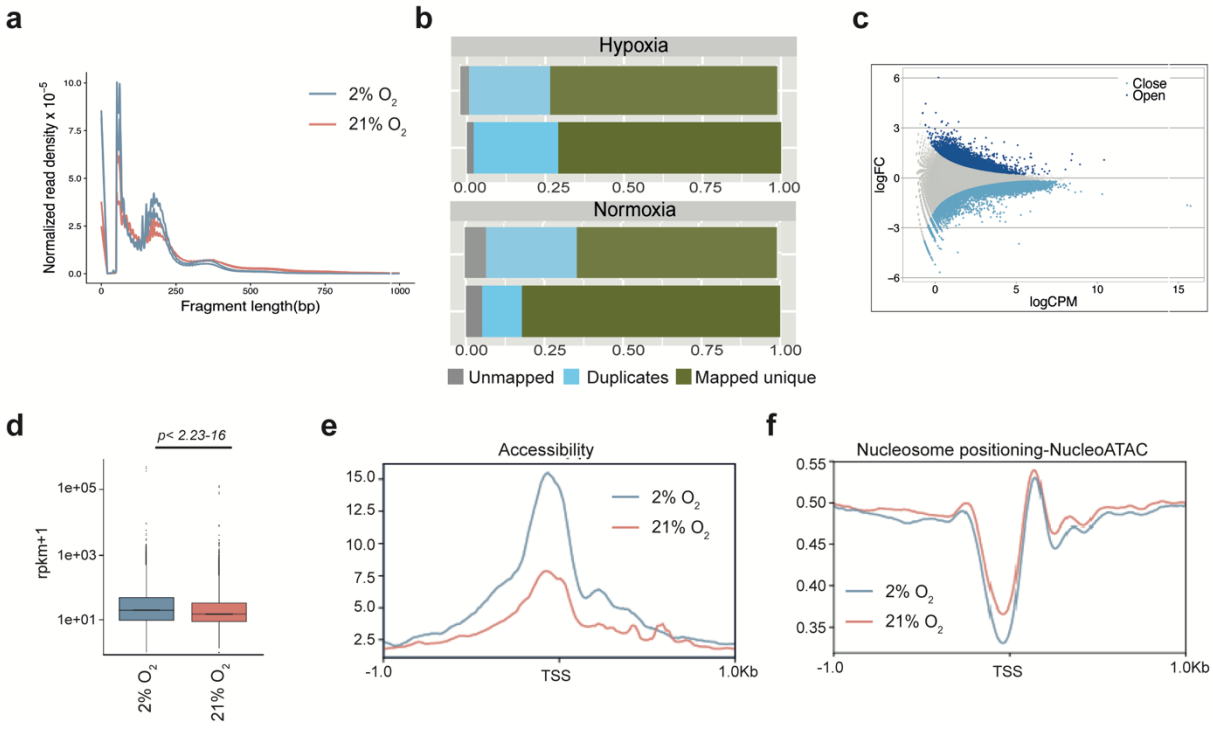

Figure 3.25. Normoxia results in lower chromatin accessibility. (**a**) Insert size distribution of each single ATAC-seq library. (**b**) Mapping statistics for each individual ATAC-seq library. (**c**) MA-plot showing opening and closing peaks upon shift to high oxygen, as determined by ATAC-seq. (**d**) Overall genome accessibility expressed as RPKM values measured by ATAC-seq. The y axis is scaled to log10 for visualization purposes. (**e**) Metaplot of ATAC-seq reads over the TSS of all protein-coding genes. (**f**) NucleoATAC metaplot to map position of all nucleosomes around the TSS of all protein-coding genes.

Plotting accessibility over the TSS, to interrogate whether the observed alterations in the chromatin accessibility would influence gene transcription, showed that gene promoters in normoxia-cultured cells displayed a strong decrease in chromatin accessibility (**Figure 3.25e**). Likewise, applying the NucleoATAC algorithm on the ATAC-seq dataset to profile nucleosome occupancy over the TSS (Schep et al., 2015), confirmed that shifting BM-MSCs to 21% O_2 led to higher nucleosome density at the promoter region (**Figure 3.25f**).

3.7.3 Lower histone acetylation correlates with chromatin compaction in normoxia-cultured BM-MSCs

Given that chromatin accessibility correlates with histone acetylation (Tessarz and Kouzarides, 2014), the findings of a more compact chromatin landscape upon culturing of BM-MSCs under high oxygen conditions, motivated me to investigate further whether this phenotype was linked to reduced histone acetylation levels. Therefore, I compared changes in histone H3 acetylation levels between hypoxia- and normoxia-cultured cells and found that normoxia-cultured cells displayed lower histone H3 acetylation in comparison to hypoxia-cultured cells (**Figure 3.26**). Of note, the loss of histone acetylation that occured after switching cells to normoxia was also confirmed by SILAC-Mass Spectrometry analysis (SILAC-MS) (data not shown).

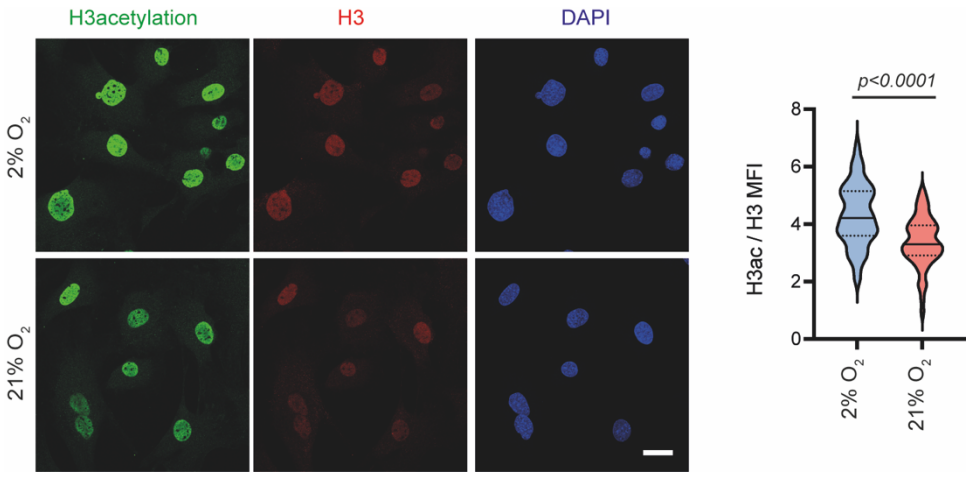

Figure 3.26. Loss of histone acetylation under high oxygen conditions. (**a**) Representative images and quantification of MFI after immunostaining against H3ac and H3 of hypoxic and normoxic cells. MFI of histone H3 was used as internal control, for normalization. Nuclei were stained with DAPI. Scale bar, 25 um.

Together, these results suggest that normoxia impairs histone acetylation and chromatin accessibility, leading to transcriptional changes that are responsible for the reduced osteogenic capacity of normoxia-cultured BM-MSCs.

3.8 High oxygen alters the cellular energetic profile

3.8.1 Changes in the epigenetic-related metabolites upon exposure to normoxia

The strong decrease in the levels of histone acetylation that was induced by high oxygen motivated me to further investigate how the histone acetylation profile was established in hypoxia- and normoxia-cultured cells. As discussed above, several metabolites have been found to influence the activity of epigenetic writers, erasers and readers, suggesting a tight crosstalk between metabolism and chromatin (Cai et al., 2011; Wellen et al., 2009). Therefore, in order to explain the normoxia-induced changes on the chromatin landscape and the transcriptional output, I compared the levels of epigenetic-related metabolites between hypoxia- and normoxia-cultured cells. Unexpectedly, acetyl-CoA levels were higher in normoxia-cultured cells (**Figure 3.27a**), contradicting their reduced histone H3 acetylation levels (**Figure 3.26).** Of note, the lower histone H3 acetylation was not due to differential regulation of the CBP histone acetyltransferase (**Figure 3.27b**).

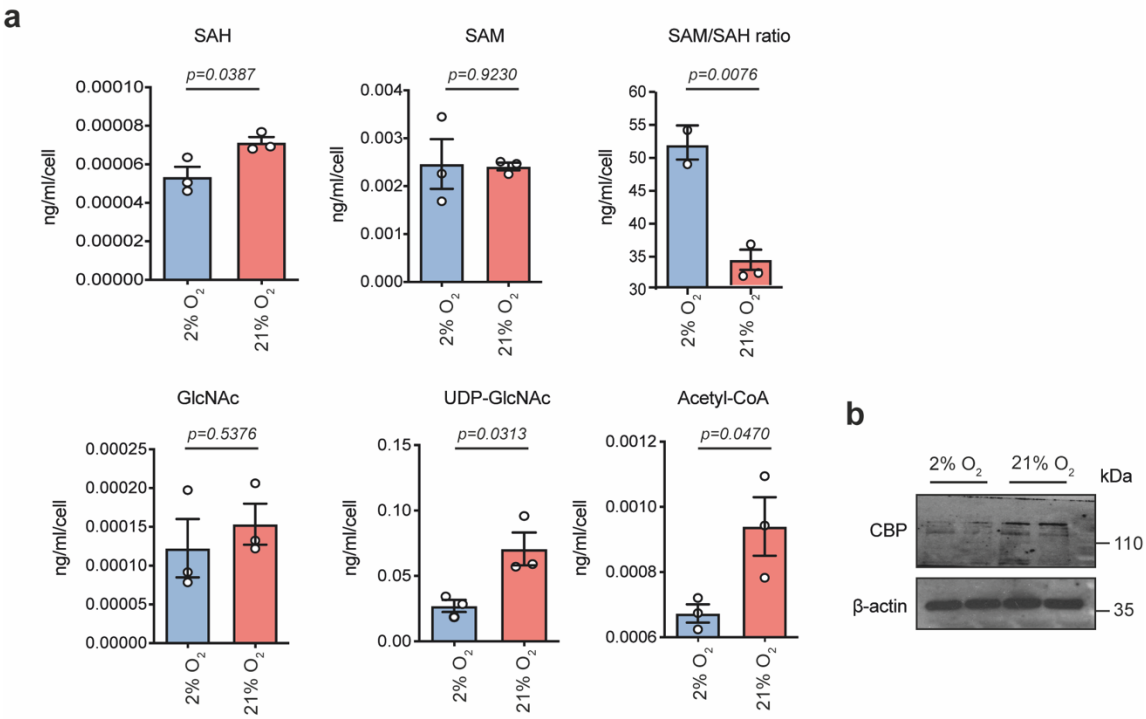

Figure 3.27. Changes in the levels of epigenetic-related metabolites. (**a**) Liquid chromatography Mass spectrometry (LC-MS) analysis of several metabolites in hypoxia- and normoxia-cultured cells.

(**b**) Representative immunoblot for CBP in hypoxia- and normoxia-cultured cells. β-actin was used as loading control.

Therefore, I next sought to explore how the BM-MSC metabolic states are altered in response to high oxygen and whether oxygen-induced activation of specific metabolic pathways could explain the accumulation of acetyl-CoA in normoxia-cultured cells.

3.8.2 Suppression of glycolysis in normoxia-cultured cells

To study how the BM-MSC energetic profile was changed during cell culture in normoxic conditions, leading to the observed differences in the abundance of epigenetic-related metabolites, I initially investigated alterations in glycolysis, since this is the prefered metabolic pathway of uncommitted stem cells. Therefore, I compared glucose consumption and lactate secretion to monitor changes in glycolysis, on day 2, day 4 and day 7 of normoxia culture. Cells shifted to normoxia consumed glucose and secreted lactate to a lower extent than cells maintained constantly under hypoxic conditions (**Figure 3.28a**), suggesting that normoxia-cultured cells did not depend heavily on glycolysis. The shift away from glycolysis upon switch to normoxia was also evident at the transcriptomic level, whereby qRT-PCR analysis revealed lower expression levels of the key glycolytic enzymes *Hk2*, *Pfk1*, *Pgk1* and *Pgam1* (**Figure 3.28b**). Supporting the oxygen-induced down-regulation of glycolysis, normoxia-cultured BM-MSCs displayed decreased extracellular acidification rate (ECAR), which is indicative of the cellular glycolytic activity (**Figure 3.28c**).

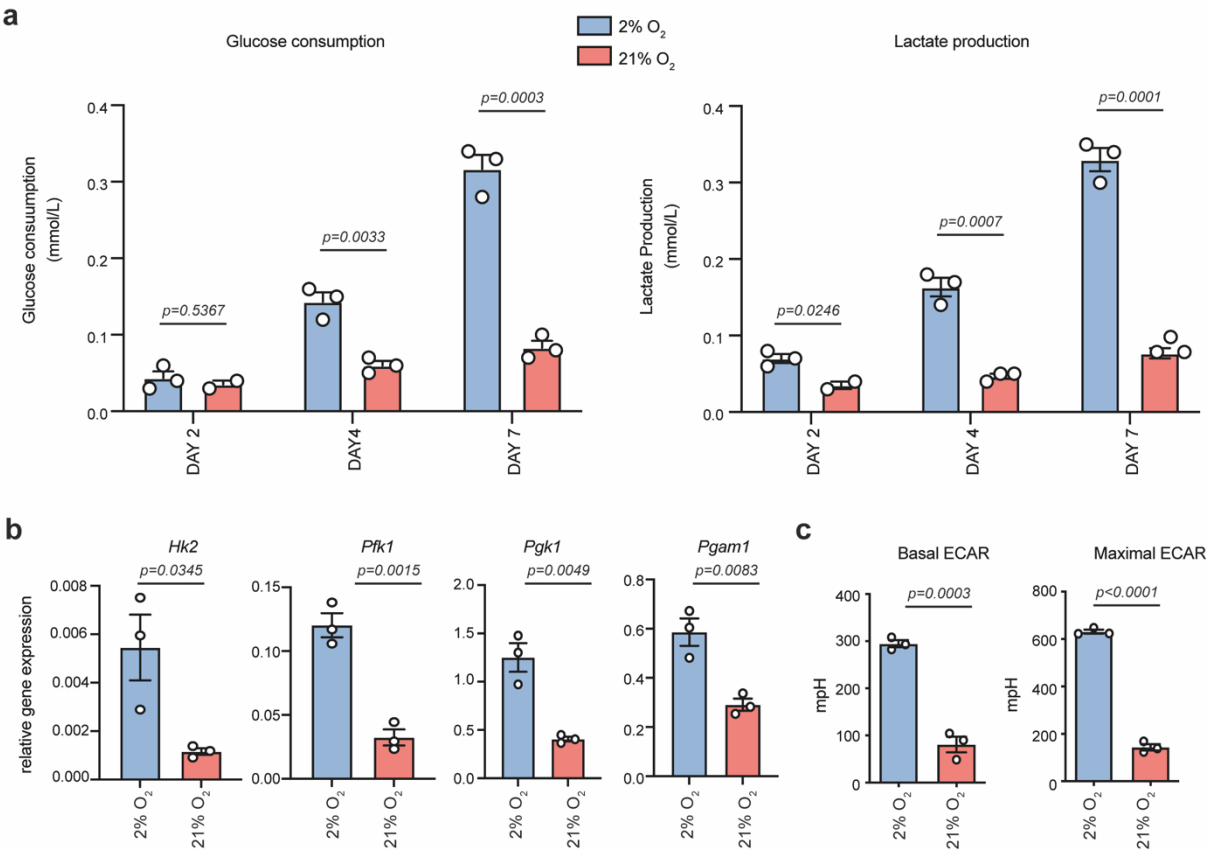

Figure 3.28. Normoxia suppresses glycolysis of BM-MSCs. (**a**) Glucose consumption and lactate production measured in the media of hypoxia- and normoxia-cultured cells using the Vi-Cell MetaFLEX instrument. (**b**) qRT-PCR analysis of glycolytic genes. *β-actin* was used as an internal control for normalization. (**c**) Basal (left) and maximal (right) ECAR in hypoxia- and normoxia-cultured BM-MSCs.

3.8.2 High oxygen stimulates mitochondrial metabolism

Since BM-MSC culture under high oxygen conditions promoted suppression of glycolysis, I next focused on the oxygen-induced changes in mitochondrial metabolism and function. Mitochondrial structure is related to mitochondrial activity, with glycolytic cells containing more fragmented mitochondria which become more elongated and tubular in the actively respiring cells (Pietilä et al., 2012; Sánchez-Aragó et al., 2013). Therefore, mitochondrial morphology of hypoxia and normoxia-cultured cells was observed using confocal and electron microscopy. Both approaches showed that the mitochondrial shape remained unaffected upon shift to normoxia (**Figure 3.29a**), with BM-MSCs cultured in both oxygen environments containing a mixed population of punctuated and elongated mitochondria. However, normoxia-cultured cells exhibited increased mitochondrial mass (**Figure 3.29b**), suggesting a potential upregulation of

mitochondrial respiration. To functionally test this, mitochondrial respiration of hypoxia- and normoxia-cultured cells was measured using SeaHorse assay. Indeed, normoxia-cultured cells displayed higher OCR, confirming increased mitochondrial activity and OXPHOS (**Figure 3.29c**).

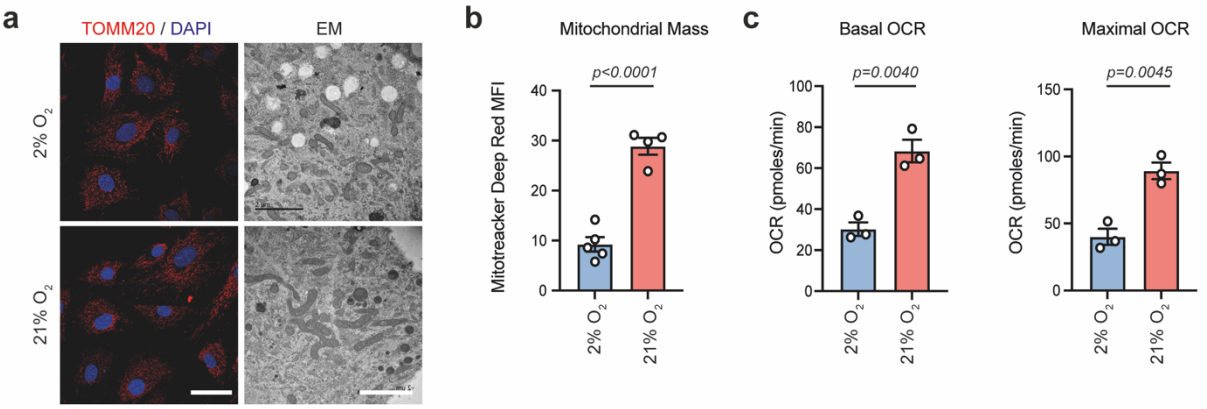

Figure 3.29. Induction of mitochondrial respiration under normoxia. (**a**) Representative images after immunostaining of hypoxia- and normoxia-cultured cells against TOMM20 (left panel) and electron microscopy images of mitochondria (right panel). Nuclei were stained with DAPI. Scale bars, 75 um in confocal images and 2 um in EM images. (**b**) MFI of hypoxia- and normoxia-cultured cells after staining with the MitoTracker Deep Red FM dye. n = 4 biologically independent experiments. (**c**) Basal (left) and maximal (right) OCR in hypoxia- and normoxia-cultured BM-MSCs.

3.8.3 Impaired lipid biosynthesis in normoxia-cultured cells

Lipid metabolism is tightly linked to mitochondrial activity and oxidative metabolism. Therefore, next I studied whether the shift in oxygen tension affected the BM-MSC lipid content. Indeed, Nile Red staining of lipid droplets revealed a dramatic loss of lipids in normoxia-cultured cells, which was also confirmed by electron microscopy (**Figure 3.30a**). The reduced lipid content in normoxia-cultured cells could be explained either by higher lipid consumption and/or by impaired lipogenesis. Hence, I initially sought to explore whether normoxia induced fatty acid oxidation. Notably, a potential increase in FAO would also explain the higher levels of acetyl-CoA in normoxia-cultured cells. To compare the endogenous β-oxidation rate of BM-MSCs cultured under the two different oxygen environments, cells were treated with etomoxir, which inhibits the CPT-1 enzyme and blocks FAO. Mitochondrial respiration was then measured in control and treated cells. Etomoxir treatment did not affect basal and maximal OCR in normoxia-cultured cells, suggesting that these cells did not rely

more heavily on endogenous FAO than the hypoxia-cultured BM-MSCs (**Figure 3.30b**). Next, to study the impact of high oxygen on lipid biosynthesis, I compared the levels of FASN and ACC1 enzymes between hypoxia- and normoxia-cultured cells. Impressively, levels of both proteins were strongly decreased upon shift to high oxygen (**Figure 3.30c**), indicating that acetyl-CoA entrance into the lipid biogenesis pathway was inhibited under normoxia. Furthermore, levels of SREBP1, which is the major regulator of lipid biosynthesis (Horton et al., 2002), were dramatically reduced in normoxia-cultured cells, explaining the lower lipid content of these cells (**Figure 3.30d**).

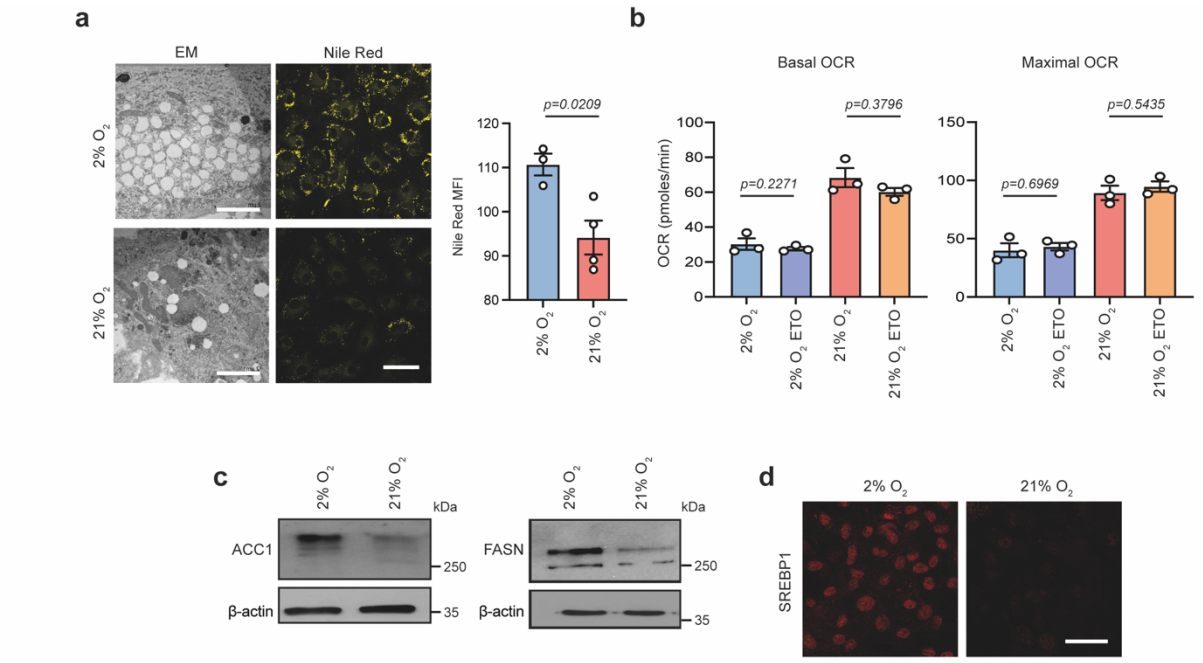

Figure 3.30. Normoxia impairs lipid biosynthesis. (**a**) Representative images and quantification of lipid droplets after observing cells under the electron microscope (left) and after staining lipids with Nile Red (right). Scale bars, 2 um for electron microscopy images and 50 um for confocal images. (**b**) Basal (left) and maximal (right) OCR in hypoxia- and normoxia-cultured BM-MSCs, after treatment with etomoxir. (**c**) Representative immunoblots for FASN and ACC1 enzymes in hypoxia- and normoxia-cultured cells. β-actin was used as loading control. (**d**) Representative images of hypoxia- and normoxia-cultured cells after immunostaining against SREBP1. Scale bar, 50 um.

Altogether, these results indicate that although hypoxia-cultured cells are primarily glycolytic, a shift in the oxygen tension results in profound metabolic alterations including suppression of glycolysis, induction of mitochondrial metabolism, and SREBP1-mediated impaired lipogenesis.

3.9 High oxygen impairs export of mitochondrial acetyl-CoA to the cytosol

Normoxia-cultured BM-MSCs contained higher levels of acetyl-CoA (**Figure 3.27a)**, but they exhibited reduced lipid biogenesis and histone hypo-acetylation, which are the two main routes of the cytosolic acetyl-CoA. Thus, one potential explanation for these observations could be a decrease in the cytosolic acetyl-CoA pool. However, levels of ACLY and ACS enzymes, which are involved in the cytosolic/nuclear generation of acetyl-CoA (Cai et al., 2011; Mews et al., 2017), were stable upon culture in high oxygen tension (**Figure 3.31a**). Hence, I speculated that normoxia-cultured BM-MSCs exhibited impaired acetyl-CoA export from mitochondria to the cytosol.

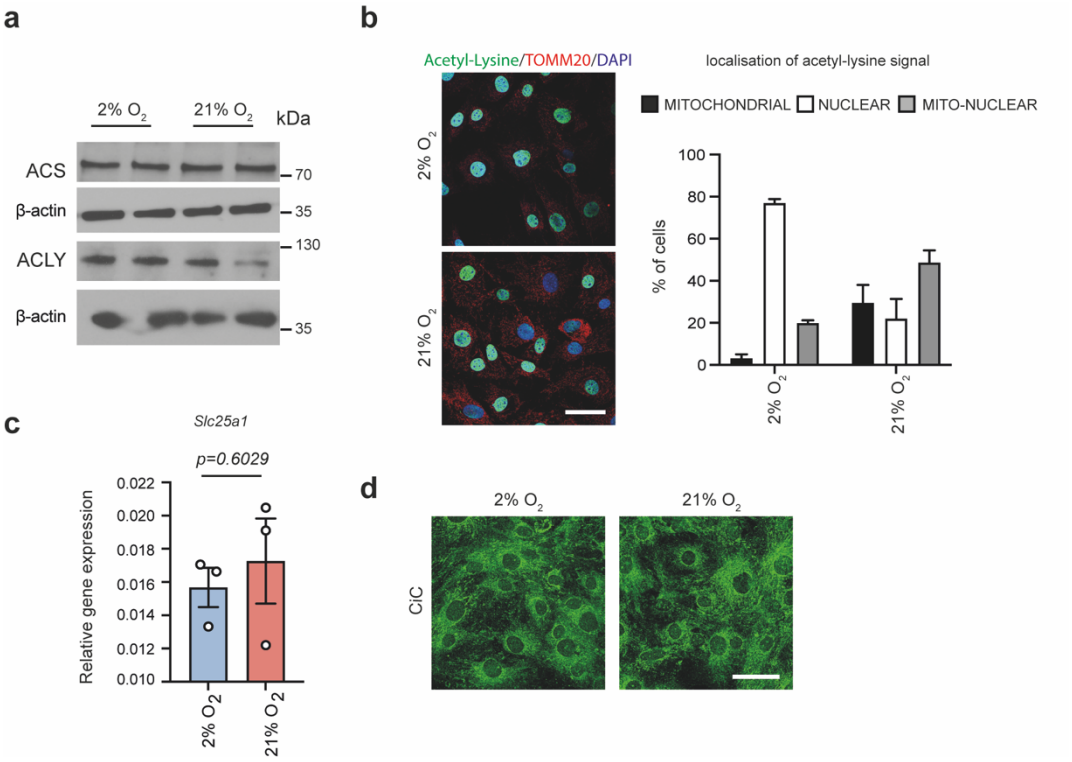

Figure 3.31. Trapping of acetyl-CoA inside mitochondria in normoxia-cultured BM-MSCs. (**a**) Representative immunoblots for ACS and ACLY enzymes in hypoxia- and normoxia-cultured cells. β-actin was used as loading control. (**b**) Representative images after immunostaining of hypoxia- and normoxia-cultured cells against acetyl-Lysine and TOMM20, and assessment of acetyl-Lysine signal localization, as described above. Nuclei were stained with DAPI. Scale bar, 25 um. (**c**) qRT-PCR analysis of *Slc25a1* gene, which encodes the Citrate Carrier. β-actin was used as internal control for normalization. (**d**) Representative images after immunostaining of hypoxia- and normoxia-cultured cells against CiC. Scale bars, 50 um.

To test this hypothesis, hypoxia- and normoxia-cultured BM-MSCs were stained with an antibody against acetyl-Lysine, whereas TOMM20 was used in parallel, as a counterstain for mitochondria. Impressively, there was a strong, oxygen-dependent change in the localization of the acetyl-Lysine signal, shifting from nuclear to mitochondrial during culture of cells to high oxygen (**Figure 3.31b**). This indicates that acetyl-CoA was indeed trapped inside mitochondria of normoxia-cultured BM-MSCs. These findings could be explained by lower levels and/or activity of the mitochondrial CiC, which is responsible for the export of mitochondrial acetyl-CoA to the cytosol. However, CiC expression and protein levels remained stable after switch to normoxia (**Figures 3.31c-3.31d**), as shown by qRT-PCR and immunostaining experiments, respectively. Therefore, I next hypothesized that although normoxia does not impact CiC levels, it might alter its activity. To functionally test this hypothesis, hypoxia-cultured cells were treated with BTA, which inhibits CiC, and normoxia-cultured cells were treated with acetate that can be used to generate cytosolic acetyl-CoA. Impressively, modulating CiC activity directly impacted lipid biogenesis and histone acetylation (**Figures 3.32a-3.32b**). In fact, CiC inhibition in hypoxia-cultured cells reduced the lipid content and promoted mitochondrial localization of the acetyl-Lysine signal, mimicking the effects of high oxygen. By contrast, acetate supplementation of normoxia-cultured BM-MSCs was sufficient to rescue the oxygen-induced defects in lipogenesis and restored the nuclear localization of the acetyl-Lysine signal.

Last, I sought to determine whether acetyl-CoA trapping within mitochondria of normoxic cells was responsible for the oxygen-induced osteogenic defects. Strikingly, supplementation of normoxia-cultured BM-MSCs with acetate prior to induction of osteogenesis, was sufficient to restore their impaired osteogenic capacity (**Figure 3.32c**).

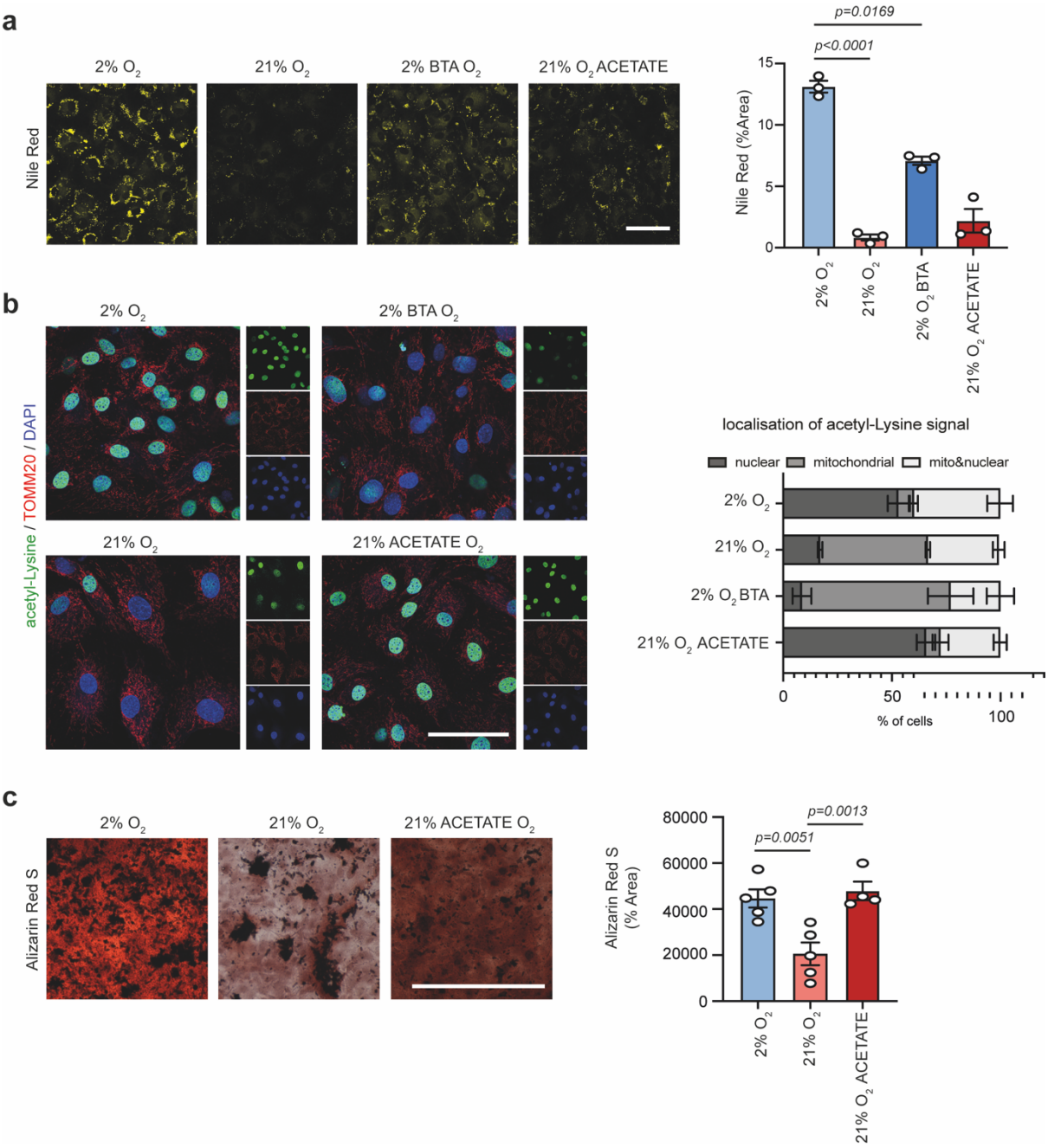

Figure 3.32. Modulating CiC activity affects lipogenesis, acetylation and osteogenesis. (a) Representative images and quantification of MFI after Nile Red staining of hypoxic control and BTA-treated cells and of normoxic control and acetate-treated cells. Scale bar, 25 um. (**b**) Representative images after immunostaining of hypoxic control and BTA-treated cells and normoxic control and acetate-treated cells against acetyl-Lysine and TOMM20, and assessment of acetyl-Lysine signal localization, as described above. Nuclei were stained with DAPI. Scale bar, 75 um. (**c**) Representative images and quantification of Alizarin Red S staining of control hypoxic and normoxic cells and of normoxic acetate-treated cells, 12 days after induction of osteogenesis. Scale bar, 500 um.

Together, these data demonstrate that shifting cells from low to high oxygen results in acetyl-CoA trapping within the mitochondria, This leads to lower levels of cytosolic acetyl-CoA that could be used for lipogenesis and histone acetylation. Decreased histone acetylation on promoters and enhancers of osteogenic genes impairs osteogenesis, which is restored upon acetate treatment.

Chapter 4

Discussion

In the present thesis, I studied the flux of acetyl-CoA from mitochondria to the nucleus and I explored how the mito-nuclear interaction is affected by different stimuli and how this impacts BM-MSC activity. First, I asked how ageing influences the metabolism-chromatin-stem cell fate axis. Secondly, I investigated the role of the oxygen tension in the regulation of stem cell function, focusing on the underlying metabolic and epigenetic determinants.

4.1 Ageing perturbs the mito-nuclear communication via degradation of CiC

The data presented here suggest a model (**Figure 4.1**) whereby the ageing-driven changes in chromatin structure lead to transcriptional alterations that are responsible for the decreased osteogenic potential of aged BM-MSCs. I showed that upon ageing, there is a shift in the subcellular localization of acetyl-CoA, which affects the epigenetic landscape. In particular, aged BM-MSCs exhibit compartmentalized acetyl-CoA localization in the mitochondria, as a result of enhanced MDV-lysosomal degradation of CiC. Strikingly, restoring histone acetylation, and thus chromatin plasticity, is sufficient to improve the impaired osteogenic capacity of aged BM-MSCs, highlighting the fundamental role of CiC in the regulation of the metabolism–chromatin–osteogenesis axis.

I found that BM-MSCs from both age groups differentiate efficiently into adipocytes, whereas aged BM-MSCs show impaired osteogenic capacity (**Figure 3.3**). Skewed adipogenic differentiation of aged BM-MSCs at the expense of osteogenesis correlates with previous reports of increased adipocyte content in the aged bone marrow and has been associated with the development of osteoporosis (Kim et al., 2012; Zhou et al., 2008).

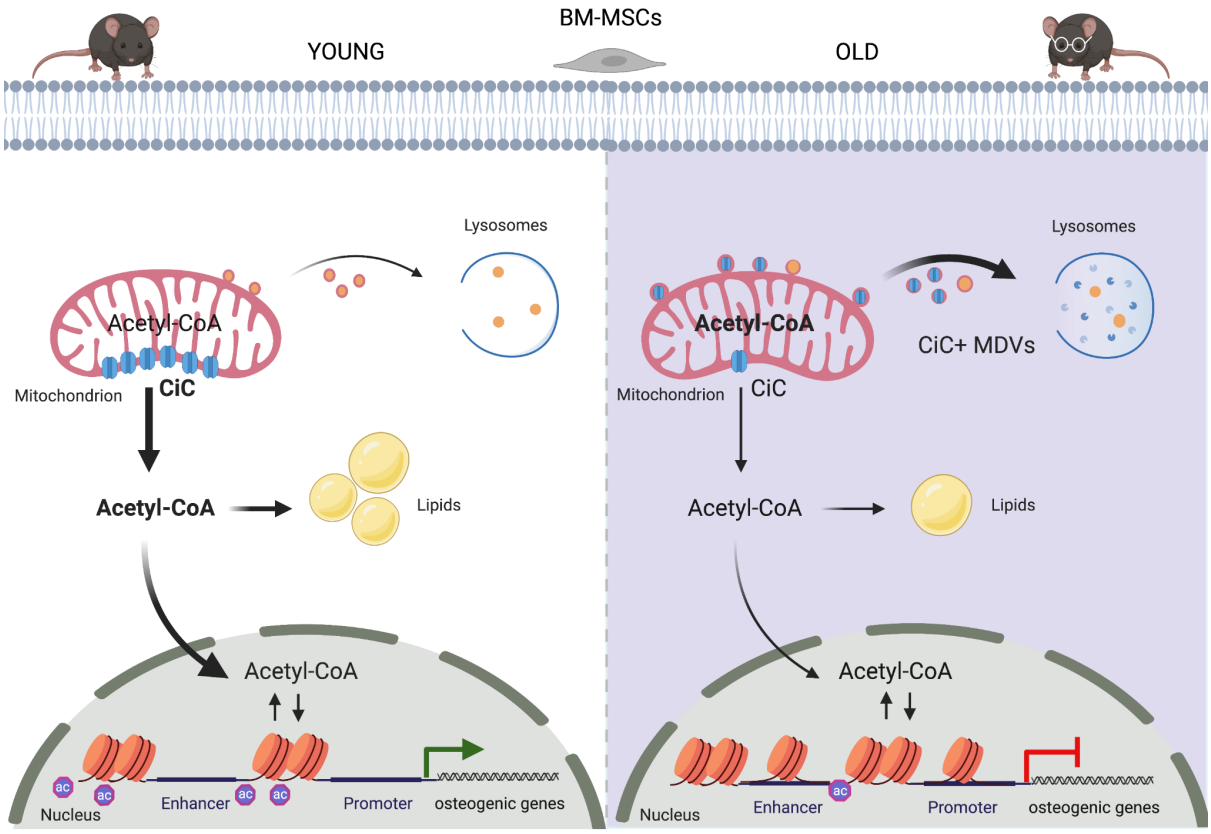

Figure 4.1. Model for CiC-mediated connection among mitochondrial quality control, chromatin and stemness in aged BM-MSCs. Upon ageing, BM-MSCs show chromatin compaction and altered profile of histone marks on promoters and enhancers of genes associated with osteogenesis, resulting in lower osteogenic capacity. Despite global reduction in histone acetylation, aged BM-MSCs contain high levels of acetyl-CoA. However, in the aged cells, acetyl-CoA is trapped inside mitochondria and cannot be used for histone acetylation and lipid biogenesis. This is due to the lower levels of CiC, which, in the aged cells, is incorporated into MDVs and transported to lysosomes for degradation. Therefore, the impaired export of acetyl-CoA from the mitochondria to the cytosol is responsible for the lower osteogenic potential of aged cells. Strikingly, acetate supplementation of aged cells rescues levels of histone acetylation and osteogenic differentiation capacity of aged cells.

The observation of enhanced adipogenic capacity of purified BM-MSCs contradicts two recent studies which reported that the gene expression profile of BM-MSCs is similar to that of osteocytes (Meyer et al., 2016; Rauch et al., 2019). In contrast to those findings, my data clearly indicate that differentiation to osteoblasts requires a more advanced level of chromatin remodeling. For instance, despite the fact that BM-MSCs isolated from young mice show active enhancer marking on osteogenesis-involved genes (**Figure 3.9**), extended duration of osteogenic induction is required for efficient differentiation to osteoblasts, contrary to the short duration of adipogenesis.

One likely explanation for the contradicting phenotypes is the different BM-MSC population used in each study. Opposite to the plastic adherence protocol for purification of a heterogenous BM-MSC population from bone marrow, I isolated and selected a homogenous and highly purified population of BM-MSCs that resides in the bone endosteum (Houlihan et al., 2012) and possesses trilineage differentiation potential both *in vitro* and *in vivo (Morikawa et al., 2009)*. This multilineage differentiation capacity is also supported by the epigenetic data, which showed active enhancer marking not only for genes involved in osteogenesis, but also for those associated with adipogenesis.

Citrate has been recently suggested to be important throughout the osteogenic differentiation of BM-MSCs, via regulating α-KG production (Hofmann et al., 2012; Morganti et al., 2020; Quinn et al., 2013). However, I showed here that the export of mitochondrial acetyl-CoA to the cytosol in the form of citrate is the critical step for BM-MSC osteogenesis. Remarkably, CiC activity is required before induction of differentiation, as evidenced by the fact that short-term inhibition of CiC function, before stimulation of differentiation, is sufficient to impair osteogenesis (**Figure 3.15e**). These data indicate that the cytosolic/nuclear acetyl-CoA pool is indispensable for the establishment of a plastic chromatin state and the acetylation of enhancers and promoters of osteogenic genes, which allow BM-MSCs to initiate a dedicated differentiation program. These results underscore the central role of the acetyl-CoA-mediated chromatin remodeling in the regulation of stem cell fate decisions. Furthermore, I demonstrated that rescuing CiC levels in aged BM-MSCs is sufficient to restore histone acetylation and improves osteogenesis in aged BM-MSCs (**Figure 3.16**), highlighting the importance of CiC in the metabolism-dependent chromatin rearrangements that are required for efficient BM-MSC lineage commitment.

BM-MSCs balance adipogenesis and osteogenesis by integrating environmental signals with their transcriptional regulatory network, and several signaling pathways modulate the chromatin landscape to fine-tune gene expression. Therefore, investigating the crosstalk between epigenetic modifications and other cellular pathways is of high importance, particularly in the context of ageing, where many cellular processes undergo profound alterations (López-Otín et al., 2013). In this study,

I revealed that mitochondrial CiC is degraded in the lysosomes of aged BM-MSCs (**Figure 3.20**), which influences stem cell fate decisions via changing the chromatin architecture. Notably, lysosomal CiC degradation in aged BM-MSCs correlates with an increase in the number of MDVs (Sugiura et al., 2014) carrying CiC, and suggests that delivery of CiC to lysosomes is probably mediated via MDVs (**Figure 3.21**). Why is MDV formation enhanced upon ageing? So far, MDVs have been studied in cells only after artificial induction of mitochondrial oxidative stress (Soubannier et al., 2012a, 2012b). Interestingly, ageing is usually accompanied by increased levels of mitochondrial stress (Baker and Haynes, 2011; Hill and Van Remmen, 2014), which could potentially explain the upregulation of MDV formation in aged BM-MSCs. Nonetheless, given that the MDV area of research is just emerging, future work in this field will shed more light on the specific mechanisms driving CiC selection and incorporation into MDVs.

Finally, the striking observation that short-term treatment of BM-MSCs with acetate resulted in increased histone acetylation and chromatin accessibility, leading to enhanced osteogenic differentiation potential, suggests that intervening in the chromatin landscape represents a promising approach to rejuvenate aged BM-MSCs.

4.2 High oxygen impairs osteogenesis in a CiC-dependent manner

The cellular microenvironment plays a critical role in the regulation of stem cell fate decisions. In this study, I investigated the role of oxygen tension on the metabolism-chromatin interplay and I explored how oxygen-induced changes in this interaction impact BM-MSC differentiation. Several studies have investigated the effects of oxygen levels in osteogenesis, with remarkably contrasting results (Lennon et al., 2001; Robins et al., 2005; Malladi et al., 2006). Nevertheless, I found that normoxia elicits permanent defects on the osteogenic differentiation potential of BM-MSCs (**Figure 3.24**), indicating that high oxygen alters dramatically the stem cell function. Many studies have shed light into the mechanisms by which oxygen tension impacts stem cell differentiation and it is now well-established that one means by which oxygen concentration regulates stem cell fate decisions is through metabolic rewiring (Leijten et al., 2014). Furthermore, specific metabolic pathways have been associated with distinct cellular states; in fact, quiescent stem cells are predominantly glycolytic, whereas differentiating cells are actively respiring. However, so far it has not been clear how chromatin and the epigenome change on a global scale upon shift in the oxygen tension and how this correlates with alterations in central metabolic pathways and stem cell activity. Here, I showed that high oxygen leads to decreased glycolysis and enhanced mitochondrial respiration (**Figures 3.28-3.29**). A similar metabolic rewiring upon exposure of cells to high oxygen levels has been described in other studies, where hypoxia was found to promote glycolysis in a HIF-1-dependent manner. Such a profound change in the cellular energetic profile could potentially alter stem cell fate decisions, given the critical role of glycolysis in the maintenance of stem cell function (Hu et al., 2016).

Indeed, the oxygen-driven upregulation of mitochondrial metabolism leads to generation of higher amounts of acetyl-CoA (**Figure 3.27**). Mitochondria-produced acetyl-CoA gets exported to the cytosol via CiC and is then used for lipid biogenesis and acetylation of cytosolic/nuclear proteins. Surprisingly, I found that although normoxia-cultured cells contain higher acetyl-CoA levels, they exhibit reduced histone acetylation and impaired lipogenesis. These results indicated that acetyl-CoA remains

trapped within the mitochondria of normoxia-cultured cells, diminishing the cytosolic acetyl-CoA pool. The final outcome of these events is chromatin compaction and loss of the transcriptional program that is required to induce osteogenesis. Acetate supplementation of cells cultured in normoxia is sufficient to rescue the histone acetylation and lipogenesis levels, and to restore the osteogenic differentiation potential (**Figure 3.32**).

But why do normoxia-cultured BM-MSCs exhibit such a compartmentalised acetyl-CoA distribution? I found that CiC levels in these cells are comparable to the levels in hypoxia-cultured BM-MSCs (**Figure 3.31d**). Therefore, impaired export of acetyl-CoA from the mitochondria to the cytosol could be due to a decrease in CiC activity. Notably, CiC protein has been found to undergo post-translational modifications, with CiC acetylation altering CiC function (Palmieri et al., 2015). Given that normoxia promotes mitochondrial respiration and OXPHOS, which lead to production of high acetyl-CoA levels, one potential explanation for the acetyl-CoA trapping could be enhanced CiC acetylation. However, this hypothesis needs to be further investigated and experiments are currently performed to confirm that normoxia-cultured BM-MSCs exhibit altered CiC acetylation levels.

Remarkably, the observed changes in the metabolism-chromatin-stemness axis upon exposure to high oxygen mimic the phenotype of aged BM-MSCs. Together, these studies highlight the central role of CiC-mediated spatial acetyl-CoA localization in inter-organelle communication that is required for efficient osteogenesis. Noteworthy, the impact of high oxygen on stem cell function is stronger than that of physiological ageing, as indicated by the fact that the loss of chromatin accessibility is much more prominent when shifting cells to high oxygen (**Figures 3.6, 3.25**). This indicates that high oxygen levels represent an extreme condition and serve as a stress factor to the cells. Notably, murine and human BM-MSCs that have been adapted to atmospheric oxygen conditions are still capable to differentiate into adipocytes, osteocytes and chondrocytes (Houlihan et al., 2012; Morikawa et al., 2009; Yang et al., 2018b). However, it is clear from the data presented here and from previously published work that the osteogenic differentiation potential of BM-MSCs is strongly enhanced under low oxygen conditions, and that normoxia shifts the differentiation balance, favoring

adipogenesis and in the expense of osteogenesis (Basciano et al., 2011; Georgi et al., 2015). Therefore, the potential effects of oxygen tension on stem cell activity should be taken into account not only when planning experiments using somatic stem cells, but especially during clinical trials.

Chapter 5

Conclusions and perspectives

5. Conclusions and perspectives

Considerable progress in the field of metabolism in the last years has revealed its crucial impact on stem cell biology. Uncommitted BM-MSCs rely almost exclusively on glycolysis in order to generate ATP, whereas their differentiation is coupled to oxidative metabolism. Recent studies have unraveled the powerful role of niche factors in the energetic profile of BM-MSCs (Scadden, 2006). However, the extent to which these factors shape the metabolic signature at each developmental stage and the exact mechanisms involved in this process need to be further investigated. Furthermore, secretion of high amounts of lactate by the highly glycolytic BM-MSCs questions the basic biological principle of energy economy. Two recent studies uncovered the importance of the glycolysis-produced lactate in the activation of hair follicle stem cells and intestinal stem cells (Flores et al., 2017; Schell et al., 2017). Therefore, whether in BM-MSCs the disposed lactate can be taken up from neighboring cells to fuel their metabolism or it simply represents an inevitable cost of the low-ROS-generating glycolysis is definitely worth further research.

One mechanism by which metabolism regulates the transcriptional output and thus stem cell identity is via modulating the activity of epigenetic enzymes (Kaelin and McKnight, 2013; Lu and Thompson, 2012; Pouikli and Tessarz, 2021; Reid et al., 2017). Research into the field of metabolism and chromatin interaction in the regulation of BM-MSC fate decisions has only started to reveal the exact role of each metabolite. Hence, further work is required to understand how to promote a coordinated mito-nuclear communication and how to accurately manipulate energy metabolism in order to regulate the epigenome in favor of stem cell proliferation and cellular homeostasis. Furthermore, one key-question in the field of metabolism and chromatin interplay is how mitochondrial and cytosolic metabolites can be sensed by nuclear enzymes to alter gene transcription. Some of these metabolites can easily diffuse in the nucleus via the pores of the nuclear membrane, constantly circulating between the cytosol and the nucleus. Yet, the exact mechanisms maintaining the two distinct pools of metabolites, preventing unnecessary inter-organelle translocation, remain elusive. In line with this, although some metabolites can easily bypass the mitochondrial and nuclear membranes, recent evidence suggests that the cytosol and

the nucleus differ in their biophysical properties, such as the stiffness and the elasticity (Dahl et al., 2008; Guilak et al., 2000; Lombardi et al., 2011). This might generate a physical barrier in the inter-organelle trafficking of metabolites, and control of their spatial availability could actively participate in the metabolic regulation of chromatin states.

Beyond their critical role in energy production and generation of intermediate metabolites, mitochondria participate in the maintenance of tissue integrity and organismal health, through regulation of protein homeostasis. Targeted degradation of misfolded or damaged mitochondrial proteins by the UPS, the UPR^{mt} and the co-ordinated function of mitochondrial proteases and chaperones are among the best-studied mechanisms of mitochondrial quality control and have been found to promote mitochondrial health. A relatively novel pathway that contributes to the surveillance of the mitochondrial proteome encompasses the mitochondrial-derived vesicles (MDVs). MDVs bud off mitochondria carrying oxidized proteins that are delivered, mostly, to lysosomes for degradation (McLelland et al., 2014; Soubannier et al., 2012a, 2012b). This MDV-mediated quality control of the mitochondrial proteome is found to be activated prior to induction of mitophagy, in order to avoid complete elimination of the entire organelle. Although recent studies have highlighted the role of MDVs in several physiological processes, including signaling and immunity (Cadete et al., 2016; Todkar et al., 2021), further work is required to elucidate the precise stimuli driving MDV formation and the molecular mechanisms facilitating scission, transport and cargo delivery to the destined organelles.

Notably, the metabolism-chromatin-stem-cell axis plays a critical role in BM-MSC biology during ageing and age-associated diseases. Recent technological advances in the field of multi-omics allow simultaneous analysis of the genome, the transcriptome, the proteome and the metabolome; integration of the multilayer information reveals the complex underlying changes during the course of stem cell differentiation and ageing. However, the limited amount of BM-MSCs represents a technical challenge and up-to-date single-cell-based methods might be a valuable tool to gain insight into the molecular principles governing stem cell and organismal ageing.

Although we have only recently started to describe the changes that occur in the epigenome of ageing stem cells, it is clear that the chromatin structure plays a fundamental role in regulating stem cell fate and function. Interestingly, since modulation of the chromatin architecture enables targeted alteration of the transcriptional output and ultimately of the stem cell identity, the epigenome might represent an attractive target for the development of strategies to direct stem cell fate decisions towards specific lineages. Of note, such approaches could be combined with the currently used methods during autologous stem cell therapy. For instance, *ex vivo* manipulation of the chromatin landscape to enhance stem cell activity prior to HSC and BM-MSC transplantation could potentially increase the efficiency of stem cell therapies. Proof-of-concept studies have been published in the last few years using model organisms to explore the potentially beneficial effects of such approaches. For example, inhibition of DNMTs by 5-AzaC has been used in various studies to enhance stem cell differentiation capacity of BM-MSCs purified from elderly humans (Kornicka et al., 2017; Yan et al., 2014). Furthermore, supplementation of BM-MSCs with the epigenetic-related metabolite α-KG improves osteogenesis in aged BM-MSCs. Mechanistically, α-KG elicits changes in the chromatin architecture, decreasing the abundance of repressive marks on the promoters of osteogenic genes (Wang et al., 2020b). In line with this, manipulating the intracellular metabolism by caloric restriction and/or pharmacological interventions, such as rapamycin and resveratrol treatment, alters the epigenome and impacts stem cell fate decisions.

With regards to the *ex vivo* manipulation of the chromatin and metabolic profile in order to direct stem cell fate decisions, attention should also be given to the oxygen conditions of cell culture. Oxygen tension has been an often-neglected parameter during cell culture, with cells residing normally in hypoxic tissues being cultured under high oxygen levels. Nevertheless, it is now evident that this may have detrimental effects on stem cell activity, increasing the risk of inefficient or failed stem cell therapies. Hence, mimicking the physiological oxygen conditions of the stem cell niche could enhance BM-MSC potential during clinical applications.

References

Acar, M., Kocherlakota, K.S., Murphy, M.M., Peyer, J.G., Oguro, H., Inra, C.N., Jaiyeola, C., Zhao, Z., Luby-Phelps, K., and Morrison, S.J. (2015). Deep imaging of bone marrow shows non-dividing stem cells are mainly perisinusoidal. Nature *526*, 126–130.

Ambrosi, T.H., Scialdone, A., Graja, A., Gohlke, S., Jank, A.-M., Bocian, C., Woelk, L., Fan, H., Logan, D.W., Schürmann, A., et al. (2017). Adipocyte Accumulation in the Bone Marrow during Obesity and Aging Impairs Stem Cell-Based Hematopoietic and Bone Regeneration. Cell Stem Cell *20*, 771–784.e6.

Andrzejewska, A., Lukomska, B., and Janowski, M. (2019). Concise Review: Mesenchymal Stem Cells: From Roots to Boost. Stem Cells *37*, 855–864.

Ayala-Cuellar, A.P., Kang, J.-H., Jeung, E.-B., and Choi, K.-C. (2019). Roles of Mesenchymal Stem Cells in Tissue Regeneration and Immunomodulation. Biomolecules & Therapeutics *27*, 25–33.

Baer, P.C., and Geiger, H. (2012). Adipose-Derived Mesenchymal Stromal/Stem Cells: Tissue Localization, Characterization, and Heterogeneity. Stem Cells International *2012*, 1–11.

Baker, B.M., and Haynes, C.M. (2011). Mitochondrial protein quality control during biogenesis and aging. Trends Biochem. Sci. *36*, 254–261.

Basciano, L., Nemos, C., Foliguet, B., de Isla, N., de Carvalho, M., Tran, N., and Dalloul, A. (2011). Long term culture of mesenchymal stem cells in hypoxia promotes a genetic program maintaining their undifferentiated and multipotent status. BMC Cell Biol. *12*, 12.

Bender, T., Lewrenz, I., Franken, S., Baitzel, C., and Voos, W. (2011). Mitochondrial enzymes are protected from stress-induced aggregation by mitochondrial chaperones and the Pim1/LON protease. Molecular Biology of the Cell *22*, 541–554.

Berger, S.L. (2007). The complex language of chromatin regulation during transcription. Nature *447*, 407–412.

Bertout, J.A., Patel, S.A., and Celeste Simon, M. (2008). The impact of O2 availability on human cancer. Nature Reviews Cancer *8*, 967–975.

Bhalla, K., Hwang, B.J., Dewi, R.E., Ou, L., Twaddel, W., Fang, H.-B., Vafai, S.B., Vazquez, F., Puigserver, P., Boros, L., et al. (2011). PGC1α Promotes Tumor Growth by Inducing Gene Expression Programs Supporting Lipogenesis. Cancer Research 71, 6888–6898.

Bielski, B.H.J., Richter, H.W., and Chan, P.C. (1975). SOME PROPERTIES OF THE ASCORBATE FREE RADICAL. Annals of the New York Academy of Sciences *258*, 231–237.

Bisaccia, F., De Palma, A., and Palmieri, F. (1989). Identification and purification of the tricarboxylate carrier from rat liver mitochondria. Biochim. Biophys. Acta 977, 171–176.

Bonyadi, M., Waldman, S.D., Liu, D., Aubin, J.E., Grynpas, M.D., and Stanford, W.L. (2003). Mesenchymal progenitor self-renewal deficiency leads to age-dependent osteoporosis in Sca-1/Ly-6A null mice. Proc. Natl. Acad. Sci. U. S. A. *100*, 5840–5845.

Bork, S., Pfister, S., Witt, H., Horn, P., Korn, B., Ho, A.D., and Wagner, W. (2010). DNA methylation pattern changes upon long-term culture and aging of human mesenchymal stromal cells. Aging Cell *9*, 54–63.

Braschi, E., Goyon, V., Zunino, R., Mohanty, A., Xu, L., and McBride, H.M. (2010). Vps35 Mediates Vesicle Transport between the Mitochondria and Peroxisomes. Current Biology *20*, 1310–1315.

Brunelle, J.K., Bell, E.L., Quesada, N.M., Vercauteren, K., Tiranti, V., Zeviani, M., Scarpulla, R.C., and Chandel, N.S. (2005). Oxygen sensing requires mitochondrial ROS but not oxidative phosphorylation. Cell Metabolism *1*, 409–414.

Buenrostro, J.D., Giresi, P.G., Zaba, L.C., Chang, H.Y., and Greenleaf, W.J. (2013). Transposition of native chromatin for fast and sensitive epigenomic profiling of open chromatin, DNA-binding proteins and nucleosome position. Nat. Methods *10*, 1213–1218.

Buettner, G.R., and Moseley, P.L. (1993). EPR Spin Trapping of Free Radicals Produced by Bleomycin and Ascorbate. Free Radical Research Communications *19*, s89–s93.

Buravkova, L.B., Andreeva, E.R., Gogvadze, V., and Zhivotovsky, B. (2014). Mesenchymal stem cells and hypoxia: Where are we? Mitochondrion *19*, 105–112.

Bustos, F., Sepúlveda, H., Prieto, C.P., Carrasco, M., Díaz, L., Palma, J., Lattus, J., Montecino, M., and Palma, V. (2017). Runt-Related Transcription Factor 2 Induction During Differentiation of Wharton's Jelly Mesenchymal Stem Cells to Osteoblasts Is Regulated by Jumonji AT-Rich Interactive Domain 1B Histone Demethylase. STEM CELLS *35*, 2430–2441.

Cadete, V.J.J., Deschênes, S., Cuillerier, A., Brisebois, F., Sugiura, A., Vincent, A., Turnbull, D., Picard, M., McBride, H.M., and Burelle, Y. (2016). Formation of mitochondrial-derived vesicles is an active and physiologically relevant mitochondrial quality control process in the cardiac system. J. Physiol. *594*, 5343–5362.

Cai, L., Sutter, B.M., Li, B., and Tu, B.P. (2011). Acetyl-CoA induces cell growth and proliferation by promoting the acetylation of histones at growth genes. Mol. Cell *42*, 426–437.

Cantó, C., Menzies, K.J., and Auwerx, J. (2015). NAD(+) Metabolism and the Control of Energy Homeostasis: A Balancing Act between Mitochondria and the Nucleus. Cell Metab. *22*, 31–53.

Caplan, A.I. (1991). Mesenchymal stem cells. J. Orthop. Res. *9*, 641–650.

Cappello, A.R., Guido, C., Santoro, A., Santoro, M., Capobianco, L., Montanaro, D., Madeo, M., Andò, S., Dolce, V., and Aquila, S. (2012). The mitochondrial citrate carrier (CIC) is present and regulates insulin secretion by human male gamete. Endocrinology 153, 1743–1754.

Catalina-Rodriguez, O., Kolukula, V.K., Tomita, Y., Preet, A., Palmieri, F., Wellstein, A., Byers, S., Giaccia, A.J., Glasgow, E., Albanese, C., et al. (2012). The mitochondrial citrate transporter, CIC, is essential for mitochondrial homeostasis. Oncotarget 3, 1220–1235.

Chandel, N.S., Maltepe, E., Goldwasser, E., Mathieu, C.E., Simon, M.C., and Schumacker, P.T. (1998). Mitochondrial reactive oxygen species trigger hypoxia-induced transcription. Proceedings of the National Academy of Sciences *95*, 11715–11720.

Chen, C.-T., Shih, Y.-R.V., Kuo, T.K., Lee, O.K., and Wei, Y.-H. (2008). Coordinated changes of mitochondrial biogenesis and antioxidant enzymes during osteogenic differentiation of human mesenchymal stem cells. Stem Cells *26*, 960–968.

Chesney, J. (2006). 6-Phosphofructo-2-kinase/fructose-2,6-bisphosphatase and tumor cell glycolysis. Current Opinion in Clinical Nutrition & Metabolic Care 9, 535–539.

Claeys, D., and Azzi, A. (1989). Tricarboxylate carrier of bovine liver mitochondria. Purification and reconstitution. J. Biol. Chem. 264, 14627–14630.

Cohen-Kfir, E., Artsi, H., Levin, A., Abramowitz, E., Bajayo, A., Gurt, I., Zhong, L., D'Urso, A., Toiber, D., Mostoslavsky, R., et al. (2011). Sirt1 Is a Regulator of Bone Mass and a Repressor of Sost Encoding for Sclerostin, a Bone Formation Inhibitor. Endocrinology *152*, 4514–4524.

Corrigan, M.A., Coyle, S., Eichholz, K.F., Riffault, M., Lenehan, B., and Hoey, D.A. (2019). Aged Osteoporotic Bone Marrow Stromal Cells Demonstrate Defective Recruitment, Mechanosensitivity, and Matrix Deposition. Cells Tissues Organs *207*, 83–96.

Couvillion, M.T., Soto, I.C., Shipkovenska, G., and Churchman, L.S. (2016). Synchronized mitochondrial and cytosolic translation programs. Nature *533*, 499–503.

Cullen, P.J., and Korswagen, H.C. (2012). Sorting nexins provide diversity for retromer-dependent

trafficking events. Nature Cell Biology *14*, 29–37.

Dahl, K.N., Ribeiro, A.J.S., and Lammerding, J. (2008). Nuclear shape, mechanics, and mechanotransduction. Circ. Res. *102*, 1307–1318.

Dai, Z., Ramesh, V., and Locasale, J.W. (2020). The evolving metabolic landscape of chromatin biology and epigenetics. Nature Reviews Genetics *21*, 737–753.

Derakhshani, M., Abbaszadeh, H., Movassaghpour, A.A., Mehdizadeh, A., Ebrahimi-Warkiani, M., and Yousefi, M. (2019). Strategies for elevating hematopoietic stem cells expansion and engraftment capacity. Life Sciences *232*, 116598.

Deshwal, S., Fiedler, K.U., and Langer, T. (2020). Mitochondrial Proteases: Multifaceted Regulators of Mitochondrial Plasticity. Annu. Rev. Biochem. *89*, 501–528.

Dobin, A., Davis, C.A., Schlesinger, F., Drenkow, J., Zaleski, C., Jha, S., Batut, P., Chaisson, M., and Gingeras, T.R. (2013). STAR: ultrafast universal RNA-seq aligner. Bioinformatics *29*, 15–21.

Dominici, M., Le Blanc, K., Mueller, I., Slaper-Cortenbach, I., Marini, F., Krause, D., Deans, R., Keating, A., Prockop, D., and Horwitz, E. (2006). Minimal criteria for defining multipotent mesenchymal stromal cells. The International Society for Cellular Therapy position statement. Cytotherapy *8*, 315–317.

Eguchi, M., Ozaki, E., Yamauchi, T., Ohta, M., Higaki, T., Masuda, K., Imoto, I., Ishii, E., and Eguchi-Ishimae, M. (2018). Manifestation of recessive combined D-2-, L-2-hydroxyglutaric aciduria in combination with 22q11.2 deletion syndrome. American Journal of Medical Genetics Part A 176, 351–358.

Endo, T., Yamano, K., and Kawano, S. (2011). Structural insight into the mitochondrial protein import system. Biochimica et Biophysica Acta (BBA) - Biomembranes *1808*, 955–970.

Etchegaray, J.-P., and Mostoslavsky, R. (2016). Interplay between Metabolism and Epigenetics: A Nuclear Adaptation to Environmental Changes. Molecular Cell *62*, 695–711.

Fallon, L., Bélanger, C.M.L., Corera, A.T., Kontogiannea, M., Regan-Klapisz, E., Moreau, F., Voortman, J., Haber, M., Rouleau, G., Thorarinsdottir, T., et al. (2006). A regulated interaction with the UIM protein Eps15 implicates parkin in EGF receptor trafficking and PI(3)K–Akt signalling. Nature Cell Biology *8*, 834–842.

Fang, L., Hemion, C., Pinho Ferreira Bento, A., Bippes, C.C., Flammer, J., and Neutzner, A. (2015). Mitochondrial function in neuronal cells depends on p97/VCP/Cdc48-mediated quality control. Frontiers in Cellular Neuroscience *9*.

Fehrer, C., Brunauer, R., Laschober, G., Unterluggauer, H., Reitinger, S., Kloss, F., Gülly, C., Gaßner, R., and Lepperdinger, G. (2007). Reduced oxygen tension attenuates differentiation capacity of human mesenchymal stem cells and prolongs their lifespan. Aging Cell *6*, 745–757.

Fiorese, C.J., Schulz, A.M., Lin, Y.-F., Rosin, N., Pellegrino, M.W., and Haynes, C.M. (2016). The Transcription Factor ATF5 Mediates a Mammalian Mitochondrial UPR. Current Biology *26*, 2037–2043.

Flores, A., Schell, J., Krall, A.S., Jelinek, D., Miranda, M., Grigorian, M., Braas, D., White, A.C., Zhou, J.L., Graham, N.A., et al. (2017). Lactate dehydrogenase activity drives hair follicle stem cell activation. Nat. Cell Biol. *19*, 1017–1026.

Friedenstein, A.J., Petrakova, K.V., Kurolesova, A.I., and Frolova, G.P. (1968). HETEROTOPIC TRANSPLANTS OF BONE MARROW. Transplantation *6*, 230.

Friedenstein, A.J., Chailakhjan, R.K., and Lalykina, K.S. (1970). THE DEVELOPMENT OF FIBROBLAST COLONIES IN MONOLAYER CULTURES OF GUINEA-PIG BONE MARROW AND SPLEEN CELLS. Cell Proliferation *3*, 393–403.

Friedenstein, A.J., Chailakhyan, R.K., Latsinik, N.V., Panasyuk, A.F., and Keiliss-Borok, I.V. (1974). Stromal cells responsible for transferring the microenvironment of the hemopoietic tissues. Cloning in

vitro and retransplantation in vivo. Transplantation *17*, 331–340.

Genchi, G., Spagnoletta, A., De Santis, A., Stefanizzi, L., and Palmieri, F. (1999). Purification and characterization of the reconstitutively active citrate carrier from maize mitochondria. Plant Physiol. 120, 841–848.

Georgi, N., Cillero-Pastor, B., Eijkel, G.B., Periyasamy, P.C., Kiss, A., van Blitterswijk, C., Post, J.N., Heeren, R.M.A., and Karperien, M. (2015). Differentiation of mesenchymal stem cells under hypoxia and normoxia: lipid profiles revealed by time-of-flight secondary ion mass spectrometry and multivariate analysis. Anal. Chem. *87*, 3981–3988.

Giacomello, M., Pyakurel, A., Glytsou, C., and Scorrano, L. (2020). The cell biology of mitochondrial membrane dynamics. Nature Reviews Molecular Cell Biology *21*, 204–224.

Gnoni, G.V., Priore, P., Geelen, M.J.H., and Siculella, L. (2009). The mitochondrial citrate carrier: metabolic role and regulation of its activity and expression. IUBMB Life *61*, 987–994.

Gomes, A.P., Price, N.L., Ling, A.J.Y., Moslehi, J.J., Montgomery, M.K., Rajman, L., White, J.P., Teodoro, J.S., Wrann, C.D., Hubbard, B.P., et al. (2013). Declining NAD Induces a Pseudohypoxic State Disrupting Nuclear-Mitochondrial Communication during Aging. Cell *155*, 1624–1638.

Greenberg, M.V.C., and Bourc'his, D. (2019). The diverse roles of DNA methylation in mammalian development and disease. Nature Reviews Molecular Cell Biology *20*, 590–607.

Guilak, F., Tedrow, J.R., and Burgkart, R. (2000). Viscoelastic properties of the cell nucleus. Biochem. Biophys. Res. Commun. *269*, 781–786.

Guzy, R.D., Hoyos, B., Robin, E., Chen, H., Liu, L., Mansfield, K.D., Simon, M.C., Hammerling, U., and Schumacker, P.T. (2005). Mitochondrial complex III is required for hypoxia-induced ROS production and cellular oxygen sensing. Cell Metab. *1*, 401–408.

Halvorsen, Y.C., Wilkison, W.O., and Gimble, J.M. (2000). Adipose-derived stromal cells—their utility and potential in bone formation. Int. J. Obes. *24*, S41–S44.

Hassan, M.Q., Tare, R., Lee, S.H., Mandeville, M., Weiner, B., Montecino, M., van Wijnen, A.J., Stein, J.L., Stein, G.S., and Lian, J.B. (2007). HOXA10 Controls Osteoblastogenesis by Directly Activating Bone Regulatory and Phenotypic Genes. Molecular and Cellular Biology *27*, 3337–3352.

Haynesworth, S.E., Goshima, J., Goldberg, V.M., and Caplan, A.I. (1992). Characterization of cells with osteogenic potential from human marrow. Bone *13*, 81–88.

Hemion, C., Flammer, J., and Neutzner, A. (2014). Quality control of oxidatively damaged mitochondrial proteins is mediated by p97 and the proteasome. Free Radical Biology and Medicine *75*, 121–128.

Hemming, S., Cakouros, D., Isenmann, S., Cooper, L., Menicanin, D., Zannettino, A., and Gronthos, S. (2014). EZH2andKDM6AAct as an Epigenetic Switch to Regulate Mesenchymal Stem Cell Lineage Specification. STEM CELLS *32*, 802–815.

Herlofsen, S.R., Bryne, J.C., Høiby, T., Wang, L., Issner, R., Zhang, X., Coyne, M.J., Boyle, P., Gu, H., Meza-Zepeda, L.A., et al. (2013). Genome-wide map of quantified epigenetic changes during in vitro chondrogenic differentiation of primary human mesenchymal stem cells. BMC Genomics *14*, 105.

Hill, S., and Van Remmen, H. (2014). Mitochondrial stress signaling in longevity: a new role for mitochondrial function in aging. Redox Biol *2*, 936–944.

Hlouschek, J., Hansel, C., Jendrossek, V., and Matschke, J. (2018). The mitochondrial citrate carrier (SLC25A1) sustains redox homeostasis and mitochondrial metabolism supporting radioresistance of cancer cells with tolerance to cycling severe hypoxia. Front. Oncol. *8*, 170.

Hofmann, A.D., Beyer, M., Krause-Buchholz, U., Wobus, M., Bornhäuser, M., and Rödel, G. (2012). OXPHOS supercomplexes as a hallmark of the mitochondrial phenotype of adipogenic differentiated human MSCs. PLoS One *7*, e35160.

Hong, S.Y., Ng, L.T., Ng, L.F., Inoue, T., Tolwinski, N.S., Hagen, T., and Gruber, J. (2016). The Role of Mitochondrial Non-Enzymatic Protein Acylation in Ageing. PLoS One *11*, e0168752.

Horton, J.D., Goldstein, J.L., and Brown, M.S. (2002). SREBPs: activators of the complete program of cholesterol and fatty acid synthesis in the liver. J. Clin. Invest. *109*, 1125–1131.

Houlihan, D.D., Mabuchi, Y., Morikawa, S., Niibe, K., Araki, D., Suzuki, S., Okano, H., and Matsuzaki, Y. (2012). Isolation of mouse mesenchymal stem cells on the basis of expression of Sca-1 and PDGFR-α. Nat. Protoc. *7*, 2103–2111.

Houtkooper, R.H., Williams, R.W., and Auwerx, J. (2010). Metabolic Networks of Longevity. Cell *142*, 9–14.

Hu, C., Fan, L., Cen, P., Chen, E., Jiang, Z., and Li L. (2016). Energy metabolism plays a critical role in stem cell maintenance and differentiation. Int. J. Mol. Sci *17*.

Hu, Z., Chen, K., Xia, Z., Chavez, M., Pal, S., Seol, J.-H., Chen, C.-C., Li, W., and Tyler, J.K. (2014). Nucleosome loss leads to global transcriptional up-regulation and genomic instability during yeast aging. Genes Dev. *28*, 396–408.

Huizing, M., Ruitenbeek, W., van den Heuvel, L.P., Dolce, V., Iacobazzi, V., Smeitink, J.A., Palmieri, F., and Trijbels, J.M. (1998). Human mitochondrial transmembrane metabolite carriers: tissue distribution and its implication for mitochondrial disorders. J. Bioenerg. Biomembr. 30, 277–284.

Iacobazzi, V., Lauria, G., and Palmieri, F. (1997). Organization and sequence of the human gene for the mitochondrial citrate transport protein. DNA Seq. 7, 127–139.

Iacobazzi, V., Infantino, V., and Palmieri, F. (2008). Epigenetic mechanisms and Sp1 regulate mitochondrial citrate carrier gene expression. Biochem. Biophys. Res. Commun. 376, 15–20.

Iacobazzi, V., Infantino, V., Bisaccia, F., Castegna, A., and Palmieri, F. (2009a). Role of FOXA in mitochondrial citrate carrier gene expression and insulin secretion. Biochem. Biophys. Res. Commun. 385, 220–224.

Iacobazzi, V., Infantino, V., Convertini, P., Vozza, A., Agrimi, G., and Palmieri, F. (2009b). Transcription of the mitochondrial citrate carrier gene: identification of a silencer and its binding protein ZNF224. Biochem. Biophys. Res. Commun. 386, 186–191.

Infantino, V., Iacobazzi, V., De Santis, F., Mastrapasqua, M., and Palmieri, F. (2007). Transcription of the mitochondrial citrate carrier gene: role of SREBP-1, upregulation by insulin and downregulation by PUFA. Biochem. Biophys. Res. Commun. 356, 249–254.

Infantino, V., Convertini, P., Cucci, L., Panaro, M.A., Di Noia, M.A., Calvello, R., Palmieri, F., and Iacobazzi, V. (2011). The mitochondrial citrate carrier: a new player in inflammation. Biochem. J 438, 433–436.

Infantino, V., Iacobazzi, V., Menga, A., Avantaggiati, M.L., and Palmieri, F. (2014). A key role of the mitochondrial citrate carrier (SLC25A1) in TNFα- and IFNγ-triggered inflammation. Biochimica et Biophysica Acta (BBA) - Gene Regulatory Mechanisms 1839, 1217–1225.

Itakura, E., Zavodszky, E., Shao, S., Wohlever, M.L., Keenan, R.J., and Hegde, R.S. (2016). Ubiquilins Chaperone and Triage Mitochondrial Membrane Proteins for Degradation. Molecular Cell *63*, 21–33.

Ito, K., and Suda, T. (2014). Metabolic requirements for the maintenance of self-renewing stem cells. Nature Reviews Molecular Cell Biology *15*, 243–256.

James, A.M., Hoogewijs, K., Logan, A., Hall, A.R., Ding, S., Fearnley, I.M., and Murphy, M.P. (2017). Non-enzymatic N-acetylation of Lysine Residues by AcetylCoA Often Occurs via a Proximal S-acetylated Thiol Intermediate Sensitive to Glyoxalase II. Cell Rep. *18*, 2105–2112.

Jesus, B.B. de, de Jesus, B.B., and Blasco, M.A. (2013). Telomerase at the intersection of cancer and aging. Trends in Genetics *29*, 513–520.

Jin, S.M., Lazarou, M., Wang, C., Kane, L.A., Narendra, D.P., and Youle, R.J. (2010). Mitochondrial membrane potential regulates PINK1 import and proteolytic destabilization by PARL. Journal of Cell Biology *191*, 933–942.

Jing, H., Liao, L., An, Y., Su, X., Liu, S., Shuai, Y., Zhang, X., and Jin, Y. (2016). Suppression of EZH2 Prevents the Shift of Osteoporotic MSC Fate to Adipocyte and Enhances Bone Formation During Osteoporosis. Mol. Ther. *24*, 217–229.

Joseph, J.W., Jensen, M.V., Ilkayeva, O., Palmieri, F., Alárcon, C., Rhodes, C.J., and Newgard, C.B. (2006). The mitochondrial citrate/isocitrate carrier plays a regulatory role in glucose-stimulated insulin secretion. J. Biol. Chem. 281, 35624–35632.

Josse, C., Schoemans, R., Niessen, N.-A., Delgaudine, M., Hellin, A.-C., Herens, C., Delvenne, P., and Bours, V. (2010). Systematic chromosomal aberrations found in murine bone marrow-derived mesenchymal stem cells. Stem Cells Dev. *19*, 1167–1173.

Jung, J.-W., Lee, S., Seo, M.-S., Park, S.-B., Kurtz, A., Kang, S.-K., and Kang, K.-S. (2010). Histone deacetylase controls adult stem cell aging by balancing the expression of polycomb genes and jumonji domain containing 3. Cellular and Molecular Life Sciences *67*, 1165–1176.

Kaelin, W.G., and McKnight, S.L. (2013). Influence of Metabolism on Epigenetics and Disease. Cell *153*, 56–69.

Kaplan, R.S., Morris, H.P., and Coleman, P.S. (1982). Kinetic characteristics of citrate influx and efflux with mitochondria from Morris hepatomas 3924A and 16. Cancer Res. 42, 4399–4407.

Kaplan, R.S., Mayor, J.A., Blackwell, R., Maughon, R.H., and Wilson, G.L. (1991a). The effect of insulin supplementation on diabetes-induced alterations in the extractable levels of functional mitochondrial anion transport proteins. Arch. Biochem. Biophys. 287, 305–311.

Kaplan, R.S., Mayor, J.A., Blackwell, R., Wilson, G.L., and Schaffer, S.W. (1991b). Functional levels of mitochondrial anion transport proteins in non-insulin-dependent diabetes mellitus. Mol. Cell. Biochem. 107, 79–86.

Kaplan, R.S., Mayor, J.A., Gremse, D.A., and Wood, D.O. (1995). High Level Expression and Characterization of the Mitochondrial Citrate Transport Protein from the Yeast Saccharomyces cerevisiae (∗). J. Biol. Chem. 270, 4108–4114.

Karakaş, N., Bay, S., Öztunç N, Öncül M, Bilgen H, et al. (2020). Neurons from human mesenchymal stem cells display both spontaneous and stimuli responsive activity. PLoS ONE *15*.

Kfoury, Y., and Scadden, D.T. (2015). Mesenchymal Cell Contributions to the Stem Cell Niche. Cell Stem Cell *16*, 239–253.

Kim, I., Rodriguez-Enriquez, S., and Lemasters, J.J. (2007). Selective degradation of mitochondria by mitophagy. Archives of Biochemistry and Biophysics *462*, 245–253.

Kim, J.-W., Tchernyshyov, I., Semenza, G.L., and Dang, C.V. (2006). HIF-1-mediated expression of pyruvate dehydrogenase kinase: A metabolic switch required for cellular adaptation to hypoxia. Cell Metabolism *3*, 177–185.

Kim, M., Kim, C., Choi, Y.S., Kim, M., Park, C., and Suh, Y. (2012). Age-related alterations in mesenchymal stem cells related to shift in differentiation from osteogenic to adipogenic potential: Implication to age-associated bone diseases and defects. Mechanisms of Ageing and Development *133*, 215–225.

Kim, N.C., Tresse, E., Kolaitis, R.-M., Molliex, A., Thomas, R.E., Alami, N.H., Wang, B., Joshi, A., Smith, R.B., Ritson, G.P., et al. (2013). VCP Is Essential for Mitochondrial Quality Control by PINK1/Parkin and this Function Is Impaired by VCP Mutations. Neuron *78*, 403.

Kohyama, J., Abe, H., Shimazaki, T., Koizumi, A., Nakashima, K., Gojo, S., Taga, T., Okano, H., Hata,

J.-I., and Umezawa, A. (2001). Brain from bone: Efficient “meta-differentiation” of marrow stroma-derived mature osteoblasts to neurons with Noggin or a demethylating agent. Differentiation *68*, 235–244.

Kolukula, V.K., Sahu, G., Wellstein, A., Rodriguez, O.C., Preet, A., Iacobazzi, V., D’Orazi, G., Albanese, C., Palmieri, F., and Avantaggiati, M.L. (2014). SLC25A1, or CIC, is a novel transcriptional target of mutant p53 and a negative tumor prognostic marker. Oncotarget *5*, 1212–1225.

Kornicka, K., Marycz, K., Marędziak, M., Tomaszewski, K.A., and Nicpoń, J. (2017). The effects of the DNA methyltranfserases inhibitor 5-Azacitidine on ageing, oxidative stress and DNA methylation of adipose derived stem cells. J. Cell. Mol. Med. *21*, 387–401.

Krysko, D.V., Agostinis, P., Krysko, O., Garg, A.D., Bachert, C., Lambrecht, B.N., and Vandenabeele, P. (2011). Emerging role of damage-associated molecular patterns derived from mitochondria in inflammation. Trends in Immunology *32*, 157–164.

Kubota, Y., Takubo, K., and Suda, T. (2008). Bone marrow long label-retaining cells reside in the sinusoidal hypoxic niche. Biochemical and Biophysical Research Communications *366*, 335–339.

Langmead, B., and Salzberg, S.L. (2012). Fast gapped-read alignment with Bowtie 2. Nat. Methods *9*, 357–359.

Lapidot, T., and Kollet, O. (2002). The essential roles of the chemokine SDF-1 and its receptor CXCR4 in human stem cell homing and repopulation of transplanted immune-deficient NOD/SCID and NOD/SCID/B2mnull mice. Leukemia *16*, 1992–2003.

Lee, H.W., Suh, J.H., Kim, A.Y., Lee, Y.S., Park, S.Y., and Kim, J.B. (2006). Histone deacetylase 1-mediated histone modification regulates osteoblast differentiation. Mol. Endocrinol. *20*, 2432–2443.

Lee, J., Saha, P.K., Yang, Q.-H., Lee, S., Park, J.Y., Suh, Y., Lee, S.-K., Chan, L., Roeder, R.G., and Lee, J.W. (2008). Targeted inactivation of MLL3 histone H3-Lys-4 methyltransferase activity in the mouse reveals vital roles for MLL3 in adipogenesis. Proc. Natl. Acad. Sci. U. S. A. *105*, 19229–19234.

Lee, W.-C., Ji, X., Nissim, I., and Long, F. (2020). Malic Enzyme Couples Mitochondria with Aerobic Glycolysis in Osteoblasts. Cell Reports *32*, 108108.

Leijten, J., Georgi, N., Moreira Teixeira, L., van Blitterswijk, C.A., Post, J.N., and Karperien, M. (2014). Metabolic programming of mesenchymal stromal cells by oxygen tension directs chondrogenic cell fate. Proc. Natl. Acad. Sci. U. S. A. *111*, 13954–13959.

Lennon D.P., Edmison, J.M., and Caplan, A.I. (2001). Cultivation of rat marrow-derived mesenchymal stem cells in reduced oxygen tension: effects on in vitro and in vivo osteochondrogenesis. J. Cell. Physiol. *187*, 345-355.

Leonhard, K., Guiard, B., Pellecchia, G., Tzagoloff, A., Neupert, W., and Langer, T. (2000). Membrane Protein Degradation by AAA Proteases in Mitochondria. Molecular Cell *5*, 629–638.

Li, H., Handsaker, B., Wysoker, A., Fennell, T., Ruan, J., Homer, N., Marth, G., Abecasis, G., Durbin, R., and 1000 Genome Project Data Processing Subgroup (2009). The Sequence Alignment/Map format and SAMtools. Bioinformatics *25*, 2078–2079.

Li, X., Egervari, G., Wang, Y., Berger, S.L., and Lu, Z. (2018). Regulation of chromatin and gene expression by metabolic enzymes and metabolites. Nature Reviews Molecular Cell Biology *19*, 563–578.

Li, Z., Liu, C., Xie, Z., Song, P., Zhao, R.C.H., Guo, L., Liu, Z., and Wu, Y. (2011). Epigenetic dysregulation in mesenchymal stem cell aging and spontaneous differentiation. PLoS One *6*, e20526.

Liao, Y., Smyth, G.K., and Shi, W. (2014). featureCounts: an efficient general-purpose program for assigning sequence reads to genomic features. Bioinformatics *30*, 923–930.

Liu, Y., Zuckier, L.S., and Ghesani, N.V. (2010). Dominant uptake of fatty acid over glucose by prostate

cells: a potential new diagnostic and therapeutic approach. Anticancer Res. 30, 369–374.

Locasale, J.W. (2013). Serine, glycine and one-carbon units: cancer metabolism in full circle. Nature Reviews Cancer *13*, 572–583.

Lombardi, M.L., Zwerger, M., and Lammerding, J. (2011). Biophysical assays to probe the mechanical properties of the interphase cell nucleus: substrate strain application and microneedle manipulation. J. Vis. Exp.

López-Otín, C., Blasco, M.A., Partridge, L., Serrano, M., and Kroemer, G. (2013). The Hallmarks of Aging. Cell *153*, 1194–1217.

Lord, B.I., Testa, N.G., and Hendry, J.H. (1975). The relative spatial distributions of CFUs and CFUc in the normal mouse femur. Blood *46*, 65–72.

Lu, C., and Thompson, C.B. (2012). Metabolic Regulation of Epigenetics. Cell Metabolism *16*, 9–17.

Lunt, S.Y., and Vander Heiden, M.G. (2011). Aerobic glycolysis: meeting the metabolic requirements of cell proliferation. Annu. Rev. Cell Dev. Biol. *27*, 441–464.

Majmundar, A.J., Wong, W.J., and Celeste Simon, M. (2010). Hypoxia-Inducible Factors and the Response to Hypoxic Stress. Molecular Cell *40*, 294–309.

Majumdar, M.K., Thiede, M.A., Haynesworth, S.E., Bruder, S.P., and Gerson, S.L. (2000). Human marrow-derived mesenchymal stem cells (MSCs) express hematopoietic cytokines and support long-term hematopoiesis when differentiated toward stromal and osteogenic lineages. J. Hematother. Stem Cell Res. *9*, 841–848.

Malladi, P., Xu, Y., Chiou, M., Giaccia, A.J., and Longaker, M.T. (2006). Effect of reduced oxygen tension on chondrogenesis and osteogenesis in adipose-derived mesenchymal cells. Am. J. Physiol. Cell Physiol. *290*, C1139-C1145.

Man, E.A.B.Y., and Man, E.A.B. Bone density and bone marrow adiposity in childhood obesity using MR spectroscopy.

Mansfield, K.D., Guzy, R.D., Pan, Y., Young, R.M., Cash, T.P., Schumacker, P.T., and Simon, M.C. (2005). Mitochondrial dysfunction resulting from loss of cytochrome c impairs cellular oxygen sensing and hypoxic HIF-alpha activation. Cell Metab. *1*, 393–399.

Masuda, S., Ageyama, N., Shibata, H., Obara, Y., Ikeda, T., Takeuchi, K., Ueda, Y., Ozawa, K., and Hanazono, Y. (2009). Cotransplantation with MSCs improves engraftment of HSCs after autologous intra-bone marrow transplantation in nonhuman primates. Experimental Hematology *37*, 1250–1257.e1.

Maynard, T.M., Meechan, D.W., Dudevoir, M.L., Gopalakrishna, D., Peters, A.Z., Heindel, C.C., Sugimoto, T.J., Wu, Y., Lieberman, J.A., and Lamantia, A.-S. (2008). Mitochondrial localization and function of a subset of 22q11 deletion syndrome candidate genes. Mol. Cell. Neurosci. 39, 439–451.

Matheoud, D., Sugiura, A., Bellemare-Pelletier, A., Laplante, A., Rondeau, C., Chemali, M., Fazel, A., Bergeron, J.J., Trudeau, L.-E., Burelle, Y., et al. (2016). Parkinson's Disease-Related Proteins PINK1 and Parkin Repress Mitochondrial Antigen Presentation. Cell *166*, 314–327.

McLelland, G.-L., Soubannier, V., Chen, C.X., McBride, H.M., and Fon, E.A. (2014). Parkin and PINK1 function in a vesicular trafficking pathway regulating mitochondrial quality control. The EMBO Journal.

McLelland, G.-L., Lee, S.A., McBride, H.M., and Fon, E.A. (2016). Syntaxin-17 delivers PINK1/parkin-dependent mitochondrial vesicles to the endolysosomal system. J. Cell Biol. *214*, 275–291.

Merkwirth, C., Jovaisaite, V., Durieux, J., Matilainen, O., Jordan, S.D., Quiros, P.M., Steffen, K.K., Williams, E.G., Mouchiroud, L., Tronnes, S.U., et al. (2016). Two Conserved Histone Demethylases Regulate Mitochondrial Stress-Induced Longevity. Cell *165*, 1209–1223.

Mews, P., Donahue, G., Drake, A.M., Luczak, V., Abel, T., and Berger, S.L. (2017). Acetyl-CoA

synthetase regulates histone acetylation and hippocampal memory. Nature *546*, 381–386.

Meyer, M.B., Benkusky, N.A., Sen, B., Rubin, J., and Pike, J.W. (2016). Epigenetic Plasticity Drives Adipogenic and Osteogenic Differentiation of Marrow-derived Mesenchymal Stem Cells. J. Biol. Chem. *291*, 17829–17847.

Mitra, R., Goodman, O.B., and Le, T.T. (2014). Enhanced detection of metastatic prostate cancer cells in human plasma with lipid bodies staining. BMC Cancer 14, 91.

Miura, Y. (2006). Mesenchymal Stem Cell-Organized Bone Marrow Elements: An Alternative Hematopoietic Progenitor Resource. Stem Cells.

Mobasheri, A., Neama, G., Bell, S., Richardson, S., and Carter, S.D. (2002). Human articular chondrocytes express three facilitative glucose transporter isoforms: GLUT1, GLUT3 and GLUT9. Cell Biol. Int. *26*, 297–300.

Moerman, E.J., Teng, K., Lipschitz, D.A., and Lecka-Czernik, B. (2004). Aging activates adipogenic and suppresses osteogenic programs in mesenchymal marrow stroma/stem cells: the role of PPAR-γ2 transcription factor and TGF-β/BMP signaling pathways. Aging Cell *3*, 379–389.

Morciano, P., Carrisi, C., Capobianco, L., Mannini, L., Burgio, G., Cestra, G., De Benedetto, G.E., Corona, D.F.V., Musio, A., and Cenci, G. (2009). A conserved role for the mitochondrial citrate transporter Sea/SLC25A1 in the maintenance of chromosome integrity. Human Molecular Genetics *18*, 4180–4188.

Morganti, C., Bonora, M., Marchi, S., Ferroni, L., Gardin, C., Wieckowski, M.R., Giorgi, C., Pinton, P., and Zavan, B. (2020). Citrate Mediates Crosstalk between Mitochondria and the Nucleus to Promote Human Mesenchymal Stem Cell In Vitro Osteogenesis. Cells *9*, 1034.

Morgenstern, M., Stiller, S.B., Lübbert, P., Peikert, C.D., Dannenmaier, S., Drepper, F., Weill, U., Höß, P., Feuerstein, R., Gebert, M., et al. (2017). Definition of a High-Confidence Mitochondrial Proteome at Quantitative Scale. Cell Reports *19*, 2836–2852.

Morikawa, S., Mabuchi, Y., Kubota, Y., Nagai, Y., Niibe, K., Hiratsu, E., Suzuki, S., Miyauchi-Hara, C., Nagoshi, N., Sunabori, T., et al. (2009). Prospective identification, isolation, and systemic transplantation of multipotent mesenchymal stem cells in murine bone marrow. J. Exp. Med. *206*, 2483–2496.

Mosaoa, R., Kasprzyk-Pawelec, A., Fernandez, H.R., and Avantaggiati, M.L. (2021). The Mitochondrial Citrate Carrier SLC25A1/CIC and the Fundamental Role of Citrate in Cancer, Inflammation and Beyond. Biomolecules 11, 141.

Moskalev, A.A., Shaposhnikov, M.V., Plyusnina, E.N., Zhavoronkov, A., Budovsky, A., Yanai, H., and Fraifeld, V.E. (2013). The role of DNA damage and repair in aging through the prism of Koch-like criteria. Ageing Research Reviews *12*, 661–684.

Moussaieff, A., Rouleau, M., Kitsberg, D., Cohen, M., Levy, G., Barasch, D., Nemirovski, A., Shen-Orr, S., Laevsky, I., Amit, M., et al. (2015). Glycolysis-mediated changes in acetyl-CoA and histone acetylation control the early differentiation of embryonic stem cells. Cell Metab. *21*, 392–402.

Naveiras, O., Nardi, V., Wenzel, P.L., Hauschka, P.V., Fahey, F., and Daley, G.Q. (2009). Bone-marrow adipocytes as negative regulators of the haematopoietic microenvironment. Nature *460*, 259–263.

Nargund, A.M., Fiorese, C.J., Pellegrino, M.W., Deng, P., and Haynes, C.M. (2015). Mitochondrial and nuclear accumulation of the transcription factor ATFS-1 promotes OXPHOS recovery during the UPR(mt). Mol Cell *58*, 123–133.

Neuspiel, M., Schauss, A.C., Braschi, E., Zunino, R., Rippstein, P., Rachubinski, R.A., Andrade-Navarro, M.A., and McBride, H.M. (2008). Cargo-selected transport from the mitochondria to peroxisomes is mediated by vesicular carriers. Curr. Biol. *18*, 102–108.

Nishida, T., Kubota, S., Aoyama, E., and Takigawa, M. (2013). Impaired glycolytic metabolism causes chondrocyte hypertrophy-like changes via promotion of phospho-Smad1/5/8 translocation into nucleus. Osteoarthritis Cartilage *21*, 700–709.

Noort, W.A., Kruisselbrink, A.B., in't Anker, P.S., Kruger, M., van Bezooijen, R.L., de Paus, R.A., Heemskerk, M.H.M., Löwik, C.W.G.M., Falkenburg, J.H., Willemze, R., et al. (2002). Mesenchymal stem cells promote engraftment of human umbilical cord blood-derived CD34(+) cells in NOD/SCID mice. Exp. Hematol. *30*, 870–878.

Nota, B., Struys, E.A., Pop, A., Jansen, E.E., Fernandez Ojeda, M.R., Kanhai, W.A., Kranendijk, M., van Dooren, S.J.M., Bevova, M.R., Sistermans, E.A., et al. (2013). Deficiency in SLC25A1, Encoding the Mitochondrial Citrate Carrier, Causes Combined D-2- and L-2-Hydroxyglutaric Aciduria. The American Journal of Human Genetics 92, 627–631.

Ott, M., Amunts, A., and Brown, A. (2016). Organization and Regulation of Mitochondrial Protein Synthesis. Annual Review of Biochemistry *85*, 77–101.

Otte, P. (1991). Basic cell metabolism of articular cartilage. Manometric studies. Z. Rheumatol. *50*, 304–312.

Palmieri, E.M., Spera, I., Menga, A., Infantino, V., Porcelli, V., Iacobazzi, V., Pierri, C.L., Hooper, D.C., Palmieri, F., and Castegna, A. (2015). Acetylation of human mitochondrial citrate carrier modulates mitochondrial citrate/malate exchange activity to sustain NADPH production during macrophage activation. Biochimica et Biophysica Acta (BBA) - Bioenergetics *1847*, 729–738.

Palmieri, F. (2013). The mitochondrial transporter family SLC25: identification, properties and physiopathology. Mol. Aspects Med. 34, 465–484.

Palmieri, F., and Monné, M. (2016). Discoveries, metabolic roles and diseases of mitochondrial carriers: A review. Biochim. Biophys. Acta 1863, 2362–2378.

Palmieri, F., Scarcia, P., and Monné, M. (2020). Diseases Caused by Mutations in Mitochondrial Carrier Genes SLC25: A Review. Biomolecules 10.

Pan, H., Guan, D., Liu, X., Li, J., Wang, L., Wu, J., Zhou, J., Zhang, W., Ren, R., Zhang, W., et al. (2016). SIRT6 safeguards human mesenchymal stem cells from oxidative stress by coactivating NRF2. Cell Research *26*, 190–205.

Paradies, G., and Ruggiero, F.M. (1990). Enhanced activity of the tricarboxylate carrier and modification of lipids in hepatic mitochondria from hyperthyroid rats. Arch. Biochem. Biophys. 278, 425–430.

Parekh, S., Ziegenhain, C., Vieth, B., Enard, W., and Hellmann, I. (2018). zUMIs - A fast and flexible pipeline to process RNA sequencing data with UMIs. Gigascience.

Pattappa, G., Heywood, H.K., de Bruijn, J.D., and Lee, D.A. (2011). The metabolism of human mesenchymal stem cells during proliferation and differentiation. J. Cell. Physiol. *226*, 2562–2570.

Pattappa, G., Thorpe, S.D., Jegard, N.C., Heywood, H.K., de Bruijn, J.D., and Lee, D.A. (2013). Continuous and Uninterrupted Oxygen Tension Influences the Colony Formation and Oxidative Metabolism of Human Mesenchymal Stem Cells. Tissue Engineering Part C: Methods *19*, 68–79.

Pedemonte, E., Benvenuto, F., Casazza, S., Mancardi, G., Oksenberg, J.R., Uccelli, A., and Baranzini, S.E. (2007). The molecular signature of therapeutic mesenchymal stem cells exposes the architecture of the hematopoietic stem cell niche synapse. BMC Genomics *8*, 65.

Perino, M., and Veenstra, G.J.C. (2016). Chromatin Control of Developmental Dynamics and Plasticity. Developmental Cell *38*, 610–620.

Peterson, K.M., Aly, A., Lerman, A., Lerman, L.O., and Rodriguez-Porcel, M. (2011). Improved survival of mesenchymal stromal cell after hypoxia preconditioning: role of oxidative stress. Life Sci. *88*, 65–73.

Pfanner, N., Warscheid, B., and Wiedemann, N. (2019). Mitochondrial proteins: from biogenesis to

functional networks. Nature Reviews Molecular Cell Biology *20*, 267–284.

Phetfong, J., Sanvoranart, T., Nartprayut, K., Nimsanor, N., Seenprachawong, K., Prachayasittikul, V., and Supokawej, A. (2016). Osteoporosis: the current status of mesenchymal stem cell-based therapy. Cell. Mol. Biol. Lett. *21*, 12.

Pickles, S., Vigié, P., and Youle, R.J. (2018). Mitophagy and Quality Control Mechanisms in Mitochondrial Maintenance. Current Biology *28*, R170–R185.

Piersma, A.H., Brockbank, K.G., Ploemacher, R.E., van Vliet, E., Brakel-van Peer, K.M., and Visser, P.J. (1985). Characterization of fibroblastic stromal cells from murine bone marrow. Exp. Hematol. *13*, 237–243.

Pietilä, M., Palomäki, S., Lehtonen, S., Ritamo, I., Valmu, L., Nystedt, J., Laitinen, S., Leskelä, H.-V., Sormunen, R., Pesälä, J., et al. (2012). Mitochondrial Function and Energy Metabolism in Umbilical Cord Blood- and Bone Marrow-Derived Mesenchymal Stem Cells. Stem Cells and Development *21*, 575–588.

Pittenger, M.F., Mackay, A.M., Beck, S.C., Jaiswal, R.K., Douglas, R., Mosca, J.D., Moorman, M.A., Simonetti, D.W., Craig, S., and Marshak, D.R. (1999). Multilineage potential of adult human mesenchymal stem cells. Science *284*, 143–147.

Pouikli, A., and Tessarz, P. (2021). Metabolism and chromatin: A dynamic duo that regulates development and ageing: Elucidating the metabolism-chromatin axis in bone-marrow mesenchymal stem cell fate decisions. Bioessays *43*, e2000273.

Prasun, P., Young, S., Salomons, G., Werneke, A., Jiang, Y.-H., Struys, E., Paige, M., Avantaggiati, M.L., and McDonald, M. (2014). Expanding the Clinical Spectrum of Mitochondrial Citrate Carrier (SLC25A1) Deficiency: Facial Dysmorphism in Siblings with Epileptic Encephalopathy and Combined D,L-2-Hydroxyglutaric Aciduria. JIMD Reports 111–115.

Priesnitz, C., and Becker, T. (2018). Pathways to balance mitochondrial translation and protein import. Genes & Development *32*, 1285–1296.

Prinz, W.A., Toulmay, A., and Balla, T. (2020). The functional universe of membrane contact sites. Nature Reviews Molecular Cell Biology *21*, 7–24.

Prowse, K.R., and Greider, C.W. (1995). Developmental and tissue-specific regulation of mouse telomerase and telomere length. Proc. Natl. Acad. Sci. U. S. A. *92*, 4818–4822.

Quiles, J.M., and Gustafsson, Å.B. (2020). Mitochondrial Quality Control and Cellular Proteostasis: Two Sides of the Same Coin. Frontiers in Physiology *11*.

Quinn, K.P., Sridharan, G.V., Hayden, R.S., Kaplan, D.L., Lee, K., and Georgakoudi, I. (2013). Quantitative metabolic imaging using endogenous fluorescence to detect stem cell differentiation. Sci. Rep. *3*, 3432.

Rauch, A., Haakonsson, A.K., Madsen, J.G.S., Larsen, M., Forss, I., Madsen, M.R., Van Hauwaert, E.L., Wiwie, C., Jespersen, N.Z., Tencerova, M., et al. (2019). Osteogenesis depends on commissioning of a network of stem cell transcription factors that act as repressors of adipogenesis. Nat. Genet. *51*, 716–727.

Rehman, J. (2010). Empowering self-renewal and differentiation: the role of mitochondria in stem cells. J. Mol. Med. *88*, 981–986.

Reid, M.A., Dai, Z., and Locasale, J.W. (2017). The impact of cellular metabolism on chromatin dynamics and epigenetics. Nature Cell Biology *19*, 1298–1306.

Renault, V.M., Rafalski, V.A., Morgan, A.A., Salih, D.A.M., Brett, J.O., Webb, A.E., Villeda, S.A., Thekkat, P.U., Guillerey, C., Denko, N.C., et al. (2009). FoxO3 regulates neural stem cell homeostasis. Cell Stem Cell *5*, 527–539.

Ritchie, M.E., Phipson, B., Wu, D., Hu, Y., Law, C.W., Shi, W., and Smyth, G.K. (2015). limma powers differential expression analyses for RNA-sequencing and microarray studies. Nucleic Acids Res. *43*, e47.

Robins, J.C., Akeno, N., Mukherjee, A., Dalal, R.R., Aronow, B.J., Koopman, P. and Clemens, T.L. (2005). Hypoxia induces chondrocyte-specific gene expression in mesenchymal cells in association with transcriptional activation of Sox9. Bone 37, 313-322.

Robinson, M.D., McCarthy, D.J., and Smyth, G.K. (2010). edgeR: a Bioconductor package for differential expression analysis of digital gene expression data. Bioinformatics *26*, 139–140.

Roger, A.J., Muñoz-Gómez, S.A., and Kamikawa, R. (2017). The Origin and Diversification of Mitochondria. Current Biology *27*, R1177–R1192.

Rogina, B., Reenan, R.A., Nilsen, S.P., and Helfand, S.L. (2000). Extended Life-Span Conferred by Cotransporter Gene Mutations in Drosophila. Science 290, 2137–2140.

Roise, D., and Schatz, G. (1988). Mitochondrial presequences. J. Biol. Chem. 263, 4509–4511.

Rossi, D.J., Jamieson, C.H.M., and Weissman, I.L. (2008). Stems cells and the pathways to aging and cancer. Cell *132*, 681–696.

Ryall, J.G. (2012). The role of sirtuins in the regulation of metabolic homeostasis in skeletal muscle. Curr. Opin. Clin. Nutr. Metab. Care *15*, 561–566.

Ryan, T.A., Phillips, E.O., Collier, C.L., Robinson, A.J.B., Routledge, D., Wood, R.E., Assar, E.A., and Tumbarello, D.A. (2020). Tollip coordinates Parkin-dependent trafficking of mitochondrial-derived vesicles. The EMBO Journal *39*.

Sánchez-Aragó, M., García-Bermúdez, J., Martínez-Reyes, I., Santacatterina, F., and Cuezva, J.M. (2013). Degradation of IF1 controls energy metabolism during osteogenic differentiation of stem cells. EMBO Rep. *14*, 638–644.

Santos, F. dos, dos Santos, F., Andrade, P.Z., Boura, J.S., Abecasis, M.M., da Silva, C.L., and Cabral, J.M.S. (2009). Ex vivo expansion of human mesenchymal stem cells: A more effective cell proliferation kinetics and metabolism under hypoxia. Journal of Cellular Physiology.

Scadden, D.T. (2006). The stem-cell niche as an entity of action. Nature *441*, 1075–1079.

Schell, J.C., Wisidagama, D.R., Bensard, C., Zhao, H., Wei, P., Tanner, J., Flores, A., Mohlman, J., Sorensen, L.K., Earl, C.S., et al. (2017). Control of intestinal stem cell function and proliferation by mitochondrial pyruvate metabolism. Nat. Cell Biol. *19*, 1027–1036.

Schep, A.N., Buenrostro, J.D., Denny, S.K., Schwartz, K., Sherlock, G., and Greenleaf, W.J. (2015). Structured nucleosome fingerprints enable high-resolution mapping of chromatin architecture within regulatory regions. Genome Res. *25*, 1757–1770.

Seaman, M.N.J. (2012). The retromer complex – endosomal protein recycling and beyond. Journal of Cell Science.

Seita, J., and Weissman, I.L. (2010). Hematopoietic stem cell: self-renewal versus differentiation. Wiley Interdiscip. Rev. Syst. Biol. Med. *2*, 640–653.

Semenza, G.L. (2012a). Hypoxia-inducible factors: mediators of cancer progression and targets for cancer therapy. Trends Pharmacol. Sci. *33*, 207–214.

Semenza, G.L. (2012b). Molecular mechanisms mediating metastasis of hypoxic breast cancer cells. Trends Mol. Med. *18*, 534–543.

Siculella, L., Sabetta, S., di Summa, R., Leo, M., Giudetti, A.M., Palmieri, F., and Gnoni, G.V. (2002). Starvation-induced posttranscriptional control of rat liver mitochondrial citrate carrier expression. Biochem. Biophys. Res. Commun. 299, 418–423.

Sivanand, S., Viney, I., and Wellen, K.E. (2018). Spatiotemporal Control of Acetyl-CoA Metabolism in Chromatin Regulation. Trends in Biochemical Sciences *43*, 61–74.

Skene, P.J., and Henikoff, S. (2017). An efficient targeted nuclease strategy for high-resolution mapping of DNA binding sites. Elife *6*.

Song, C.G., Zhang, Y.Z., Wu, H.N., Cao, X.L., Guo, C.J. et al. (2018). Stem cells: a promising candidate to treat neurological disorders. Neural Regen Res *13*, 1294–1304.

Song, M., Chen, Y., Gong, G., Murphy, E., Rabinovitch, P.S., and Dorn, G.W. (2014). Super-Suppression of Mitochondrial Reactive Oxygen Species Signaling Impairs Compensatory Autophagy in Primary Mitophagic Cardiomyopathy. Circulation Research *115*, 348–353.

Soubannier, V., McLelland, G.-L., Zunino, R., Braschi, E., Rippstein, P., Fon, E.A., and McBride, H.M. (2012a). A vesicular transport pathway shuttles cargo from mitochondria to lysosomes. Curr. Biol. *22*, 135–141.

Soubannier, V., Rippstein, P., Kaufman, B.A., Shoubridge, E.A., and McBride, H.M. (2012b). Reconstitution of Mitochondria Derived Vesicle Formation Demonstrates Selective Enrichment of Oxidized Cargo. PLoS ONE *7*, e52830.

Sözen, T., Özışık, L., and Başaran, N.Ç. (2017). An overview and management of osteoporosis. Eur. J. Rheumatol. Inflamm. *4*, 46–56.

Spencer, J.A., Ferraro, F., Roussakis, E., Klein, A., Wu, J., Runnels, J.M., Zaher, W., Mortensen, L.J., Alt, C., Turcotte, R., et al. (2014). Direct measurement of local oxygen concentration in the bone marrow of live animals. Nature *508*, 269–273.

Su, X., Wellen, K.E., and Rabinowitz, J.D. (2016). Metabolic control of methylation and acetylation. Current Opinion in Chemical Biology *30*, 52–60.

Suda, T., Takubo, K., and Semenza, G.L. (2011). Metabolic regulation of hematopoietic stem cells in the hypoxic niche. Cell Stem Cell *9*, 298–310.

Sugimura, R., and Li, L. (2010). Shifting in Balance Between Osteogenesis and Adipogenesis Substantially Influences Hematopoiesis. Journal of Molecular Cell Biology *2*, 61–62.

Sugiura, A., McLelland, G., Fon, E.A., and McBride, H.M. (2014). A new pathway for mitochondrial quality control: mitochondrial-derived vesicles. The EMBO Journal *33*, 2142–2156.

Suhm, T., Kaimal, J.M., Dawitz, H., Peselj, C., Masser, A.E., Hanzén, S., Ambrožič, M., Smialowska, A., Björck, M.L., Brzezinski, P., et al. (2018). Mitochondrial Translation Efficiency Controls Cytoplasmic Protein Homeostasis. Cell Metabolism *27*, 1309–1322.e6.

Sutendra, G., Kinnaird, A., Dromparis, P., Paulin, R., Stenson, T.H., Haromy, A., Hashimoto, K., Zhang, N., Flaim, E., and Michelakis, E.D. (2014). A nuclear pyruvate dehydrogenase complex is important for the generation of acetyl-CoA and histone acetylation. Cell *158*, 84–97.

Tan, J., Lu, J., Huang, W., Dong, Z., Kong, C., Li, L., Gao, L., Guo, J., and Huang, B. (2009). Genome-Wide Analysis of Histone H3 Lysine9 Modifications in Human Mesenchymal Stem Cell Osteogenic Differentiation. PLoS ONE *4*, e6792.

Tan, M., Mosaoa, R., Graham, G.T., Kasprzyk-Pawelec, A., Gadre, S., Parasido, E., Catalina-Rodriguez, O., Foley, P., Giaccone, G., Cheema, A., et al. (2020). Inhibition of the mitochondrial citrate carrier, Slc25a1, reverts steatosis, glucose intolerance, and inflammation in preclinical models of NAFLD/NASH. Cell Death Differ. 27, 2143–2157.

Taudt, A., Nguyen, M.A., Heinig, M., Johannes, F., and Colome-Tatche, M. (2016). chromstaR: Tracking combinatorial chromatin state dynamics in space and time.

Tessarz, P., and Kouzarides, T. (2014). Histone core modifications regulating nucleosome structure and dynamics. Nature Reviews Molecular Cell Biology *15*, 703–708.

Todkar, K., Chikhi, L., Desjardins, V., El-Mortada, F., Pépin, G., and Germain, M. (2021). Selective packaging of mitochondrial proteins into extracellular vesicles prevents the release of mitochondrial DAMPs. Nat. Commun. *12*, 1971.

Tormos, K.V., Anso, E., Hamanaka, R.B., Eisenbart, J., Joseph, J., Kalyanaraman, B., and Chandel, N.S. (2011). Mitochondrial complex III ROS regulate adipocyte differentiation. Cell Metab. *14*, 537–544.

Tothova, Z., Kollipara, R., Huntly, B.J., Lee, B.H., Castrillon, D.H., Cullen, D.E., McDowell, E.P., Lazo-Kallanian, S., Williams, I.R., Sears, C., et al. (2007). FoxOs Are Critical Mediators of Hematopoietic Stem Cell Resistance to Physiologic Oxidative Stress. Cell *128*, 325–339.

Tseng, P.-C., Hou, S.-M., Chen, R.-J., Peng, H.-W., Hsieh, C.-F., Kuo, M.-L., and Yen, M.-L. (2011). Resveratrol promotes osteogenesis of human mesenchymal stem cells by upregulating RUNX2 gene expression via the SIRT1/FOXO3A axis. Journal of Bone and Mineral Research *26*, 2552–2563.

Wang, G.L., and Semenza, G.L. (1993). General involvement of hypoxia-inducible factor 1 in transcriptional response to hypoxia. Proc. Natl. Acad. Sci. U. S. A. *90*, 4304–4308.

Wang, C., Wang, J., Li, J., Hu, G., Shan, S., Li, Q., and Zhang, X. (2016). KDM5A controls bone morphogenic protein 2-induced osteogenic differentiation of bone mesenchymal stem cells during osteoporosis. Cell Death & Disease *7*, e2335–e2335.

Wang, R., Wang, Y., Zhu, L., Liu, Y., and Li, W. (2020a). Epigenetic Regulation in Mesenchymal Stem Cell Aging and Differentiation and Osteoporosis. Stem Cells Int. *2020*, 8836258.

Wang, Y., Deng, P., Liu, Y., Wu, Y., Chen, Y., Guo, Y., Zhang, S., Zheng, X., Zhou, L., Liu, W., et al. (2020b). Alpha-ketoglutarate ameliorates age-related osteoporosis via regulating histone methylations. Nat. Commun. *11*, 5596.

Wei, Q., and Frenette, P.S. (2018). Niches for Hematopoietic Stem Cells and Their Progeny. Immunity *48*, 632–648.

Weiss, A.R.R., and Dahlke, M.H. (2019). Immunomodulation by Mesenchymal Stem Cells (MSCs): Mechanisms of Action of Living, Apoptotic, and Dead MSCs. Front. Immunol. *10*, 1191.

Weissman, I.L., Anderson, D.J., and Gage, F. (2001). Stem and progenitor cells: origins, phenotypes, lineage commitments, and transdifferentiations. Annu. Rev. Cell Dev. Biol. *17*, 387–403.

Wellen, K.E., Hatzivassiliou, G., Sachdeva, U.M., Bui, T.V., Cross, J.R., and Thompson, C.B. (2009). ATP-citrate lyase links cellular metabolism to histone acetylation. Science *324*, 1076–1080.

Willems, P.H.G.M., Rossignol, R., Dieteren, C.E.J., Murphy, M.P., and Koopman, W.J.H. (2015). Redox Homeostasis and Mitochondrial Dynamics. Cell Metab. *22*, 207–218.

Winklhofer, K.F. (2014). Parkin and mitochondrial quality control: toward assembling the puzzle. Trends in Cell Biology *24*, 332–341.

Woodbury, D., Reynolds, K., and Black, I.B. (2002). Adult bone marrow stromal stem cells express germline, ectodermal, endodermal, and mesodermal genes prior to neurogenesis. Journal of Neuroscience Research *69*, 908–917.

Wu, S., Zhou, F., Zhang, Z., and Xing, D. (2011). Mitochondrial oxidative stress causes mitochondrial fragmentation via differential modulation of mitochondrial fission-fusion proteins. FEBS J. *278*, 941–954.

Xu, S., Peng, G., Wang, Y., Fang, S., and Karbowski, M. (2011a). The AAA-ATPase p97 is essential for outer mitochondrial membrane protein turnover. Mol. Biol. Cell *22*, 291–300.

Xu, W., Yang, H., Liu, Y., Yang, Y., Wang, P., Kim, S.-H., Ito, S., Yang, C., Wang, P., Xiao, M.-T., et al. (2011b). Oncometabolite 2-Hydroxyglutarate Is a Competitive Inhibitor of α-Ketoglutarate-Dependent Dioxygenases. Cancer Cell *19*, 17–30.

Yalcin, A., Clem, B.F., Simmons, A., Lane, A., Nelson, K., Clem, A.L., Brock, E., Siow, D., Wattenberg, B., Telang, S., et al. (2009). Nuclear Targeting of 6-Phosphofructo-2-kinase (PFKFB3) Increases Proliferation via Cyclin-dependent Kinases. Journal of Biological Chemistry 284, 24223–24232.

Yamano, K., and Youle, R.J. (2013). PINK1 is degraded through the N-end rule pathway. Autophagy *9*, 1758–1769.

Yamano, K., Wang, C., Sarraf, S.A., Münch, C., Kikuchi, R., Noda, N.N., Hizukuri, Y., Kanemaki, M.T., Harper, W., Tanaka, K., et al. (2018). Endosomal Rab cycles regulate Parkin-mediated mitophagy. eLife *7*.

Yan, X., Ehnert, S., Culmes, M., Bachmann, A., Seeliger, C., Schyschka, L., Wang, Z., Rahmanian-Schwarz, A., Stöckle, U., De Sousa, P.A., et al. (2014). 5-azacytidine improves the osteogenic differentiation potential of aged human adipose-derived mesenchymal stem cells by DNA demethylation. PLoS One *9*, e90846.

Yang, R., Yu, T., Kou, X., Gao, X., Chen, C., Liu, D., Zhou, Y., and Shi, S. (2018a). Tet1 and Tet2 maintain mesenchymal stem cell homeostasis via demethylation of the P2rX7 promoter. Nature Communications *9*.

Yang, Y.-H.K., Ogando, C.R., Wang See, C., Chang, T.-Y., and Barabino, G.A. (2018b). Changes in phenotype and differentiation potential of human mesenchymal stem cells aging in vitro. Stem Cell Res. Ther. *9*, 131.

Yoshino, J., Mills, K.F., Yoon, M.J., and Imai, S.-I. (2011). Nicotinamide Mononucleotide, a Key NAD Intermediate, Treats the Pathophysiology of Diet- and Age-Induced Diabetes in Mice. Cell Metabolism *14*, 528–536.

Zara, V., Iacobazzi, V., Siculella, L., Gnoni, G.V., and Palmieri, F. (1996). Purification and characterization of the tricarboxylate carrier from eel liver mitochondria. Biochem. Biophys. Res. Commun. 223, 508–513.

Zara, V., Ferramosca, A., Palmisano, I., Palmieri, F., and Rassow, J. (2003). Biogenesis of rat mitochondrial citrate carrier (CIC): the N-terminal presequence facilitates the solubility of the preprotein but does not act as a targeting signal. J. Mol. Biol. 325, 399–408.

Zara, V., Ferramosca, A., Papatheodorou, P., Palmieri, F., and Rassow, J. (2005). Import of rat mitochondrial citrate carrier (CIC) at increasing salt concentrations promotes presequence binding to import receptor Tom20 and inhibits membrane translocation. J. Cell Sci. 118, 3985–3995.

Zee, B.M., Levin, R.S., Xu, B., LeRoy, G., Wingreen, N.S., and Garcia, B.A. (2010). In Vivo Residue-specific Histone Methylation Dynamics. Journal of Biological Chemistry *285*, 3341–3350.

Zhang, H., Ryu, D., Wu, Y., Gariani, K., Wang, X., Luan, P., D'Amico, D., Ropelle, E.R., Lutolf, M.P., Aebersold, R., et al. (2016). NAD^+ repletion improves mitochondrial and stem cell function and enhances life span in mice. Science *352*, 1436–1443.

Zhang, J., Niu, C., Ye, L., Huang, H., He, X., Tong, W.-G., Ross, J., Haug, J., Johnson, T., Feng, J.Q., et al. (2003). Identification of the haematopoietic stem cell niche and control of the niche size. Nature *425*, 836–841.

Zhang, J., Li, X., Mueller, M., Wang, Y., Zong, C., Deng, N., Vondriska, T.M., Liem, D.A., Yang, J.-I., Korge, P., et al. (2008). Systematic characterization of the murine mitochondrial proteome using functionally validated cardiac mitochondria. Proteomics *8*, 1564–1575.

Zhang, Y., Marsboom, G., Toth, P.T., and Rehman, J. (2013). Mitochondrial respiration regulates adipogenic differentiation of human mesenchymal stem cells. PLoS One *8*, e77077.

Zhao, Z., and Shilatifard, A. (2019). Epigenetic modifications of histones in cancer. Genome Biology *20*.

Zhou, S., Greenberger, J.S., Epperly, M.W., Goff, J.P., Adler, C., LeBoff, M.S., and Glowacki, J. (2008).

Age-related intrinsic changes in human bone-marrow-derived mesenchymal stem cells and their differentiation to osteoblasts. Aging Cell *7*, 335–343.

Zhou, Y., Zhou, B., Pache, L., Chang, M., Khodabakhshi, A.H., Tanaseichuk, O., Benner, C., and Chanda, S.K. (2019). Metascape provides a biologist-oriented resource for the analysis of systems-level datasets. Nat. Commun. *10*, 1523.

Zimorski, V., Ku, C., Martin, W.F., and Gould, S.B. (2014). Endosymbiotic theory for organelle origins. Current Opinion in Microbiology *22*, 38–48.

Zuk, P.A., Zhu, M., Mizuno, H., Huang, J., Futrell, J.W., Katz, A.J., Benhaim, P., Lorenz, H.P., and Hedrick, M.H. (2001). Multilineage cells from human adipose tissue: implications for cell-based therapies. Tissue Eng. *7*, 211–228.

Appendix A

Measurement of bone quality parameters

Murine femurs were scanned with a high resolution μCT scanner with an isotropic voxel size of 8.8 um^3. The x-ray settings for each scan were 50 kV and 200 μA, using a 0.5 mm aluminum filter. All scans were performed over 360 degrees, with a rotation step of 0.3 degrees and a frame averaging of 1. Images were reconstructed and analyzed using NRecon software (version 2.0) and CTAn software (version 1.18), respectively. Trabecular and cortical bone regions of distal femurs were selected with reference to the growth plate (0.44-2.2 mm and 2.2-2.64 mm from growth plate, respectively). Bone mineral density was determined based on calibration with two phantoms of known density, which were scanned under the same conditions as the bone samples.

Appendix B

Electron microscopy

Samples were fixed in fixation buffer for 30 minutes at RT and for 30 minutes at 4°C. They were then washed with 0.1 M sodium cacodylate buffer, incubated for 1 hour on ice-cold OsO_4, and washed again with 0.1 M sodium cacodylate buffer. After ethanol washes, samples were incubated with EPON buffer and embedded. Sections (70 nm) were cut using an Ultracut device and put in ddH_2O at 37 °C in the dark, on negatively stained grids with 1.5% uranyl acetate. Images were acquired using a JEM 2100 plus microscope.

Fixation buffer
2% glutaraldehyde
2.5% sucrose
3 mM $CaCl_2$
100 mM HEPES, pH=7.4

0.1 M sodium cacodylate buffer
1% osmium
1.25% sucrose
10 mg/ml potassium ferricyanide in 0.1 M sodium cacodylate

Appendix C

Targeted liquid chromatography mass spectrometry (LC-MS) analysis

The extracted metabolites were resuspended in UPLC-grade acetonitrile:water in ratio 80:20 v:v. The samples were analyzed on the Acquity iClass UPLC using a SeQuant ZIC-HILIC 5 µm polymer 100 ×2.1 mm column connected to the Xevo TQ-S triple quadrupole mass spectrometer. 8 µl of metabolite extract were injected onto the column and separated using a flow rate of 500 µl/min of buffer A and buffer B, with the following gradient: 0–0.5 minutes 20% A; 0.5–1.4 minutes 20–35% A; 1.4–2.5 minutes 35–65% B. After 2.5 minutes, the system is set back to 20% A and re-equilibrated for 2.5 minutes.

Next, the eluted metabolites were detected in positive ion mode using ESI MRM (multi-reaction monitoring) applying the following settings: capillary voltage 1.5 kV, desolvation temperature 550 °C, desolvation gas flow rate 800 L/h, collision cell gas flow 0.15 ml/min. The following MRM transitions were used for relative compound quantification of metabolite m/z precursor mass (M+H+) 810, fragment mass (M+H+) m/z 303, using a cone voltage of 98 V and a collision energy of 28 V. For each compound, two further fragments were monitored as qualitative controls for compound identity. Data analysis and peak integration were performed using the TargetLynx software (version 4.1).

Buffer A

10mM ammonium acetate
0.1% acetic acid

Buffer B

Acetonitrile

Appendix D

Analysis of sequencing data

RNA-sequencing (RNA-seq) analysis

RNA-libraries were sequenced as single-end 150 bp reads on the HiSeq 4000 sequencer. The sequenced reads of RNA-seq dataset were processed using zUMIs (version 2.2.1) (Parekh et al., 2018) with STAR (version 2.6.1a) (Dobin et al., 2013), Samtools (version 1.9) (Li et al., 2009) and featureCounts from Rsubread (version 1.32.4) (Liao et al., 2014). The reads were mapped to the mouse genome (mm10 version) with the ensembl annotation (version GRCm38.91). The generated count matrix was further analyzed using R (version 3.5.1). First, genes were filtered using the 'filterByExpr' function of edgeR (Robinson et al., 2010) with min.count =5. The differential gene expression analysis was carried out using the limma-trend (Ritchie et al., 2015) approach at the adjusted p-value=0.05. Obtained sets of genes were further analyzed, for example through GO enrichment analysis.

Assay for Transposase Accessible Chromatin-sequencing (ATAC-seq)

The fastq files of ATAC-sequenced reads were mapped to the mouse genome (mm10 version) using local alignment on bowtie2 (Langmead and Salzberg, 2012), with parameters -x mm10 and -X 2000. The resulting BAM files were sorted, indexed using Samtools (version 1.3.1) and duplicates were removed using MarkDuplicates of Picard Tools. The peaks were called using chromstaR (Taudt et al., 2016) R package in differential mode, with bin size=300, step size=100 and minimum mapping quality threshold=15. The per sample peak RPKM (reads per kilobase of transcript per million mapped reads) table was pulled out from the chromstaR model and differential accessibility analysis was performed using edgeR (Robinson et al., 2010). The normalizing factors were calculated using 'RLE' method in 'calcNormFactors', tagwise dispersion trend was estimated using the default parameters in 'estimateDisp' function

and a generalized linear model was then fit on the data using ‘glmQLFit’ function in robust mode.

The peaks called by chromstaR were then used in nucleoATAC (Schep et al., 2015) for nucleosome positioning. For visualization purposes, the replicates were merged using ‘samtools merge’ and the bigwig files were generated using ‘bamCoverage–normalizeUsing RPGC’.

CUT and RUN-sequencing (CUT&RUN)

The fastq reads were mapped to mm10 version of genome using bowtie2 (Langmead and Salzberg, 2012) and duplicates were removed using MarkDuplicates program of Picard Tools. For mapping spike-in fragments to yeast, the ‘no-overlap–no-dovetail’ options were set and mapped to a repeat-masked version of the yeast genome, in order to avoid cross-mapping the mouse genome to that of the yeast genome. The peaks were then called using the chromstaR (Taudt et al., 2016) package in differential modes for each histone mark (H3K27ac, H3K27me3 and H3ac), with bin size=1,000, step size=500 and minimum mapping quality threshold=15. Differential analysis was performed using edgeR, similarly to that of the ATAC-seq analysis. For visualization purposes, the replicates were merged using ‘samtools merge’ and the bigwig files were generated using ‘bamCoverage–normalizeUsing RPGC’. The differential regions in the H3ac data were identified using chromstaR in differential mode with eight states. The segments with the different states in old, acetate-treated old and young samples were obtained from multivariate peak call.

Erklärung zur Dissertation

gemäß der Promotionsordnung vom 12. März 2020

Hiermit versichere ich an Eides statt, dass ich die vorliegende Dissertation selbstständig und ohne die Benutzung anderer als der angegebenen Hilfsmittel und Literatur angefertigt habe. Alle Stellen, die wörtlich oder sinngemäß aus veröffentlichten und nicht veröffentlichten Werken dem Wortlaut oder dem Sinn nach entnommen wurden, sind als solche kenntlich gemacht. Ich versichere an Eides statt, dass diese Dissertation noch keiner anderen Fakultät oder Universität zur Prüfung vorgelegen hat; dass sie - abgesehen von unten angegebenen Teilpublikationen und eingebundenen Artikeln und Manuskripten - noch nicht veröffentlicht worden ist sowie, dass ich eine Veröffentlichung der Dissertation vor Abschluss der Promotion nicht ohne Genehmigung des Promotionsausschusses vornehmen werde. Die Bestimmungen dieser Ordnung sind mir bekannt. Darüber hinaus erkläre ich hiermit, dass ich die Ordnung zur Sicherung guter wissenschaftlicher Praxis und zum Umgang mit wissenschaftlichem Fehlverhalten der Universität zu Köln gelesen und sie bei der Durchführung der Dissertation zugrundeliegenden Arbeiten und der schriftlich verfassten Dissertation beachtet habe und verpflichte mich hiermit, die dort genannten Vorgaben bei allen wissenschaftlichen Tätigkeiten zu beachten und umzusetzen. Ich versichere, dass die eingereichte elektronische Fassung der eingereichten Druckfassung vollständig entspricht.

Teilpublikationen:

1. Pouikli et al. Chromatin remodeling due to degradation of citrate carrier impairs osteogenesis of aged mesenchymal stem cells. *Nat. Aging (*2021).
2. Pouikli A. and Tessarz P. Metabolism and Chromatin: A Dynamic Duo that regulates development and ageing. *BioEssays* (2021).
3. Pouikli A. and Tessarz P. Epigenetic alterations in stem cell aging - a promising target for age-associated interventions? *Brief. Genomics* (2021).

Köln, den 14 November 2021

Andromachi Pouikli